A Thesis Submitted for the Degree of PhD at the University of Warwick

Permanent WRAP URL:

http://wrap.warwick.ac.uk/95507

Copyright and reuse:

This thesis is made available online and is protected by original copyright.

Please scroll down to view the document itself.

Please refer to the repository record for this item for information to help you to cite it.

Our policy information is available from the repository home page.

For more information, please contact the WRAP Team at: wrap@warwick.ac.uk

warwick.ac.uk/lib-publications

Computational Studies of Paddlewheel Complexes in Isolation and Incorporated into Metal Organic Frameworks

By

Khalid Ahmad Alzahrani

A thesis submitted in partial fulfilment of the requirements for the degree of Doctor of Philosophy in Chemistry

Department of Chemistry,
University of Warwick,
CV4 7AL

August 2017

Contents

Tables and Illustrations

6

Acknowledgements

Firstly I would like to acknowledge the support of the King Abdulaziz University and the Ministry of Education, Kingdom of Saudi Arabia, for the provision of a PhD scholarship as without their support this PhD would not have happened.

I would like to acknowledge the University of Warwick for providing me everything needed for writing up this thesis. Many thanks to the Royal Society of Chemistry for allowing me to access the Cambridge Structural Database.

I would like to acknowledge the efforts of my supervisor Prof. Robert Deeth who has guided me through the last four years, offered invaluable support and more recently has assisted in proof reading half of this thesis. I would also like to thank my second supervisor Dr. Scott Habershon for his great support and advice through the last two years (After RD took early retirement in 2015), and for his assistance in proof reading the second half of this thesis. My thanks to Ben Houghton for helping organise and focus me at the beginning, and to Scott's and Alessandro's group members for their support in the last two years. Many thanks to all my Saudi friends in Coventry for the enjoyable gathering meetings during weekends and holydays.

Finally I would like to thank my wife Rasha and my beautiful daughters Dina and Lana for their understanding and support during the writing process. I would like also to thank my parents, brothers, and sisters for their encouragements and emotional support. It has been difficult and long and I couldn't have done it without them.

Declaration

This thesis is submitted to the University of Warwick in support of my application for the degree of Doctor of Philosophy. It has been composed by myself and has not been submitted in any previous application for any degree.

The work presented was carried out by the author, including data generated and data analysis except in the cases outlined below:

- The SVL coding files in Chapter 3 and Chapter 4 were written by Robert J. Deeth (PhD supervisor).
- The DFT calculations in Chapter 5 using ADF software were carried out by Robert J. Deeth.

Parts of this thesis have been published by the author:

- K. A. H. Alzahrani and R. J. Deeth, *J. Mol. Model.*, 2016, **22**, 80.
- K. A. H. Alzahrani and R. J. Deeth, *Dalton Trans*, 2016, **45**, 11944-11948.
- Chapter 4 and the transferable version of CPW-FF are in preparation.

Abstract

The aim of the work presented in this thesis is to develop computational approaches to the modelling of zinc and copper paddlewheel complexes both in isolation and when incorporated into metal organic frameworks (MOFs). We considered both 'ab initio' and empirical force field methods based mainly on DFT and ligand field molecular mechanics (LFMM) respectively.

A new all-atom first-principles force field (FF) is constructed for the bimetallic, four-bladed zinc paddlewheel (ZPW) motif. Zinc-ligand interactions are described via Morse functions and the angular geometry at the metal centres is modelled with a pure ligand-ligand repulsion term. The ZPW-FF is principally based on 21 DFT-optimized model systems of general formula ZnPR.nL, where ZnP is the base $Zn_2(O_2CR)_4$ unit, R=H, CH_3 or CF_3, L=NH_3, pyridine, or water and n = 0, 1 or 2. It correctly generates the distorted tetrahedral coordination of the uncapped $[Zn_2(O_2CR)_4]$ species in their ground states as well as giving reasonable structures and energies for the higher symmetry D_{4h} transition state conformations. The zinc-ligand Morse function reference distance, r_0, is further refined against some experimental complexes located in the Cambridge Structural Database and this FF is applied to pore models of the flexible MOF $[Zn(bdc)_2(dabco)]_n$ and also used to assess the system under water vapour. A single pore model reproduces the unit cell of the evacuated MOF system while a 3×3 grid model is necessary to provide good agreement with the observed pronounced structural changes upon adsorption of either dimethylformamide or benzene. The ZPW-FF is also applied to 2D and 3D crystal systems of MOF-2 which comprises $Zn(bdc)(H_2O).(dmf)$ building units and provides good results.

In the second part of this thesis, our density functional theory calculations on four-bladed copper paddlewheel (CPW) systems $[Cu_2(O_2CR)_4L_2]$ reveal a change in ground state with increasing Cu–L bond strength. For L = N-heterocyclic carbene (NHC), the Jahn–Teller axis switches from parallel to orthogonal to the Cu–Cu vector and the copper coordination geometry becomes highly flexible. While the calculated dimer/monomer equilibrium for isolated complexes slightly favours monomers, the preformed paddlewheel units embedded in many metal organic frameworks are potential targets for developing novel materials. Therefore, the preliminary LFMM parameters for constructing a generic CPW-FF are reported. However, a definitive version of the CPW-FF remains a task for the future.

Abbreviations

MOF – Metal Organic Framework

ZPW – Zinc Paddlewheel

CPW – Copper Paddlewheel

ZPW-FF – Zinc Paddlewheel Force Field

CPW-FF – Copper Paddlewheel Force Field

CSD – Cambridge Structure Database

DFT – Density Functional Theory

HF – Hartree Fock

ADF – Amsterdam Density Functional

QM - Quantum Mechanics

MOE – The Molecular Operating Environment

DommiMOE – d-Orbital Molecular Mechanics in MOE

MM - Molecular Mechanics

MD – Molecular Dynamic

LFMM – Ligand Field Molecular Mechanics

LFSE - Ligand Field Stabilization Energy

LFT – Ligand Field Theory

AOM – Angular Overlap Model

FF – Force Field

BCI – Bond Charge Increment

Chapter 1: Introduction to Metal Organic Frameworks

1.1 Motivation

"What would happen if we could arrange the atoms one by one the way we want them?" This is one of the most famous questions in material science, which was asked, in 1959, by Richard P. Feynman. Since then, chemists have tried to answer the question by involving themselves intensively in studying the structures and interactions of molecules and atoms in gases, liquids and solids. From our perspective, a partial answer of Feynman's question is to identify which effects are important for the controlled arrangement or rearrangement of molecules or atoms.

This work deals generally with crystalline porous materials where the atoms are arranged to generate ordered pores within structures. In addition, changing the pore size and/or shape by modifying the structure itself or the adsorbed molecules are mainly considered in this work. Therefore, applying Feynman's question to these kind of compounds, would lead chemists to define the cavities on a molecular level. However, this thesis deals theoretically with a special structural type of porous materials, known as metal organic frameworks (MOFs) and how the overall system, particularly the pore size and/or shape, is influenced by the type of metal centres, organic ligands, and adsorbed molecules such as dimethylformamide (DMF) and benzene. These type of MOF systems are known as flexible MOFs and may also be called soft porous crystals (SPCs):

''Soft porous crystals are defined as porous solids that possess both a highly ordered network and structural transformability. They are bistable or multistable crystalline materials with long range structural ordering, a reversible transformability between states, and permanent porosity. The term porosity means that at least one crystal phase possesses space that can be occupied by guest molecules, so that the framework exhibits reproducible guest adsorption '' (quoted from S. Horike et al.) [1]

In addition, some existing experimental examples of the interactions between MOFs systems and guest molecules and their associated structural transformability are addressed in this work. These objectives are investigated by developing an accurate theoretical method to help understand the fundamental aspects of chosen MOFs.

As mentioned above, MOFs are featured by defined cavities which are often accessible for guest molecules. Thus, the main goal of this thesis is to develop a theoretical method that can accurately reproduce flexible MOF systems, including their pore size and/or shape changes. Then, the dynamic behaviour of these systems would be easily studied to understand the adsorption mechanism between its framework and adsorbed species. Hence, this thesis is organized as follows. The world of MOFs and some of their applications will be considered briefly in this Chapter. All theoretical methods background used in this thesis are described in Chapter 2. In Chapters 3 - 6 computational studies, including methods, results, and discussions, on some existing flexible MOF systems and paddle wheel complexes containing zinc and copper metals are explained in detail. Chapter 7 has the conclusion of the thesis and some remarks on future work.

1.2 Metal organic frameworks (MOFs)

Metal-organic frameworks (MOFs), also known as coordination networks or coordination polymers in the literature, are now considered as one of the most promising classes of porous materials.[2-6] Over the past fifty years, research into such materials has resulted in many applications which have affected our lives and industrial processes (Figure 1.1).[7-13] MOFs are crystalline materials consisting of central metal ions, metal clusters, or metal oxide clusters and organic ligands acting as linkers to form one-, two-, or three-dimensional structures (Figure 1.2).[14-16]
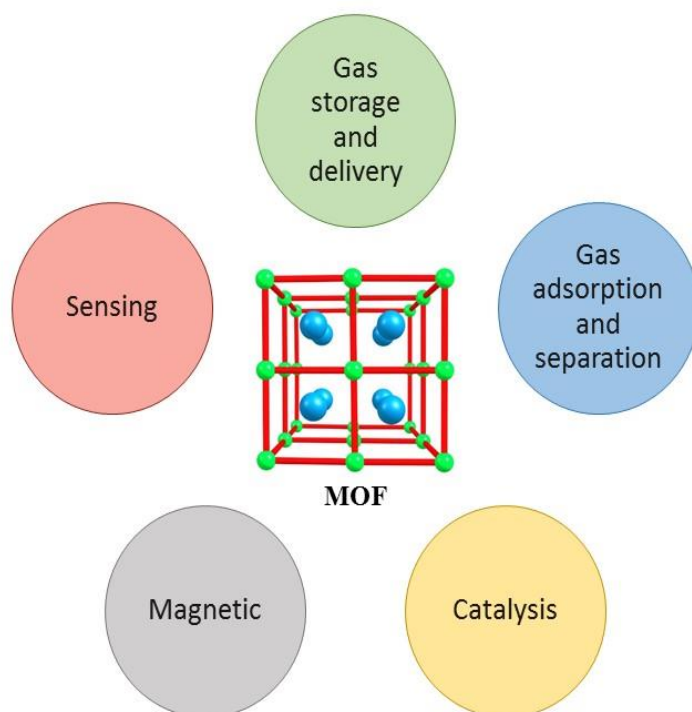
Figure 1.1; Potential applications of metal organic frameworks (MOFs).
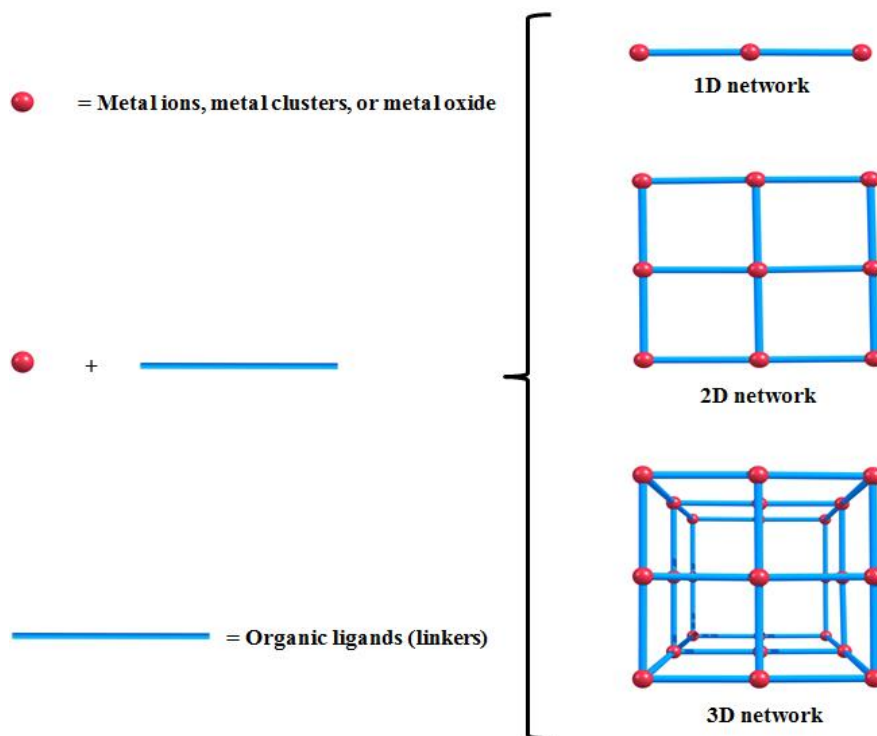
Figure 1.2; Schematic representation of one-, two-, or three-dimensional structures of MOFs built from metal units and organic ligands (linkers).

Controlling the framework dimensionality and topology in forming MOFs allows researchers to target specific properties of materials such as gas storage and delivery, gas adsorption and separation, catalysis, sensing, and magnetic.[17] The properties of MOF systems are depending on the type of the metal centre and linkers between them. For example, replacing zinc by copper atoms or verse versa can affect the flexibility and stability of the whole MOFs systems.[18] In addition, tuning the size, shape, and the surface properties of MOFs systems for a targeted application can also be controlled by the length, geometry, ratio, and functional groups of the linkers.[19] Figure 1.3 illustrates some organic linkers used regularly for producing MOF systems.
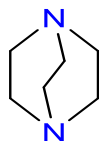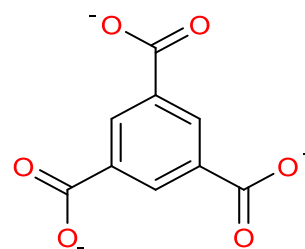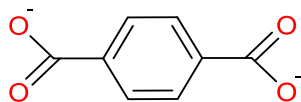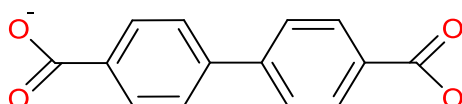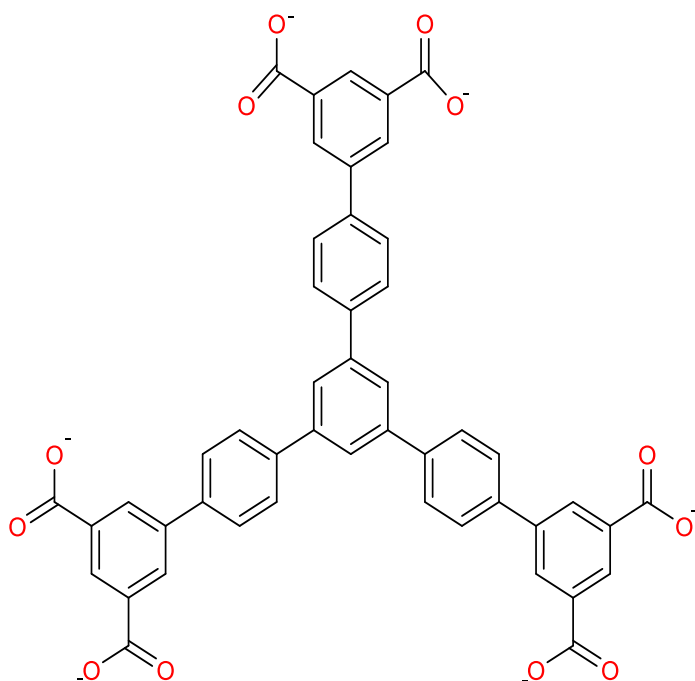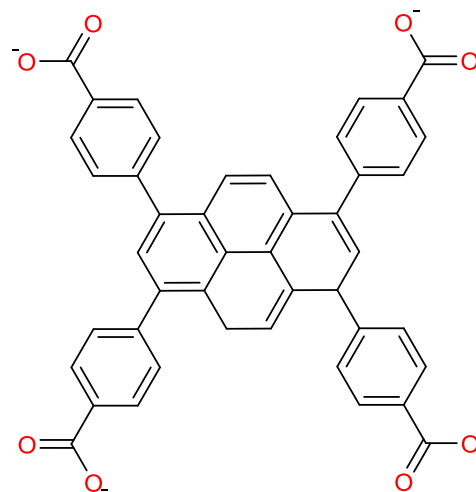
Figure 1.3; Some organic linkers used in producing the most useful MOF systems. Pyrazine and DABCO are usually used as axial linkers.

Since the pioneering work of Robson and co-workers [20] thousands of scientific articles, which feature the term 'metal-organic framework', have been published. Yaghi, Fujita, Zaworotko, Kitagawa, Moore/Lee, and Ferey research groups have contributed to produce a number of MOFs systems (such as MOF-5, HKUST-1 [21], MIL-53 [22] etc.) which are built from different metals connected by a variety of organic linkers (Figure 1.4)

MOF-5 **HKUST-1** **MIL-53**
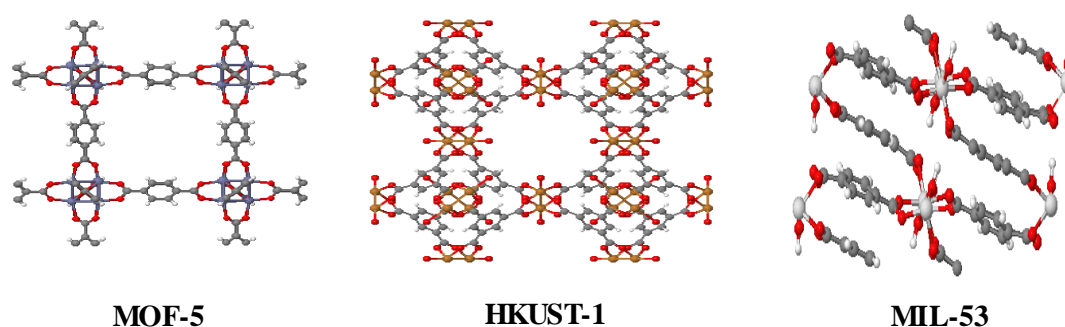
Figure 1.4; Schematic view of some MOFs built from metals unit and organic linkers (ligands). MOF-5 built from Zn4O nodes with 1,4-benzodicarboxylic acid linkers, HKUST-1 built from copper nodes with 1,3,5-benzenetricarboxylic acid between them, and MIL-53 built from scandium and oxygen (ScO_6) nodes with 1,4-benzodicarboxylic acid linkers between the nodes. These structures are adapted from ChemTube3D home website, University of Liverpool.

Theoretically, the plentiful sources of organic linkers and metals ions lead to design of a wide variety of MOFs. However, in this thesis, the flexible MOFs containing a paddle-wheel secondary building units (SBUs), where the paddle-wheel motif is a transition metal (TM) dimer bridged by four carboxylate units is emphasized (Figure 1.5). While many MOFs have relatively rigid frameworks which therefore define a fixed pore size, other MOFs display a degree of flexibility or 'breathing' (Figure

1.6).[23, 24] The pore size and/or shape changes as a function of adsorbate offering exciting possibilities for using these materials particularly in separations[25-28] and sensing[29, 30]. As mentioned previously, some flexible MOFs systems contain a paddle-wheel SBU. The paddle-wheel motif is a TM dimer bridged by three or four carboxylate units. In combination with linear linkers, the latter generates planar $[M_2L_2]_n$ grids which can be interconnected by ditopic pillars like 1,4-diazabicyclo(2.2.2)octane (dabco) or pyrazine to generate a 3-D framework.
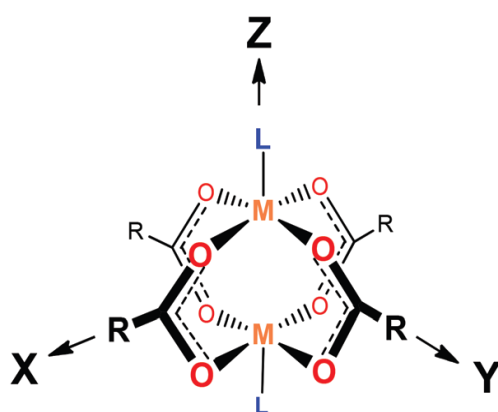
Figure 1.5; Schematic representation of four-bladed paddlewheel complex.

DMF/WATER   **EMPTY**   **BENZENE**
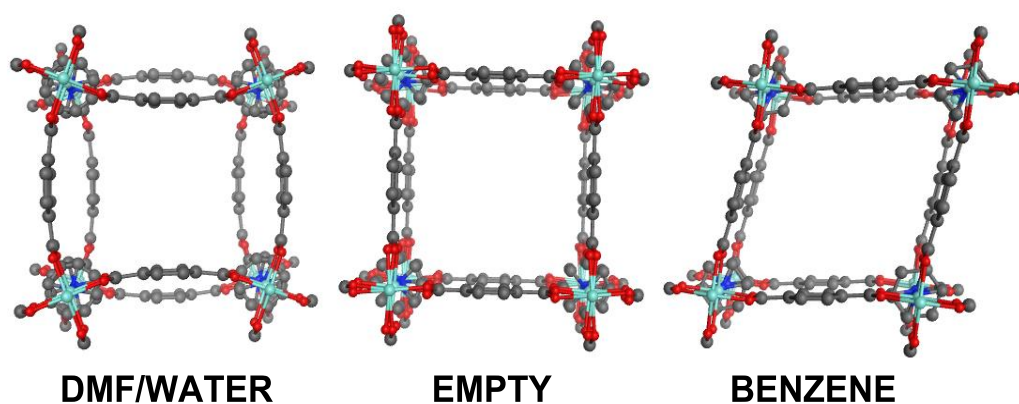
Figure 1.6; Pore framework structures for [Zn2(bdc)2(dabco)]n derived from published CIF files. Hydrogens and encapsulated solvent removed. dabco and carboxylate disorder as per CIF file.

1.3 Current and Potential applications of MOFs

Nanoporous materials, such as zeolites, carbon nanotubes, activated carbon, and MOFs have been used widely in several energy-related applications.[7, 31] However, due to their crystalline nature, the potential applications of MOFs are much greater than other Nanoporous materials. Additionally, the ability of introducing different functional groups through their hybrid framework makes MOFs a promising candidates for a variety of applications. All of these features motivate scientists to obtain unique porous materials with various functionality and selectively as well. In this introduction, therefore, the potential applications of MOFs have been classified into five broad groups which are presented below briefly. Although this thesis concentrates on modelling flexible MOFs systems, introducing some potential applications of MOFs systems, whether rigid or flexible, are crucial here to provide the readers a general information regarding the MOF systems and their applications.

1.3.1 Gas Storage and Delivery

Gas storage and delivery applications are considered as one of the primary research fields of MOFs. Recent studies have suggested that the abilities of MOFs to store, capture and deliver gases, including natural gases, would be widely used in gas storage applications.[32, 33] There are several existing MOFs with high porosity and very large surface areas which make these materials promising candidates in this particularly application. For instance, the storage of molecular hydrogen, H_2, within MOFs cavities is known as an efficient energy carrier for the future. Thus, these systems are investigated intensively at present. One of the most interesting application is in the

hydrogen-fuelled automobiles. The development of a safe and viable approach for the storage of H_2 would likely accelerate the wide spread commercialization of this application.[34] Beside the storage of H_2 other molecules like carbon dioxide and methane which would be used within MOFs as a greenhouse gas and energy carrier applications respectively.[35] MOFs have also an abilities to store both small and large molecule and release them in a controlled manner.[36, 37] This feature have been used widely in pharmaceutical applications especially for drug delivery.[38] Therefore, understanding the interactions between MOFs and guest molecules is highly essential in this area.

1.3.2 Gas Adsorption and Separation

The high porosity (the largest pore = 98 Å)[39] and surface areas (ranging from 1000 to 10,000 m^2/g)[7] properties of MOFs have nominated this type of materials to be an excellent candidate for gas adsorption and separation applications. Compared to other inorganic porous materials, the pores in MOFs can be affected by systematically introducing functional groups into the framework. Thus, gas adsorption and separation characterisations of MOFs can be tuned, not only by changing the pore size and shape, but also by the specific tailoring of the interaction between guest molecules and frameworks. This property leads researchers to use MOFs for separation of liquid and gas mixtures.[25-28]

Another commendable properties of MOFs is their thermal stability, which allows the process of removal guest species from MOFs pores very simple. This feature makes MOFs potential and suitable for gas adsorption and separation. In regard to the former,

MOFs have widely play an important role in capturing the greenhouse gases (e.g. carbon dioxide, CO_2) from industrial emissions, which contribute to global warming. [40-42] In regard to the latter, some studies have shown the possibility of achieving kinetic-based separations using MOFs.[43] Therefore, understanding the interaction between MOFs and guest molecule with respect to the mobility and the ordering of the guest species into the pores is very important.

1.3.3 Catalysis

As mentioned previously, the high crystallinity and thermal stability of MOFs, including the possibility of tuning their pore properties, would make this material highly desirable in industrial catalysis applications. In addition, the arrangement of the active sites, including their distance and orientation, is well ordered and can be controlled, which makes synergetic effects possible. Therefore, some MOFs models can be used simply as an active support or as a support partner in some reaction processes. The former can be observed in MOFs possessing unsaturated metal sites.[44] Compared to homogeneous catalytic systems, MOFs have proven their efficiencies in separation products from the chemical mixture and facilitate the recyclability process of catalyst applications. Although, this feature is available in heterogeneous catalytic systems, MOFs have the advantage of better catalyst stability.[45] The availability of highly concentrated organized metals within MOFs leads to many reports of efficient reaction catalysis.[46-48] Additionally, the possibility of controlling the pore size and shape of MOFs has influenced the selectivity toward desired products.[31]

All of these properties associated with MOF systems will attract more researchers to investigate the MOF-based catalysis applications in the near future. However, a better understanding of the reaction mechanism at the active centre is basically required. Moreover, studying the mobility and the ordering of all reactants within the pores are also needed to enhance systematically the performance of MOF-based catalysis.

1.3.4 Luminescent MOFs and Sensing

The presence of metals ions and organic linkers, with various functional groups, within MOFs have nominated these materials to be promising candidates as sources of emissive phenomena. It is known that luminescent materials have been widely used in making sensing, lighting, display, and optoelectronic devices. Nevertheless, nowadays, developing a suitable luminescent MOFs for practical applications is substantially interesting.[31] Moreover, producing MOFs-based sensing systems is interesting at the moment.[29, 30]

Although the surface nature of the materials is neglected in most MOFs applications, it has a significant function in sensing applications. Therefore the possibility of controlling the tunable porosity and functionality of MOFs plays an important role in developing sensing devices for specific applications. Additionally, the ability of changing MOF properties enables researchers to produce specific detection devices.[49] For example, Yanai *et al*,[50] have used the flexible MOF system, shown in Figure 1.6, for the selective detection of C_2H_2 and CO_2 based on fluorescence responses to these guest molecules. Moreover, In 2008, Allendorf *et al*, have developed the first sensor based on thin film of rigid HKUST-1 system.[51] This device has shown its ability to

detect some molecules, such as water and alcohols, which their adsorption does not required a large structural transformation.

1.3.5 Magnetic MOFs

In recent years, MOFs materials have been used in many applications based on their magnetics properties. The design possibilities that allow embedding paramagnetic metal ions such as Cu^{+2}, or using open-shell organic linkers within MOFs would result in magnetic properties and strong magnetic interactions between the centres of spin.[52] Moreover, the ligand diversity and topology design possibilities incorporated within MOFs can maximize and control the magnetic interactions between linker and/or metal sites to enhance system's cooperativity. This type of materials are known as magnetic framework composites (MFCs) which are recently used in many technological field such as catalysis, storage, drug delivery, imaging and sensing.[53]

1.4 Design and Characterization of MOFs

In the past decade, thousands of MOFs systems have been reported and studied including their design, characterization, modification, and applications. The possibility of controlling size, shape and functionality of MOFs systems motivates researchers to develop specific periodic systems. To date, hundreds of scientists have been contributed to designing MOF systems for applications using generally two approaches. The first approach is based on designing crystal structure experimentally. As mentioned previously, various metals and polydentate ligands using within MOFs can be used to incorporate desired properties and functional groups into the framework. Subsequently, the obtained systems made for certain applications, such

as gas storage, gas separation, gas adsorption, and catalysis, can be characterized. Despite that this approach is widely used, it is nevertheless time consuming and expensive especially for characterization.[54-56]

The second approach is to use computational modelling where the topologies of MOFs can be predicted and formed theoretically from various metal and organic linkers. This approach involves usually constructing large libraries of potential MOFs materials.[57, 58] The enumeration of MOF topologies would be followed by screening for targeted properties such as higher pore sizes, presence of open metal sites, and stability and higher selectivity for certain gas molecules. The predicted MOFs with desired properties can be then synthesised and characterized experimentally.[59] For example, Farah et al,[8] have initially used molecular simulations tools to design and characterize a MOF system named NU-100 with a particularly high surface area which enables storage of hydrogen and carbon dioxide. Subsequently, NU-100 was synthesized and characterized experimentally yielded a material being in excellent agreement with calculated structure.

In recent years, the availability of computational models have contributed widely to prediction of the properties of the potential MOFs. However, there are two methods of computational simulation for MOFs. The first one is the electronic structure methods which is based on the principles of quantum mechanics, including Hartree-Fock (HF) theory and density functional theory (DFT). The second method is classical simulation methods which define the potential energy functions by using interatomic potentials. In the next section, more details of computational studies of MOFs are explained in general before getting to the computational theories and approximations in chapter 2.

1.5 Computational Studies of MOFs

Exploring the properties of thousands of MOFs reported in the literature using available experimental techniques is very expensive and time consuming. Furthermore, some detailed information such as the microscopic properties of MOFs are very difficult to be studied using only experimental methods. Therefore, molecular modelling methods have provided a valuable complement to experimental studies giving researchers a deeper and more thorough understating of these materials at the molecular level, including mechanisms of host-guest interactions involved.[60-62] In addition, molecular modelling has been used significantly by chemists and engineering for large-scale screening of hypothetical and existing materials, including MOFs.[58] Thus, during the past decade, significant computational approaches studies have been done for investigating the performance and properties of MOFs.[14-16]

To date, there are thousands of published research articles using computational tools to understand some aspects of MOFs. Therefore, in this introduction some intrinsic reviews focusing on summarizing various topics of computational studies on MOFs are briefly highlighted. For example, Samuel *et al.*[63] explained in their review the most recent theories of the quantum mechanical electronic calculations that have been applied to MOFs. Moreover, in a comprehensive overview of the successes and the limitations of different computational methodologies for MOFs, Qingyuan *et al.*[64] provided a state-of-the-art review on the most recent modelling approaches of particularly gas separations applications in MOFs. Meek *et al.*[65] have also reviewed the most important applications of MOFs, together with a brief description of the development in molecular modelling of MOFs. Sholl and co-workers [66] wrote a review focusing on quantal and classical simulations methods that have been used for studying

specific adsorption and transport applications of MOFs. However, to our knowledge, there is no comprehensive review covering the significant advances of computational methodologies those have been achieved so far with respect to MOFs. Thus, reading the recent textbooks, papers, and reviews, particularly for newcomers, is highly demanded to understand the features of MOFs and the relevant computational methodologies developed so far.

1.6 Aims and Objectives

High quality computational modelling would be of enormous benefit to help understand the structure-function relationships of MOFs. However, one of the most difficult problem that faces researchers in the area is how to capture the types of structural change displayed by flexible MOF systems as a function of adsorbate. Quantum mechanical methods such as density functional theory (DFT) would be desirable but the size and complexity of MOFs makes the application of QM methods extremely time consuming. Alternatively, molecular mechanics methods should be developed to give a good agreement between the calculated structures of MOFs and experiments. From our point of view, the problem can be solved by extending the force field software 'DommiMOE' to enable the accurate and efficient simulation of the targeted MOFs systems. In this thesis, modelling zinc paddle wheel (ZPW) and copper paddle wheel (CPW) complexes in isolation and incorporated into metal organic frameworks will be highlighted, including their structural flexibilities and their dynamic behaviour based on particular adsorbed molecules such as benzene and DMF. Theoretical methods used in this work and obtained results are explained in more detail in the following chapters.

1.7 References

1.   S. Horike, S. Shimomura and S. Kitagawa, *Nat. Chem.*, 2009, **1**, 695-704.

2.   H. K. Chae, D. Y. Siberio-Pérez, J. Kim, Y. Go, M. Eddaoudi, A. J. Matzger, M. O'Keeffe and O. M. Yaghi, *Nature*, 2004, **427**, 523-527.

3.   M. Eddaoudi, J. Kim, N. Rosi, D. Vodak, J. Wachter, M. O'Keeffe and O. M. Yaghi, *Science*, 2002, **295**, 469-472.

4.   G. Férey, C. Mellot-Draznieks, C. Serre, F. Millange, J. Dutour, S. Surblé and I. Margiolaki, *Science*, 2005, **309**, 2040-2042.

5.   R. Kitaura, K. Seki, G. Akiyama and S. Kitagawa, *Angew. Chem. Int. Ed.*, 2003, **42**, 428-431.

6.   J. L. Rowsell and O. M. Yaghi, *Micropor. Mesopor. Mat.*, 2004, **73**, 3-14.

7.   H. Furukawa, K. E. Cordova, M. O'Keeffe and O. M. Yaghi, *Science*, 2013, **341**, 1230444.

8.   O. K. Farha, A. Ö. Yazaydın, I. Eryazici, C. D. Malliakas, B. G. Hauser, M. G. Kanatzidis, S. T. Nguyen, R. Q. Snurr and J. T. Hupp, *Nat. Chem.*, 2010, **2**, 944-948.

9.   G. Férey, *Chem. Soc. Rev.*, 2008, **37**, 191-214.

10.   S. Kitagawa and R. Matsuda, *Coord. Chem. Rev.*, 2007, **251**, 2490-2509.

11.   S. Ma, D. Sun, J. M. Simmons, C. D. Collier, D. Yuan and H.-C. Zhou, *J. Am. Chem. Soc.*, 2008, **130**, 1012-1016.

12.   A. Phan, C. J. Doonan, F. J. Uribe-Romo, C. B. Knobler, M. O'keeffe and O. M. Yaghi, *Acc. Chem. Res*, 2010, **43**, 58-67.

13.   S. Xiang, Y. He, Z. Zhang, H. Wu, W. Zhou, R. Krishna and B. Chen, *Nat. Commun.*, 2012, **3**, 954.

14.   S. M. Cohen, *Chem. Rev.*, 2011, **112**, 970-1000.

15.   K. J. Gagnon, H. P. Perry and A. Clearfield, *Chem. Rev.*, 2011, **112**, 1034-1054.

16.   M. O'Keeffe and O. M. Yaghi, *Chem. Rev.*, 2011, **112**, 675-702.

17.   F. o.-X. Coudert, *Chem. Mater.*, 2015, **27**, 1905-1916.

18.   S. Bureekaew, S. Amirjalayer and R. Schmid, *J. Mater. Chem.*, 2012, **22**, 10249-10254.

19.   W. Lu, Z. Wei, Z.-Y. Gu, T.-F. Liu, J. Park, J. Park, J. Tian, M. Zhang, Q. Zhang and T. Gentle III, *Chem. Soc. Rev.*, 2014, **43**, 5561-5593.

20.   B. Hoskins and R. Robson, *J. Am. Chem. Soc.*, 1990, **112**, 1546-1554.

21.   S. S.-Y. Chui, S. M.-F. Lo, J. P. Charmant, A. G. Orpen and I. D. Williams, *Science*, 1999, **283**, 1148-1150.

22. C. Serre, F. Millange, C. Thouvenot, M. Noguès, G. Marsolier, D. Louër and G. Férey, *J. Am. Chem. Soc.*, 2002, **124**, 13519-13526.

23. L. Sarkisov, R. L. Martin, M. Haranczyk and B. Smit, *J. Am. Chem. Soc.*, 2014, **136**, 2228-2231.

24. A. Schneemann, V. Bon, I. Schwedler, I. Senkovska, S. Kaskel and R. A. Fischer, *Chem. Soc. Rev.*, 2014, **43**, 6062-6096.

25. C. S. Hawes, Y. Nolvachai, C. Kulsing, G. P. Knowles, A. L. Chaffee, P. J. Marriott, S. R. Batten and D. R. Turner, *Chem. Commun.*, 2014, **50**, 3735-3737.

26. B. Li, H.-M. Wen, W. Zhou and B. Chen, *J. Phys. Chem. Lett.*, 2014, **5**, 3468-3479.

27. S. Mukherjee, B. Joarder, A. V. Desai, B. Manna, R. Krishna and S. K. Ghosh, *Inorg. Chem.*, 2015, **54**, 4403-4408.

28. Q.-G. Zhai, N. Bai, S. n. Li, X. Bu and P. Feng, *Inorg. Chem.*, 2015, **54**, 9862-9868.

29. D. Liu, K. Lu, C. Poon and W. Lin, *Inorg. Chem.*, 2013, **53**, 1916-1924.

30. Z. Hu, B. J. Deibert and J. Li, *Chem. Soc. Rev.*, 2014, **43**, 5815-5840.

31. R. J. Kuppler, D. J. Timmons, Q.-R. Fang, J.-R. Li, T. A. Makal, M. D. Young, D. Yuan, D. Zhao, W. Zhuang and H.-C. Zhou, *Coord. Chem. Rev.*, 2009, **253**, 3042-3066.

32. D. A. Gómez-Gualdrón, C. E. Wilmer, O. K. Farha, J. T. Hupp and R. Q. Snurr, *J. Phys. Chem. C*, 2014, **118**, 6941-6951.

33. H. Zhang, P. Deria, O. K. Farha, J. T. Hupp and R. Q. Snurr, *Energy Environ Sci*, 2015, **8**, 1501-1510.

34. L. J. Murray, M. Dincă and J. R. Long, *Chem. Soc. Rev.*, 2009, **38**, 1294-1314.

35. G. Férey, C. Serre, T. Devic, G. Maurin, H. Jobic, P. L. Llewellyn, G. De Weireld, A. Vimont, M. Daturi and J.-S. Chang, *Chem. Soc. Rev.*, 2011, **40**, 550-562.

36. M. Müller, A. Devaux, C.-H. Yang, L. De Cola and R. A. Fischer, *Photochem. Photobiol. Sci.*, 2010, **9**, 846-853.

37. P. Horcajada, T. Chalati, C. Serre, B. Gillet, C. Sebrie, T. Baati, J. F. Eubank, D. Heurtaux, P. Clayette and C. Kreuz, *Nat. Mater.*, 2010, **9**, 172-178.

38. P. Horcajada, R. Gref, T. Baati, P. K. Allan, G. Maurin, P. Couvreur, G. Ferey, R. E. Morris and C. Serre, *Chem. Rev.*, 2011, **112**, 1232-1268.

39. H. Deng, S. Grunder, K. E. Cordova, C. Valente, H. Furukawa, M. Hmadeh, F. Gándara, A. C. Whalley, Z. Liu and S. Asahina, *science*, 2012, **336**, 1018-1023.

40. D. Britt, H. Furukawa, B. Wang, T. G. Glover and O. M. Yaghi, *Proc. Natl. Acad. Sci.*, 2009, **106**, 20637-20640.

41.   J.-R. Li, Y. Ma, M. C. McCarthy, J. Sculley, J. Yu, H.-K. Jeong, P. B. Balbuena and H.-C. Zhou, *Coord. Chem. Rev.*, 2011, **255**, 1791-1823.

42.   T. M. McDonald, J. A. Mason, X. Kong, E. D. Bloch, D. Gygi, A. Dani, V. Crocellà, F. Giordanino, S. O. Odoh and W. S. Drisdell, *Nature*, 2015, **519**, 303-308.

43.   C. Y. Lee, Y.-S. Bae, N. C. Jeong, O. K. Farha, A. A. Sarjeant, C. L. Stern, P. Nickias, R. Q. Snurr, J. T. Hupp and S. T. Nguyen, *J. Am. Chem. Soc.*, 2011, **133**, 5228-5231.

44.   K. K. Tanabe, Z. Wang and S. M. Cohen, *J. Am. Chem. Soc.*, 2008, **130**, 8508-8517.

45.   J. Lee, O. K. Farha, J. Roberts, K. A. Scheidt, S. T. Nguyen and J. T. Hupp, *Chem. Soc. Rev.*, 2009, **38**, 1450-1459.

46.   M. J. Beier, W. Kleist, M. T. Wharmby, R. Kissner, B. Kimmerle, P. A. Wright, J. D. Grunwaldt and A. Baiker, *Chem. Eur. J.*, 2012, **18**, 887-898.

47.   F. Carson, S. Agrawal, M. Gustafsson, A. Bartoszewicz, F. Moraga, X. Zou and B. Martín-Matute, *Chem. Eur. J.*, 2012, **18**, 15337-15344.

48.   K. Leus, Y.-Y. Liu and P. Van Der Voort, *Cat. Rev.*, 2014, **56**, 1-56.

49.   D. Zacher, O. Shekhah, C. Wöll and R. A. Fischer, *Chem. Soc. Rev.*, 2009, **38**, 1418-1429.

50.   N. Yanai, K. Kitayama, Y. Hijikata, H. Sato, R. Matsuda, Y. Kubota, M. Takata, M. Mizuno, T. Uemura and S. Kitagawa, *Nat. Mater.*, 2011, **10**, 787-793.

51.   M. D. Allendorf, R. J. Houk, L. Andruszkiewicz, A. A. Talin, J. Pikarsky, A. Choudhury, K. A. Gall and P. J. Hesketh, *J. Am. Chem. Soc.*, 2008, **130**, 14404-14405.

52.   Q. Li, X. Jiang and S. Du, *RSC Advances*, 2015, **5**, 1785-1789.

53.   R. Ricco, L. Malfatti, M. Takahashi, A. J. Hill and P. Falcaro, *J. Mater. Chem. A*, 2013, **1**, 13033-13045.

54.   M. Eddaoudi, D. B. Moler, H. Li, B. Chen, T. M. Reineke, M. O'keeffe and O. M. Yaghi, *Acc. Chem. Res.*, 2001, **34**, 319-330.

55.   O. M. Yaghi, M. O'Keeffe, N. W. Ockwig, H. K. Chae, M. Eddaoudi and J. Kim, *Nature*, 2003, **423**, 705-714.

56.   B. J. Burnett, P. M. Barron, C. Hu and W. Choe, *J. Am. Chem. Soc.*, 2011, **133**, 9984-9987.

57.   C. E. Wilmer, O. K. Farha, Y.-S. Bae, J. T. Hupp and R. Q. Snurr, *Energy Environ Sci*, 2012, **5**, 9849-9856.

58.   C. E. Wilmer, M. Leaf, C. Y. Lee, O. K. Farha, B. G. Hauser, J. T. Hupp and R. Q. Snurr, *Nat. Chem.*, 2012, **4**, 83-89.

59.   D. Farrusseng, C. Daniel, C. Gaudillere, U. Ravon, Y. Schuurman, C. Mirodatos, D. Dubbeldam, H. Frost and R. Q. Snurr, *Langmuir*, 2009, **25**, 7383-7388.

60. D. Wu, Q. Yang, C. Zhong, D. Liu, H. Huang, W. Zhang and G. Maurin, *Langmuir*, 2012, **28**, 12094-12099.

61. R. Vaidhyanathan, S. S. Iremonger, G. K. Shimizu, P. G. Boyd, S. Alavi and T. K. Woo, *Angew. Chem. Int. Ed.*, 2012, **51**, 1826-1829.

62. N. S. Suraweera, R. Xiong, J. Luna, D. M. Nicholson and D. J. Keffer, *Mol. Simul.*, 2011, **37**, 621-639.

63. S. O. Odoh, C. J. Cramer, D. G. Truhlar and L. Gagliardi, *Chem. Rev.*, 2015, **115**, 6051-6111.

64. Q. Yang, D. Liu, C. Zhong and J.-R. Li, *Chem. Rev.*, 2013, **113**, 8261-8323.

65. S. T. Meek, J. A. Greathouse and M. D. Allendorf, *Adv. Mater.*, 2011, **23**, 249-267.

66. S. Keskin, J. Liu, R. B. Rankin, J. K. Johnson and D. S. Sholl, *Ind. Eng. Chem. Res.*, 2008, **48**, 2355-2371.

Chapter 2: Computational Chemistry

2.1 Introduction

In recent years, a variety of computational chemistry methods have contributed significantly in investigating and modelling many chemical systems, ranging from diatomic molecules to more complex systems such as MOFs and proteins. Simple diatomic molecules require merely a very high level of theory to model the structure and energies accurately, whereas for much more complicated structures such as transition metal (TM) systems, more approximate methods must be applied.

This work considers MOFs systems where the more complicated electronic structures of TM centres are present. Quantum mechanical (QM) approaches, are relatively compute intensive and are impractical for dynamics simulations of large systems which can require hundreds of thousands of energy and/or force evaluations. Density functional theory (DFT) is efficient and gives a satisfactory results for a wide range of TM systems. However, for large (i.e. many atoms and periodic boundaries) systems such as MOFs, DFT is also too expensive, especially if dynamical properties are of interest. The alternative faster approach is to use empirical methods, such as molecular mechanics (MM). However, conventional MM is not appropriate for TM systems, so Deeth *et al*, have contributed successfully to make MM smarter and more applicable to TM systems by proposing the Ligand Field Molecular Mechanics (LFMM) approach.[1] More details regarding LFMM will be provided in the following sections.

The earlier introduction chapter has dealt briefly with MOFs, including applications, design, characterization, and some computational studies on MOFs systems. This

chapter will describe the theoretical methods that have been considered specifically within this work, including quantum mechanics (QM), molecular mechanics (MM), and molecular dynamics (MD) approaches.

2.2 Quantum Mechanics (QM)

In 1900, Max Planck [2] proposed that the radiation emitted by black bodies is quantised with limited discrete value. By the early days of the twentieth century, the idea of quantisation was extended by various scientists to cover not only a characteristic of light but also many others aspects of physical and chemical theories. One of the most significant example is Rutherford -Bohr model of atom which is based on the Max Plank's solution. This model was accurately indicate the emission spectra of the Hydrogen atom which proved that the energy levels of electrons are quantised. These theories are in opposition to classical mechanics view (Newtonian physics) where levels of energy can be vary continuously. Therefore, developing a new kind of mechanics to describe microscopic systems was crucial. The possible alternative solution was based on wave mechanics as standing waves are also a quantised phenomenon. However, accounting the properties of a chemical systems required an advanced new approach. Therefore quantum mechanics theory have been developed and expanded analogous with the developing of computer science in last four decades.

2.2.1 The Schrödinger equation and Born-Oppenheimer Approximation

The Wavefunction, Ψ, is one of the most important physical fundamentals of quantum mechanics which exists for any chemical system. Applying appropriate operators to Ψ gives expectation values of a given physical observable. The Hamiltonian operator, $\hat{H}$, is the most common operator used in quantum mechanics which is applied to Ψ to give the total energy, E, of a chemical system. Equation 2.1 represents the time-independent Schrödinger equation which provides a starting point for *ab initio* methods used in computational chemistry,

$$\hat{H}\Psi = E\Psi. \tag{2.1}$$

The Hamiltonian operator for nuclei (N) and electrons (n) consists of five contributions to the total energy of a system; the kinetic energy of the electrons, T_e, and neutrons, T_n, the interelectron repulsion, V_{ee}, the internuclear repulsion, V_{nn}, and the electrostatic attraction between electrons and the nuclei, V_{en} (Eq. 2.2). Therefore, the Hamiltonian operator is comprised of two parts for describing the kinetic energy T and the potential energy V as shown in Equation 2.1,

$$\hat{H} = T_e + T_n + V_{ee} + V_{nn} + V_{en}. \tag{2.2}$$

Calculating the properties of a molecule using a quantum mechanics method is essentially obtained from the interactions between nuclei and electrons. However, the

mass of a proton in a nucleus equal about 1800 times greater than that of an electron. Therefore, nuclei are much heavier than electrons and their velocity are much more slowly. Consequently, it is possible to treat electrons quantum mechanically and nuclei as fixed classical points. This is known as the Born-Oppenheimer approximation where the nuclei are assumed to be stationary and, therefore, the kinetic energy of the neutrons, T_n, must be zero.[3] Therefore, by applying the Born-Oppenheimer approximation, the Hamiltonion operator should be written as,

$$\hat{H} = T_e + V_{ee} + V_{nn} + V_{en}. \tag{2.3}$$

The Schrödinger Equation (Eq. 2.1) provides exactly a solution of a one-electron system such as Hydrogen. Others theories and solutions to the Schrödinger equation have been developed in last century considering the solutions of multi electrons systems.

2.2.2 Hartree-Fock (HF) Theory

Hartree-Fock (HF) theory is the basis of several *ab initio* computational chemistry methods.[2] It is generally based on a number of approximations to solve the Schrödinger equation for systems possessing more than one electron. The first employed approximation, is the Born-Oppenheimer approximation which separates the motion of nuclear and electron, and, therefore, considers the nuclei to be clamped and the electronic wavefunction is obtained quantum mechanically. In consequence, the Hamiltonian being separated into two parts; the nuclear part which contains merely the

nuclear-nuclear repulsion and an electronic part. The electronic Schrödinger Equation (Eq.2.3) can be separated into one-electron terms and two-electron terms. The former consists of electron kinetic energy and electron-nuclear attraction terms, and the later contains the electron-electron repulsion term. In order to obtain the correct asymmetrical behavior of the wavefunction, the orbitals are arranged within a single Slater determinant of n spin orbitals as shown in,

$$\psi\,(1,2,...,n) = \left(\frac{1}{\sqrt{n\,!}}\right) \begin{vmatrix} \varphi_1\,(1) & \varphi_2\,(1) & \cdots & \varphi_n\,(1) \\ \varphi_1\,(2) & \varphi_2\,(2) & \cdots & \varphi_n\,(2) \\ \vdots & \vdots & \ddots & \vdots \\ \varphi_1\,(n) & \varphi_2\,(n) & \cdots & \varphi_n\,(n) \end{vmatrix} \tag{2.4}$$

In Eq.2.4, the number of electrons in the system and the spin of orbitals are represented by n and ϕ_n respectively. In the HF method, adjusting the coefficients of the atomic orbitals (AOs) within the limitations imposed by a selected basis set and a single determinant approximation should lead to a minimum energy. However, the variational principle states that any trial wavefunction will have an energy expectation value equal to or higher than the true ground state wavefunction corresponding to the selected Hamiltonian. Therefore, the energy of the true ground state is lower than the HF energy of a computed molecule. In addition, the single determinant approximation considers only one electronic configuration and ignores computing the electronic correlation energy. Thus, the HF approximation is insufficient for computing an electronic state accurately, especially for transition metal (TM) systems, and lead to large differences from experimental results.

A number of methods have been developed to capture this weakness and account the electron correlation energy of a given system. These are collectively referred as post Hartree-Fock methods which includes theories such as configuration interaction (Cl), coupled cluster (CC), Møller–Plesset perturbation theory (MP2, MP3, MP4...), and multi-configurational self-consistent field (MCSCF). However, these methods are computationally expensive particularly for TM systems where a large number of electrons exist, resulting in a significant correlation energy. Additionally, these methods limited the size of system as the wavefunction depends on four variables for each electron; three spatial variables and one spin variable. Table 2.1 shows how the computational expense of different quantum mechanics methods scale, in terms of computational cost, depending on the number of electrons n.

Table 2.1; Scaling of different QM methods with respect to the number of electrons n.

Method	Scaling factor
DFT	n^3
HF	n^4
MP2	n^5
CCSD	n^6
CCSD(T)	n^7
MP4	n^8

Table 2.1 shows why methods that scale more favorably with systems size, such as density functional theory (DFT), have become more popular and attractive in last decades. In this work all the quantum mechanics calculations have been done using DFT. Therefore, the following section will consider DFT, including some developed approximations associated with it, such as the local density approximation [4] and the gradient corrected approximation (GGA).[2]

2.2.3 Density Functional Theory (DFT)

DFT and HF approaches are both considered as independent particle models. However, DFT considers the correlation of one electron against the electron density, whereas HF considers the correlation of one electron against an average potential of all electrons interactions within a given system in purpose of obtaining the correlation energy. Therefore, for large systems, such as transition metal systems, HF method fails to account correctly for electron correlation. For this reason DFT has become more attractive especially for a large systems such as TM-based solids and MOFs which contains many atoms and electrons.

DFT is based on the Hohenberg-Kohn theorem [5] which states that the ground state density, $\rho(r)$, of a system of interacting electrons in an external field, $V(r)$, defines the ground state energy uniquely. Unlike others quantum mechanics methods where the many-body electron wavefunction depends on 4N variables for each electron, in DFT method, the electron density depends only on a function of three variables regardless of the number of electron in the system. Therefore, the energy of the electronic ground state, $E[\rho]$, can be expressed as a functional of the density, ρ, where T represents the

kinetic energy of the system, and V describes the external potential acting on the system,

$$E[\rho] = T[\rho] + V_{en}[\rho] + V_{ee}[\rho]. \tag{2.5}$$

In addition, under the Born-Oppenheimer approximation the interactions between nuclei is constant which can be added later. $T[\rho]$ is the kinetic energy, $V_{en}[\rho]$ is the nucleus-electron potential energy, and $V_{ee}[\rho]$ is electron-electron potential energy. The latter can be divided into two contributions, the coulomb energy, $J[\rho]$, and the exchange-correlation function, $E_{xc}[\rho]$,

$$E[\rho] = T[\rho] + V_{en}[\rho] + J[\rho] + E_{xc}[\rho]. \tag{2.6}$$

However, the nucleus-electron potential energy function, is known exactly, whereas the kinetic energy function and the exchange function, are unknown. Moreover, the unknown terms are not so easily derived. Equation (2.6) is known as Thomas-Ferim-Dirac (TFD) model, which is consider as one of earliest approximations to derive the kinetic energy. However, this approximation is based on deriving the kinetic energy using the free uniform electron gas which means the orbitals and the bonding between molecules are not considered. This leads to a very poor representation of the kinetic energy.

The alternative modern DFT approximation is based on the work of Kohn-Sham (KS)[6] where orbitals used to describe the electron density. In this approximation the

electrons are treated as non-interacting electron with the same density and, therefore, the kinetic energy can be described in terms of a Slater determinant of molecular orbitals, ϕ_i,

$$T_S[\rho] = \sum_i^N \left\langle \phi_i \left| -\frac{1}{2}\nabla^2 \right| \phi_i \right\rangle.$$

(2.7)

This can provide a correct solution to the Schrödinger equation and gives the exact kinetic energy functional which depends merely on the density. However, this approach requires the exact density which is not known. Therefore, the ground state electron density can be represented by a set of one-electron spatial orbitals (Equation 2.8)

$$\rho(r) = \sum_i^n \left| \phi_i(r) \right|^2.$$

(2.8)

Although this approach does not give an absolute answer, it is considered as one of most useful methods in modern quantum chemistry. The remaining kinetic energy along with the exchange function is incorporated into the exchange-correlation function and the Kohn-Sham DFT energy can be represented as,

$$E[\rho] = T_s[\rho] + V_{en}[\rho] + J[\rho] + E_{xc}[\rho].$$

(2.9)

Expanding the orbitals terms, $\phi_!$, for a one electron basis set leads to solution of the Kohn-Sham equations in a self-consistent manner to yield the optimum set of orbitals and hence the optimal electron density,

$$\left[-\frac{1}{2}\nabla^2 + V_{en}(r_1) + \int \frac{\rho(r_2)}{|r_1 - r_2|} dr_2 + V_{xc}(r_1) \right] \phi_!(r_1) = \in_! \phi_!(r_1).$$
(2.10)

The challenge of the above equation is to find the exact functional form of the exchange-correlation energy which in principle would give the exact energy from DFT. However, E_{xc} is usually approximated and a number of different methods to account the exchange-correlation functional are developed and will be explained briefly in the following sections.

2.2.4 The Local Density Approximation

The local density approximation is the simplest methods for approximating the exchange-correlation energy, E_{xc}. This method assumes that E_{xc} can be expressed in a terms of uniform electron gas based on the density $\rho(r)$ at a given point in the system (Equation 2.11).

$$E_{XC} = \int \rho(r) \varepsilon_{xc}(\rho(r)) dr.$$
(2.11)

The ε_{xc} (ρ(r)) represents the exchange-correlation energy associated with an electron in a uniform electron gas of density ρ(r). The exchange contribution of a uniform electron gas is given by the Dirac formula,

$$\varepsilon_x^{LDA} = -\frac{3}{4}\sqrt[3]{\frac{3\rho(r)}{\pi}} \, .$$

(2.12)

Additionally, the correlation energy functional has been interpolated analytically by schemes developed by Vosko, Wilk, and Nusair.[7] Although the LDA approximation gives reasonable results in calculating geometries and vibrational frequencies, it gives large errors in energies. The reason behind this is the lack of the exchange and correlation energy estimations which can be corrected by implementing the generalized gradient approximation.

2.2.5 The generalized gradient approximation

The generalized gradient approximation (GGA) can be implemented to improve upon LDA. In fact, the true electron density of a system is not a homogeneous electron gas which requires a realistic method to describe the exchange-correlation energy correctly. Therefore, the inhomogeneity of the electron density can be accounted for by including its gradient, which leads to significant improvements over LDA.

In the GGA approximation the exchange and correlation terms are treated separately and the exchange energy can be written as,

$$E_X^{GGA} = E_X^{LDA} - \sum_\sigma \int F(s_\sigma) \rho_\sigma^{4/3}(r) dr \ . \tag{2.13}$$

F represents the exchange functional which can take a range of functional forms, including those with empirical parameters such as Becke's functional.[8] Moreover, S_σ represents the reduced density gradient which can be described by the equation below (Equation 2.14).

$$S_\sigma = \frac{|\nabla \rho_\sigma(r)|}{\rho_\sigma^{4/3}(r)} \ . \tag{2.14}$$

Despite that the quantum mechanical (QM) approaches give an accurate and satisfactory results for a wide range of transition metal systems, they are impractical for dynamics simulations of flexible MOFs systems. The alternative is to consider fully atomistic molecular mechanics/ molecular dynamics (MM/MD) simulations. Therefore, the following sections will consider a theoretical background of both molecular mechanics and molecular dynamics approaches used in this work.

2.3 Molecular Mechanics (MM)

In the Molecular Mechanics (MM) approach a system is treated classically as a collection of weights connected to each other by springs that obey simple mathematical rules such as Hooke's law. In this method, the positions of the atoms of a chemical system are determined by forces between them, including bonded and non-bonded terms. The total energies obtained from these forces are linked to the positions of the nuclei in the system leading to enforce the entire molecular structure. However, using MM treatment for specific systems requires a suitable and flexible force field (FF). The FF is set of functions parameterized by terms such as the force constant, the ideal bond length, the ideal bond angle, etc. The values of these terms can be obtained either experimentally or theoretically, using spectroscopy data like the infrared spectrum or QM methods, respectively. Once a force field has been chosen for a particular system, the MM local optimization would be able to find the optimized geometry of that system.
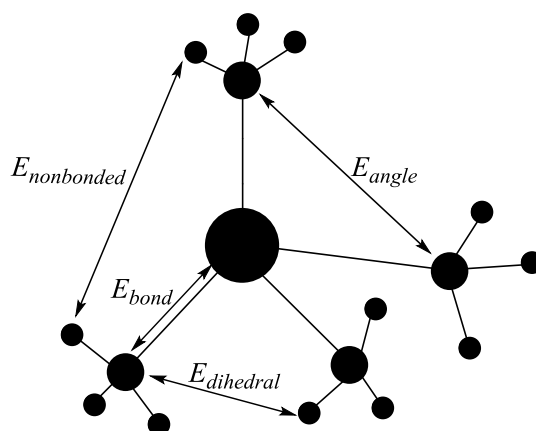
Figure 2.1; The model of molecular mechanics.

According to Comba et al,[9] the conventional molecular mechanics method defines the strain energy U_{total} that generally arises from the total bond deformation energy ($\sum E_b$), the total bond angle bending energy, ($\sum E_\theta$), the total dihedral angle energy ($\sum E_\phi$), and the total nonbonded energy ($\sum E_{nb}$) consisting of van der Waals (vdW) and electrostatic interactions (Equation 2.15).

$$U_{total} = \sum E_b \ + \sum E_\theta + \sum E_\phi + \sum E_{nb} \tag{2.15}$$

Each energy term is calculated mathematically using simple functions such as there shown below in equations 2.16 – 2.20,

$$E_b = \frac{1}{2} k_b \, (r_{ij} - r_0)^2 \tag{2.16}$$

where k_b is the force constant and r_0 is the ideal bond length. Similar way can be used to model valence angles,

$$E_\theta = \frac{1}{2} k_\theta \, (\theta_{ijk} - \theta_0)^2 \tag{2.17}$$

where k_θ is the strength of holding the angle at θ_0 which represents the angle ideal value. However, since a periodic function is required to model dihedral angles, the E_ϕ can be defined as,

$$E_\phi = \frac{1}{2} k_\phi (1 + cos \, (m \, (\phi_{ijkl} + \phi_{offset}))) \tag{2.18}$$

where k_ϕ is the strength barrier value to rotate about ϕ_{ijkl} which is the torsion angle. ϕ_{offset} presents the offset of the lowest energy from a staggered arrangement. The non-bonded interactions, E_{nb}, are calculated based on a function that includes an attractive and repulsion components,

$$E_{nb} = Ae^{-Bdij} - C\,d_{ij}{}^{-6} \tag{2.19}$$

where d_{ij} represents the distance between the two nuclei, and A, B, and C are constant values based on Lennard-Jones vdW parameters.

In addition, Comba et al states that a number of energy terms can be added to the potential energy expression such as out – of – plane deformation E_δ and electrostatic interactions $E\varepsilon$ to model aromatic or sp² hybridized systems and the interaction of metal complexes with biological systems respectively. The E_δ function can be expressed as,

$$E_\delta = \frac{1}{2}\,k_\delta\,\delta^2 \tag{2.20}$$

Where k_δ is the force constant and δ is the angle between the centre of plane of three atoms bonded to a fourth atom. The electrostatic interactions are based on Coulomb law and expressed as,

$$E\varepsilon = q_i\,q_j\,/\,\varepsilon\,d_{ij} \tag{2.21}$$

where ε is dielectric constant, d_{ij} is the interatomic separation, and q_i q_j are the partial charges on i and j atoms.

Combined with a suitable empirical parameters, these potential energy terms define the force field (FF). However, some complicated FFs are based on more complex functional forms than the harmonic oscillator expression for bond length deformation. This function can be replaced by simpler function such as a Morse function, E_{Morse}, for describing bond stretching (Equation 2.22).[10] Additionally, some FFs add terms for better describing conformational and vibrations energies. For example, the Merck molecular force field (MMFF) which used the stretch-bend cross terms, E_{stb} (Equation 2.23).[11]

$$E_{Morse} = D\left[1 - e^{a(r-r_0)}\right]^2 - D \tag{2.22}$$

$$E_{stb} = \sum_{i,j,k}\left\{k_{ijk}(r_{ij} - r_{0,ij}) + k_{kji}(r_{jk} - r_{0,jk})\right\}\theta_{0,ijk} \tag{2.23}$$

Molecular mechanics model (Equation 2.15) is very successful and used widely these days. However, it sometimes requires a very large number of parameters to obtain a suitable FF for a specific type of a chemical system, particularly TM systems. Therefore, developing a truly comprehensive FF has become an enormous challenge for computational chemists in the last two decades. Nevertheless, there are some well-known force field which have been proposed especially for studying a small organic

molecules, such as MMFF [12-14], and for large biomolecules like DNA and proteins, such as AMBER [15] and CHARMM [16]. Fortunately, these force field can be revised to increase their applicability and cover more chemical systems, including TM systems.

2.3.1 Shortcomings of MM for TM systems

The conventional MM method has been used widely in carbon chemistry which has only three common geometries; liner, trigonal planar, and tetrahedral, and each of these geometries has associated with 180°, 120°, and 109.5^o single valence angle respectively. However, a rich diversity of geometry structures, coordination numbers, oxidation states, spin states, and electronic effects such as Jahn-Teller distortions associated with TM systems cannot easily be accommodated by the conventional MM method. The reason of that is the difficulty of identifying the angular geometry at the metal centre where each angle-bend has a different reference value. For example, the trigonal bipyramidal and the octahedral coordination symmetries, associated often with TM systems, have multiple reference angles for the same A-M-A set (Figure 2.2).
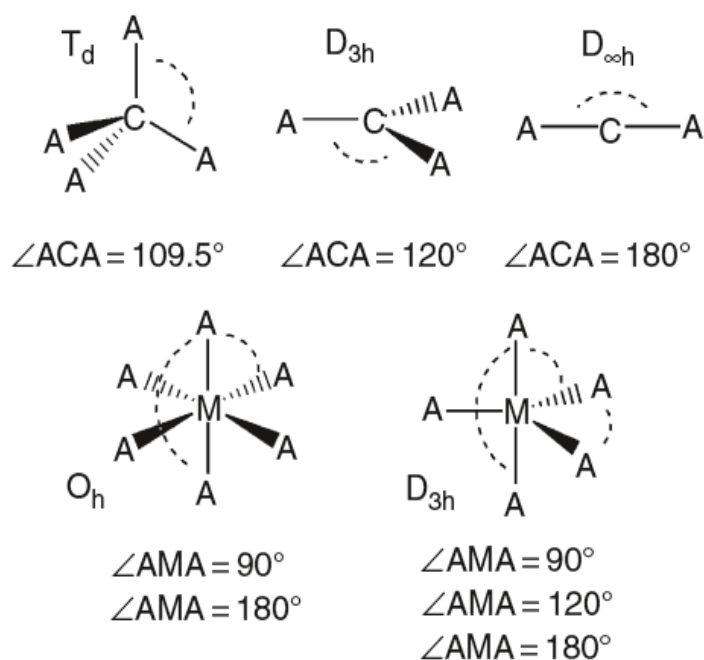
Figure 2.2; Angles bending of central atom for different common geometries.

However, a number of ingenious MM methods have been created to capture the angular geometry of metals centres in coordination compounds such as SHAPES [17] and VALBOND [18]. MOMEC is another ingenious approach proposed by Comba et al.[8] It deals with the angle bending of coordination compounds by employing the ligand-ligand repulsion method analogous to points on a sphere (POS).[19] Consequently, the reference θ_0 values are not required. Deeth et al.[20] have followed this approach and contributed successfully in solving this issue by the implementation of the ligand field molecular mechanics (LFMM) model within molecular operating environment (MOE). [21] MOE is a software package possessing a range of force fields which are particularly designed for the treatment of biomolecular chemistry and drug discovery. The implementation of LFMM model within MOE has proposed an extended version of MOE software which was christened DommiMOE. This software

has proven its ability to represent the angular geometries around the metal centres correctly, and gives an accurate value of the strain energy for various TM complexes. Since this work considers zinc (Zn^{+2}) and copper (Cu^{+2}) containing MOF systems, all the MM calculation are based on the LFMM method. Therefore, the following section will provide a detailed description of LFMM method.

2.3.2 Ligand Field Molecular Mechanics

Ligand field molecular mechanics (LFMM) approach is considered as one of the most effective solutions for the d-orbital effect problems. The LFMM model incorporates the ligand field stabilization energy (LFSE) directly into the potential energy expression of conventional MM,

$$U_{total} = \sum E_b + \sum E_\theta + \sum E_\phi + \sum E_{nb} + LFSE. \qquad (2.24)$$

This approach uses the concept of LFSE to account for d-electrons effects, which have a significant impact on reactivity and structure of TM complexes. For example, the effect of the LFSE was proven by the experimental hydration enthalpies for hexaaqua complexes of divalent first row metal ions (Figure 2.3).[22] The typical "double hump" behaviour shown in figure 2.3 is usually rationalized in terms of the LFSE function which can provide the d configuration and the magnitude values of the ligand field splitting, Δ_{oct} (Figure 2.4). However, these values can be corrected experimentally using the spectroscopic Δ_{oct} data giving a remarkably smooth line as shown in figure 2.3 (open circles).
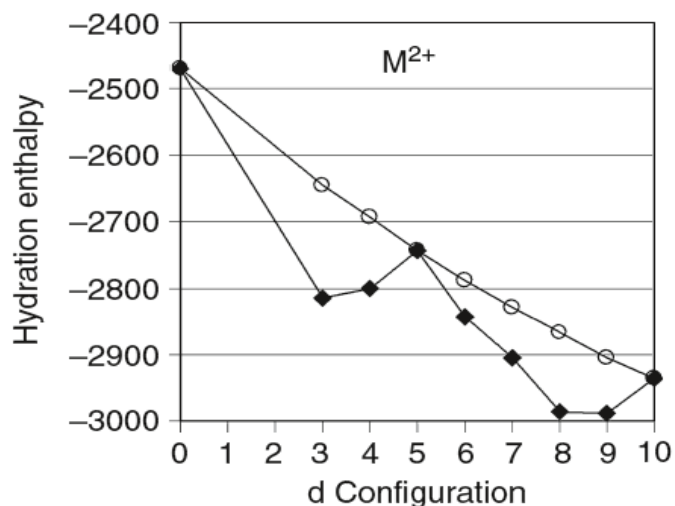
Figure 2.3; Experimental hydration enthalpies values from Ca^{2+} (d^0) through to Zn^{2+} (d^{10}). The open circles expressed the values once the effects of LFSE are removed.
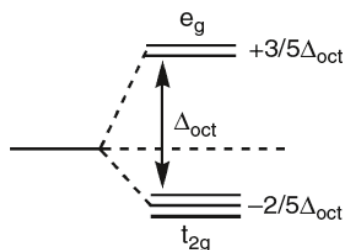
Figure 2.4; Octahedral (O_h) d-orbital splitting diagram.

Therefore, to accurately represent the experimental data for TM systems using computational methods, the LFSE must be correctly accounted for. This is not a problem for QM methods as the d-electron effects are treated implicitly, but in MM methods the LFSE value must be added explicitly. For over half a century, the ligand field theory (LFT) is considered as the simplest general model to describe d-orbital energies. Although there are some limitations in computing the properties of

coordination complexes, the LFT has provided a useful picture of metal-ligand bonding in such complexes. Therefore, Deeth et al, have added the LFT model to the conventional MM to propose the ligand field molecular mechanics (LFMM) approach.[1]

The angular overlap model (AOM) of Schaeffer and Jorgensen [23] is used within LFMM to capture the LFSE. This model is a bond centred approach and assumes the total ligand field potential, V_{LF}, to be the sum of the M-L bonds contributions. Each bond can be modelled individually by AOM parameters which can be derived from spectroscopic data of the d-d splitting or theoretical studies to describe separate σ and π interactions as shown in the figure 2.5 below.
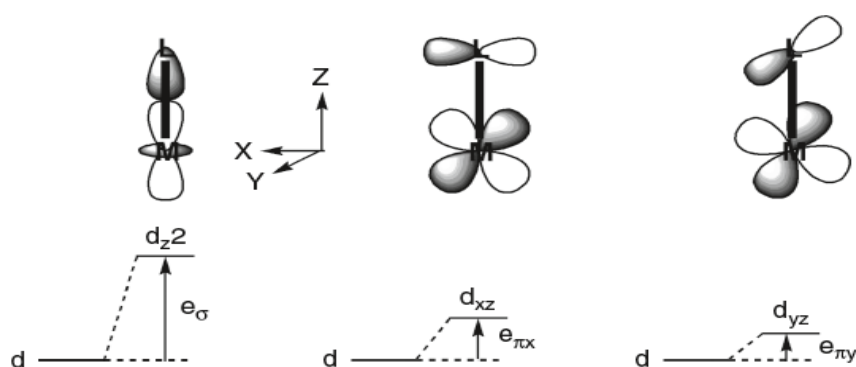
Figure 2.5; Introduction of AOM parameters of local M-L bonding showing the differences between σ and π   interactions.

Using the AOM within LFMM has provided a more physical realistic description of the M-L bond. Additionally, this model is superior to crystal field theory (CFT) since it can represent all the appropriate symmetry behaviour and allows us to treat each ligand individually. Therefore, in general, the d-orbital energies are a function of all

the ligands regardless their symmetries. For example, in high-symmetry geometry such as the octahedral, O_h, the splitting Δ_{oct} is expressed by equation 2.20, and illustrated for more clarity in Figure 2.6.

$$\Delta_{oct} = 3e_\sigma - 4e_\pi \tag{2.20}$$
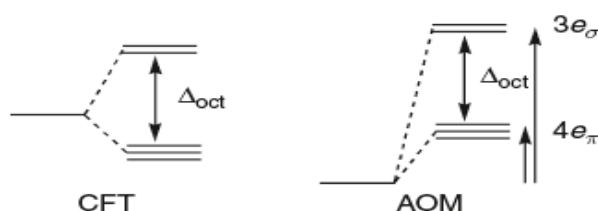
Figure 2.6; Comparison between CFT barycentre (left) and AOM barycentre (right) in case of a π-donor ligand where e_π is positive.

Furthermore, LFMM requires additional parameters over conventional MM to be applicable to TM complexes. The conventional MM is mainly responsible for computing organic parts, and the LFSE for the metal centre is treated by AOM approach (Figure 2.7). Since the LFSE is only computed for the d electrons effects, the M-L stretching and L-M-L angle bending terms must be included in the force field. Therefore, Deeth et al, have followed Comba et al, and used the Morse function and the ligand-ligand POS terms to describe the M-L stretching and L-M-L angle bending respectively. However, unlike Comba's MM/AOM method,[24] the LFMM method includes the LFSE contribution directly into the MM calculations to determine the structure and energy. Therefore, the LFMM method can be applied in TM systems to mimic more expensive QM methods or even experimental data.
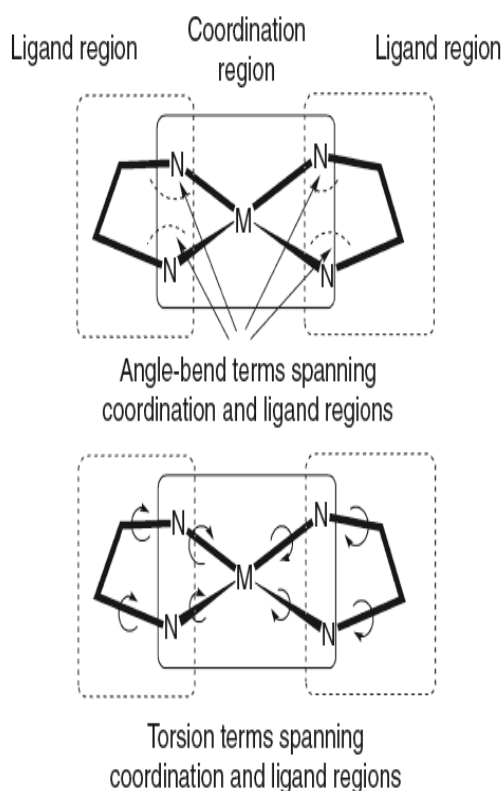
Figure 2.7; Schematic representation of ligand and coordination regions and force field terms which represent them.

2.4 Molecular Dynamics

Based on the computational efficiency of a FF approach, studying the dynamical behaviour of MOF systems, using molecular dynamic (MD) approach, is more applicable and flexible. On the other hand, ab inito molecular dynamics (AIMD) is also possible and has been applied for some dynamical studies of MOF systems and an impressive agreement with experiment data was obtained with a short simulation times of only a few ps.[25] Classical methods such as grand canonical Monte Carlo (GCMC) have been widely employed to model the thermodynamics of adsorbate-MOF interactions[26, 27] but these generally assume a fixed framework which may be

inappropriate in the case of flexible MOFs. However, modelling very large flexible systems for a long time, or carrying out virtual high throughput screening remains the province of classical simulation techniques.

In MD, the motion for a system of N atoms are described by the classical equation called the Newton equation. Under a specific thermodynamic conditions, such as constant temperature and/or constant pressure, a trajectory of a reaction can be generated. The trajectory can provide a crucial thermodynamic properties information for each atom which, for example, may contribute in calculating the free energy or diffusion coefficients properties. However, the MD is time-dependent approach and requires very short time (~ 1 fs) to avoid numerical instability which leads to strong limitations on the total simulation time. Nevertheless, classical MD is still the valuable approach to compute the dynamical behaviour of large systems, whether flexible or not, such as MOF and biomolecules systems for any appreciable length of time.

2.5 References

1. R. J. Deeth, *Coord. Chem. Rev.*, 2001, **212**, 11-34.

2. C. J. Cramer, *Essentials of computational chemistry: theories and models*, John Wiley & Sons, 2013.

3. M. Born and R. Oppenheimer, *Annalen der Physik*, 1927, **389**, 457-484.

4. D. Farrusseng, C. Daniel, C. Gaudillere, U. Ravon, Y. Schuurman, C. Mirodatos, D. Dubbeldam, H. Frost and R. Q. Snurr, *Langmuir*, 2009, **25**, 7383-7388.

5. P. Hohenberg and W. Kohn, *Phys. Rev.*, 1964, **136**, B864.

6. W. Kohn and L. J. Sham, *Phys. Rev.*, 1965, **140**, A1133.

7. S. H. Vosko, L. Wilk and M. Nusair, *Can. J. Phys.*, 1980, **58**, 1200-1211.

8. A. D. Becke, *Phys. Rev. A*, 1988, **38**, 3098.

9. P. Comba, T. W. Hambley and B. Martin, *Molecular modeling of inorganic compounds*, John Wiley & Sons, 2009.

10. P. E. Siegbahn and M. R. Blomberg, *Chem. Rev.*, 2000, **100**, 421-438.

11. V. J. Burton, R. J. Deeth, C. M. Kemp and P. J. Gilbert, *J. Am. Chem. Soc.*, 1995, **117**, 8407-8415.

12. T. A. Halgren, *J. Comput. Chem.*, 1996, **17**, 490-519.

13. T. A. Halgren, *J. Comput. Chem.*, 1996, **17**, 520-552.

14. T. A. Halgren, *J. Comput. Chem.*, 1996, **17**, 553-586.

15. D. A. Pearlman, D. A. Case, J. W. Caldwell, W. S. Ross, T. E. Cheatham, S. DeBolt, D. Ferguson, G. Seibel and P. Kollman, *Comput. Phys. Commun.*, 1995, **91**, 1-41.

16. B. R. Brooks, R. E. Bruccoleri, B. D. Olafson, D. J. States, S. Swaminathan and M. Karplus, *J. Comput. Chem.*, 1983, **4**, 187-217.

17. V. S. Allured, C. M. Kelly and C. R. Landis, *J. Am. Chem. Soc.*, 1991, **113**, 1-12.

18. T. K. Firman and C. R. Landis, *J. Am. Chem. Soc.*, 2001, **123**, 11728-11742.

19. D. L. Kepert, *Inorganic stereochemistry*, Springer Science & Business Media, 2012.

20. R. J. Deeth, N. Fey and B. Williams–Hubbard, *J. Comput. Chem.*, 2005, **26**, 123-130.

21. M. Moe, *Quebec: Montreal*, 2006.

22. D. A. Johnson and P. G. Nelson, *Inorg. Chem.*, 1995, **34**, 5666-5671.

23. C. E. Schäffer and C. K. Jørgensen, *Mol. Phys.*, 1965, **9**, 401-412.

24. P. Comba, T. W. Hambley, M. A. Hitchman and H. Stratemeier, *Inorg. Chem.*, 1995, **34**, 3903-3911.

25. L. Chen, J. P. Mowat, D. Fairen-Jimenez, C. A. Morrison, S. P. Thompson, P. A. Wright and T. Düren, *J. Am. Chem. Soc.*, 2013, **135**, 15763-15773.

26. J. A. Gee and D. S. Sholl, *J. Phys. Chem. C*, 2015, **119**, 16920-16926.

27. H. Wu, J. M. Simmons, Y. Liu, C. M. Brown, X. S. Wang, S. Ma, V. K. Peterson, P. D. Southon, C. J. Kepert and H. C. Zhou, *Chem. Eur. J.*, 2010, **16**, 5205-5214.

Chapter 3: Molecular Modelling of Zinc Paddlewheel Molecular Complexes and the Pores of a Flexible Metal Organic Framework

3.1 Introduction

Metal organic frameworks (MOFs) are porous materials with a remarkable range of potential applications.[1-3] The framework comprises combinations of secondary building units (SBUs) connected by linkers which can generate a remarkable array of 3-dimensional networks. The SBUs are transition metal complexes or clusters while the linkers are typically organic carboxylates often in combination with polytopic nitrogen-donor 'pillar' ligands such as, for example, 1,4-diazabicyclo(2.2.2)octane (dabco) or pyrazine.

While many MOFs have relatively rigid frameworks which therefore define a fixed pore size, other MOFs display a degree of flexibility or 'breathing'.[4, 5] The pore size and/or shape changes as a function of adsorbate offering exciting possibilities for using these materials in separations [6-9] and sensing.[10, 11]

Some flexible MOFs contain a paddle-wheel SBU. The paddle-wheel motif is a TM dimer bridged by three or four carboxylate units. In combination with linear linkers, the latter generates planar $[M_2L_2]_n$ grids which can be interconnected by ditopic pillars like dabco to generate a 3-D framework. The classic example is the MOF $[Zn_2(bdc)_2(dabco)]_n$ (bdc = 1,4-benzenedicarboxylate) which displays a remarkable degree of flexibility depending on the adsorbate.[12]

As synthesized, the $[Zn_2(bdc)_2(dabco)]_n$ pore contains one water and four dimethylformamide (DMF) molecules. The framework-adsorbate interactions lead to a pronounced bending deformation of the pore bdc edges (Figure 3.1, left) but this disappears on evacuation leaving a more regular cuboidal pore (Figure 3.1, middle) which further distorts (and contracts) to a rhombohedral structure upon adsorption of benzene (Figure 3.1, right).


DMF/WATER   **EMPTY**   **BENZENE**
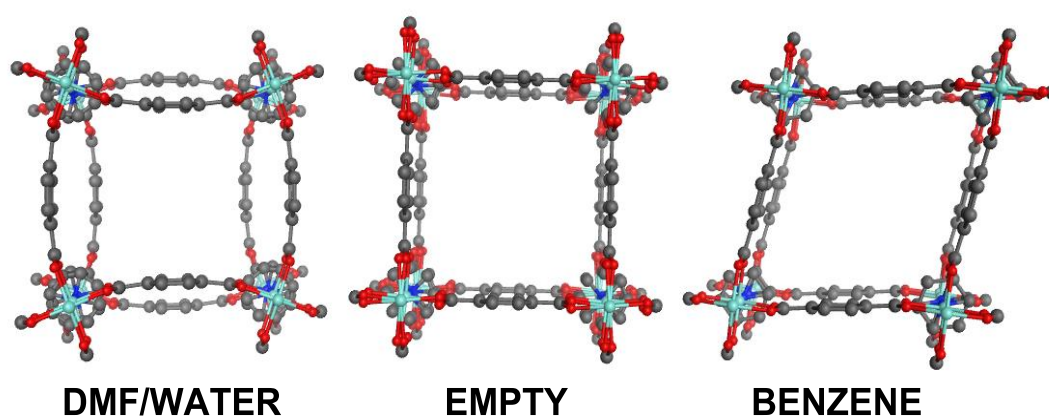
Figure 3.1; Pore framework structures for $[Zn_2(bdc)_2(dabco)]_n$ derived from published CIF files.[12] Hydrogens and encapsulated solvent removed. dabco and carboxylate disorder as per CIF file.

Computer modeling of MOFs can provide important atomic level insights into their structures and properties but the structural changes of the type shown in Figure 3.1 are computationally challenging and demand a sophisticated theoretical method.[13] As explained in Chapter 2, quantum chemical (QC) approaches such as density functional theory (DFT) are fairly general, reasonably accurate and give satisfactory results for a wide range of transition-metal systems. However, MOFs are relatively large and QC is computationally expensive, especially if dynamical properties are of interest.[13]

Nevertheless, ab initio molecular dynamics (AIMD) is possible and has been applied, for example, to the breathing of MIL-53(Sc).[14] Despite the short simulation times of only a few ps, impressive agreement with experiment was obtained. Given its general applicability, we can anticipate many more QC and AIMD studies in the future. Meanwhile, modelling very large systems for a long time, or carrying out virtual high throughput screening,[15] remains the province of classical simulation techniques.

Classical methods such as grand canonical Monte Carlo (GCMC) have been widely employed to model the thermodynamics of adsorbate-MOF interactions [16, 17] but these generally assume a fixed framework which may be inappropriate in the case of flexible MOFs. The alternative is to consider fully atomistic molecular mechanics/molecular dynamics (MM/MD) simulations.

The critical feature of MM/MD is the underlying force field (FF). Generic FFs like UFF[18] and Dreiding[19] can be applied to MOFs but their performance may be of limited accuracy.[20] Thus, while a universal force field is attractive, it is also an extremely challenging undertaking and most of the recent FF development targeted at MOF systems has involved so-called 'first principles' parameterization wherein the FF parameters are derived from quantum-chemically-generated training data.[21-23] Bespoke FFs designed for MOFs such as BTW-FF[24], MOF-FF[22] and UFF4MOF[25] should give better accuracy but perhaps at the expense of development time and transferability – i.e., the FF may only work well for the subset of MOFs on which they are trained. In the case of the flexible MOF NH_2-MIL-53(Al), Garcia-Perez et al. even argue[26] that a fully flexible FF is unnecessary and that a combination of rigid FF combined with some judicious experimental work is sufficient to predict adsorption and diffusion of CO_2 and methane through this material.

In our work deriving accurate FFs targeted at specific transition-metal/ligand combinations, we have used both experimental and/or quantum chemical data.[27-35] In this chapter, we focus on a particular class of flexible MOFs which incorporate the four-bladed zinc paddlewheel (ZPW) motif capped by apical N donor and construct a new, specialized valence FF, ZPW-FF, based on molecular ZPW complexes which then automatically captures the types of structural change displayed by $[Zn_2(bdc)_2(dabco)]_n$ as a function of adsorbate. To achieve this, we consider the DFT-calculated chemistry of simple model ZPW systems including those for which there are no experimental data such as the uncapped 'bare' $Zn_2(carboxylate)_4$ unit. The latter has either not been explicitly included in the FF development (BTW-FF [24] and MOF-FF [22]) or the structure employed was not the ground state (UFF4MOF [25]). Our new FF is thus based on a consistent set of theoretical data but is then further refined using the structural chemistry of experimentally characterized, single-ZPW systems to reduce the systematic errors from our chosen DFT protocol. The focus on the local coordination environment of the zinc centers gives the ZPW-FF an unprecedented ability to reproduce subtle variations in bond lengths and bond angles and provides DFT-like accuracy at a small fraction of the computational cost. The good accuracy extends to modelling MOFs and we demonstrate that the structural changes observed for $[Zn_2(bdc)_2(dabco)]_n$ can be successfully reproduced using non-periodic models of its pores. Significantly, the ZPW-FF is based on single ZPW systems so that the subsequent flexibility of the multiple-ZPW pore models emerges as a natural property predicted by ZPW-FF.

3.2 Theoretical methods

All the DFT calculations reported in this chapter used the ORCA suite version 3.0.1.[36] The general protocol employed the Becke-Perdew BP86 functional[37, 38] with Ahlrichs' def2-SVP basis sets.[39] Condensed phase effects[40] were accounted for using the conductor like screening model (COSMO)[41-43] as implemented in ORCA with water as the solvent. Molecular mechanics optimizations used DommiMOE,[44] our extension of the 2011 version of the molecular operating environment (MOE).[45] The as-distributed Merck molecular force field, MMFF94, (mmff94x.ff) was augmented with additional Zn-L-A angle-bending terms and Zn-L-A-B torsional terms. Ligand field molecular mechanics (LFMM) parameters were defined for the zinc coordination.[46] Zn-L interactions were described via Morse functions and the explicit angle bending terms were replaced by a pure ligand-ligand repulsion term of the form A_{LL}/d^n. For these d^{10} Zn^{2+}, there is no ligand field stabilization energy and hence all angular overlap model parameters and spin-pairing terms were set to zero. The MOE and LFMM parameter files and partial-charge-setting scripts are included in the Appendix 1 and are also available from the author upon request.[47] Unless otherwise noted, electrostatic interactions employ a distance-dependent dielectric term with a damped cut-off starting at 8 Å going to zero at 10 Å.

A typical NVT ensemble molecular dynamics annealing protocol was as follows: starting T = 50K; heat to 330K in 10ps, hold for 10ps, and cool to 0 K in 10ps. The Nosé-Poincaré-Andersen algorithm was employed with a 2 fs time step. Bond lengths to H atoms were frozen. A 0.1 fs temperature damping constant was used with configurations sampled every 0.5 ps.

3.3 Results and discussion

A good force field for coordination compounds relies on a diverse set of training data.[48, 49] The previous experience with Cu(II) FFs shows that the inherent 'plasticity' of the Jahn-Teller active d^9 center yields sufficient diversity that an accurate FF can be constructed using structural data derived solely from experimental X-ray diffraction studies.[50] This is not quite the case for ZPW systems which, at first sight, all seem remarkably similar.

The Cambridge Structural Database (CSD) is a rich source of experimental structural data. Our initial searches were restricted to a central ZPW motif such that none of the Zn-O(carboxylate) bonds were coded as 'polymeric'. This search thus excludes the majority of (but not all) ZPW MOFs in favor of compounds with isolated, molecular ZPW units and yielded 77 ZPW structures. The Zn-O(carboxylate) distances do not vary very much and average at 2.04 Å with a standard deviation of ~ 0.03 Å.

Starting with the extremes, the shortest Zn-O(carboxylate) bond length is reported to be 1.88 Å for catena-(tetrakis(μ_6-1,1',1''-(1,3,5-triazine-2,4,6-triyl)tripiperidine-4-carboxylic acid)-hexaaqua-hexa-zinc(II) pyridine dimethyl sulfoxide solvate (CSD refcode WUHHEN)[51]. Although this compound is actually a MOF, the unit cell is sufficiently large to accommodate complete ZPW units and hence pass our test of not having polymeric Zn-O contacts. However, there are a number of anomalous structural features as illustrated in Figure 3.2.
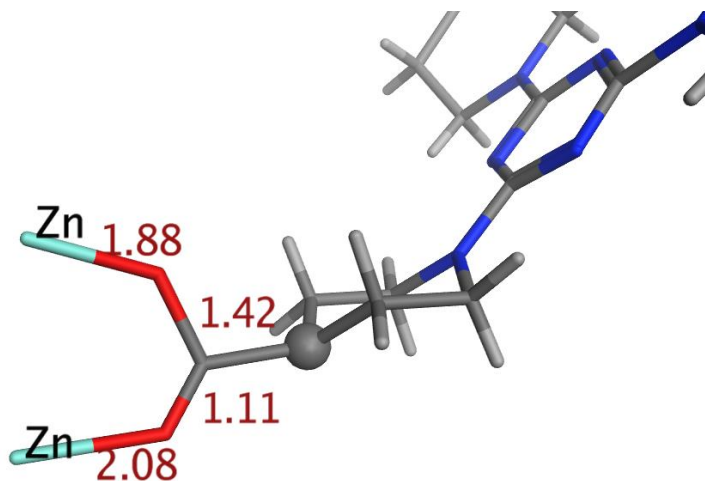
Figure 3.2; Local detail of carboxylate coordination in WUHHEN. Bond lengths (Å) shown in dark red. The upper Zn-O contact is anomalously short, the carboxylate C-O bonds too asymmetric and one hydrogen is missing off the highlighted carbon (grey sphere).

The carboxylates are oddly coordinated, the internal C-O distances are very asymmetric and the hydrogen attached to the adjoining carbon atom is not reported in the CIF file. Given that there is significant disorder of incorporated solvent molecules and the overall R factor for the refinement is relatively high (8.4%), the short Zn-O contact seemed anomalous to us. In any event, this system has water apical ligands and this chapter focuses on apical N donor. The extension of ZPW-FF to apical oxygen donors and the anomalous X-ray structure of WUHHEN will be the subject of chapter 4.

The longest Zn-O (carboxylate) bond length in the set of 2.13 Å in (tetrakis(μ_2-benzoato)-bis(pyridine-4-carbaldehyde oxime)-di-zinc(II) (TUFLOW), has a ready experimental interpretation in terms of the intermolecular H-bond between the carboxylate oxygen and the 4-pyridyl-oxime ligand of a neighboring ZPW complex as highlighted in magenta in Figure 3.3. This example hints at the sensitivity of the ZPW

structure which appears to be relatively easy to distort. This should also provide an exacting test of a force field's ability to model inter-molecular interactions accurately. However, the initial FF development focuses more on intra-molecular interactions.
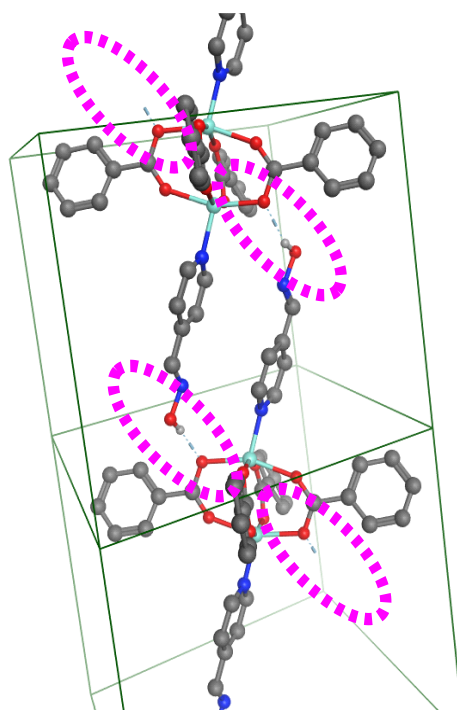

Figure 3.3; Packing detail for TUFLOW showing intermolecular H-bond contacts (dotted magenta oval) responsible for the long Zn-O distance. (The extra connecting molecules top right and bottom left are omitted for clarity as are all the H atoms bar those involved in the H-bond.)

Although the overall metal coordination in ZPW system is invariant – every example in the CSD shows five-coordinate Zn centers – there are some subtle variations which a FF should deal with. Given the geometric constraints of the paddle-wheel motif, the local zinc coordination is approximately square pyramidal, especially with nitrogen in the apical position. However, in the absence of electronic effects, as would be expected here for d^{10} Zn (II) species, five-coordinate complexes should prefer to be trigonal

bipyramidal. In addition, pentacoordinate species are well known to be quite flexible and readily undergo Berry pseudorotations. The zinc sites in ZPWs are thus inherently unstable from a mechanical perspective and this manifests itself is a subtle sensitivity of the ZPW to intra- and inter-molecular interactions.

A number of distortions from a regular ZPW structure can be conceived (Figure 3.4): (i) a twist around the Zn-Zn vector, (ii) a shear of one ZnO_4L unit relative to the other, and (iii) a sliding motion of a pair of trans-related carboxylates parallel to the Zn-Zn vector towards one of the zinc centres while the other two carboxylates move in the opposite direction. This makes both Zn geometries more trigonal bipyramidal.
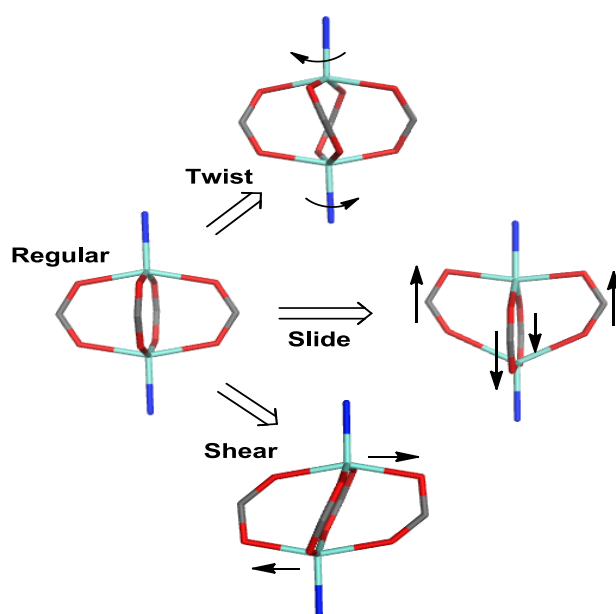
Figure 3.4; Schematic idealizations of possible distortions of a regular zinc paddlewheel structure.

Examples of twisted and sheared structures can readily be found in the CSD data but there are apparently no good experimental examples of a pronounced sliding distortion at least with capping N donor ligands. However, such structures can be generated computationally. DFT is the obvious method and we optimized the structures of a number of ZPW systems both to test the viability of the DFT protocol (BP86/SVP/COSMO(water)) as well as to investigate the source of any apparent distortions in the crystallographic structures. Our choice of functional is based on previous experience[52] plus we note that it was also used for UFF4MOF[25] although the latter employed the ADF program[53], triple-ζ STO basis sets and ZORA[54] relativistic corrections. In any event, a recent benchmarking study suggests that comparable results can be obtained for a wide range of functionals[55] so the particular choice made here is not expected to be especially significant.
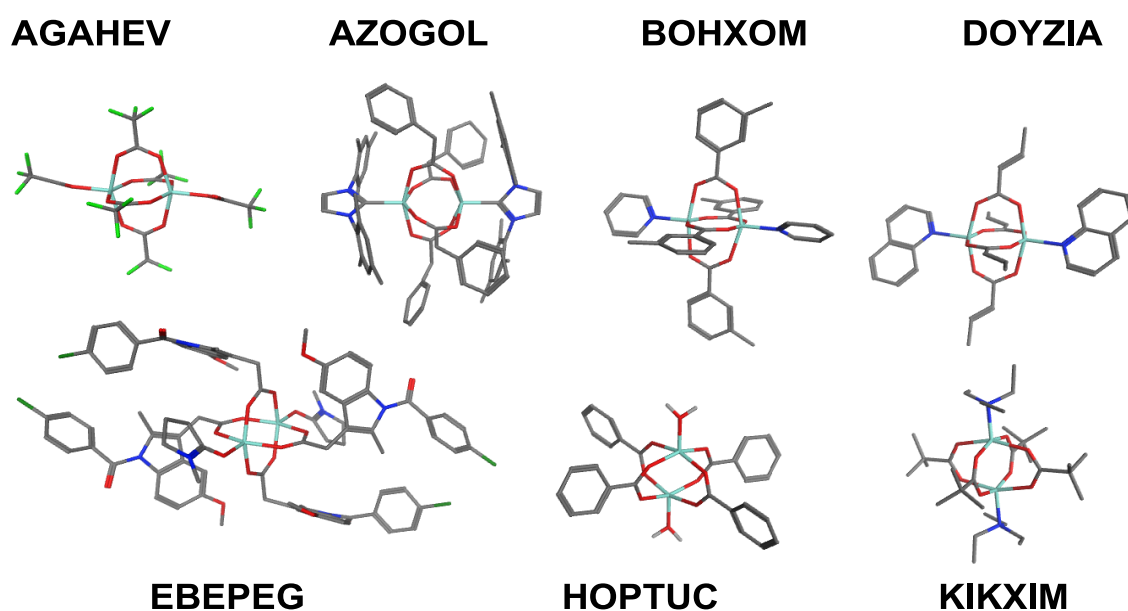
Figure 3.5; A selection of entries from the CSD used to validate the DFT protocol.

As expected, the BP86/DFT/COSMO protocol generally reproduces the experimental structures very well (See Figure 3.6 for overlaid structures). However, the averaged data in Table 3.1 also show that the chosen DFT methodology systematically overestimates the zinc-ligand distances by around 0.03 to 0.05 Å. The FF will be corrected for this error subsequently.
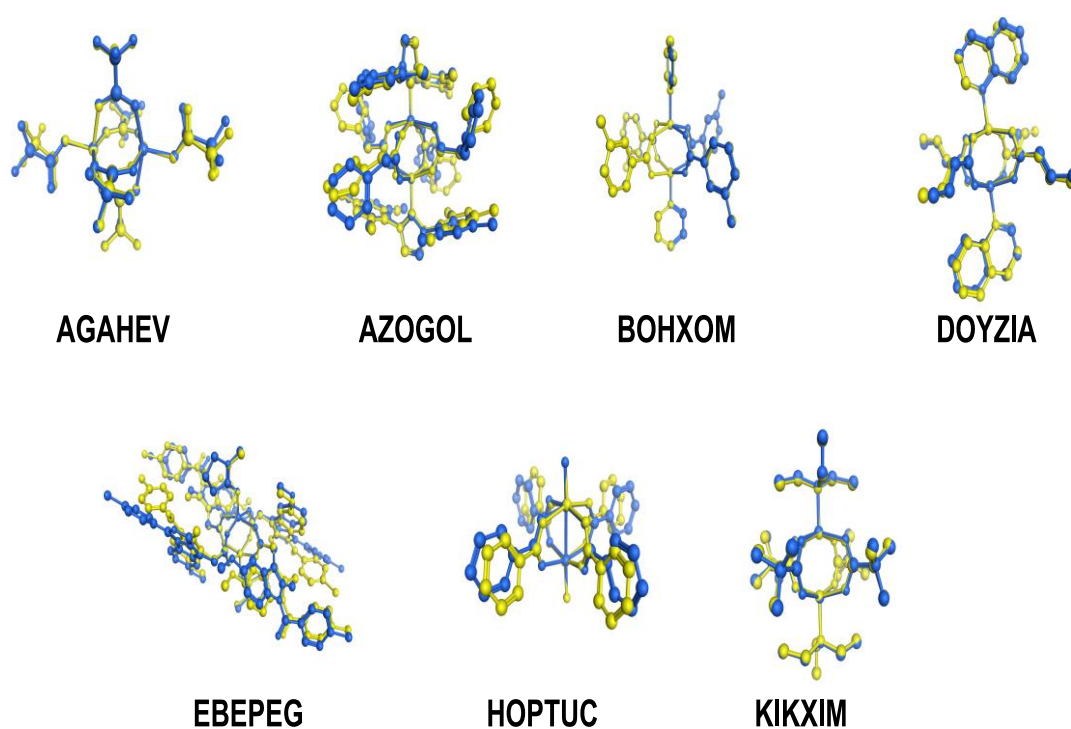
Figure 3.6; Overlays of X-ray (yellow) and DFT-optimized (blue) structures for selected ZPW systems. Hydrogen omitted for clarity.

Table 3.1; Comparison of experimental and calculated bond lengths (Å) for the complexes shown in Figure 3.5. The Zn-O(CBX) entry is the averaged Zn-O(carboxylate) distance. Zn-L refers to the bond to the capping group.

CSD Refcode	AGAHEV		AZOGOL		BOHXOM		DOYZIA		EBEPEG		HOPTUC		KIKXIM	
	X-ray	DFT	X-ray	DFT	X-ray	DFT	X-ray	DFT	X-ray	DFT	X-ray	DFT	X-ray	DFT
Zn-Zn	3.23	3.23	3.19	3.22	2.98	2.93	2.98	2.96	2.93	2.96	2.98	2.83	2.97	3.05
Zn-O (CBX)	2.05	2.09	2.07	2.10	2.04	2.07	2.04	2.07	2.03	2.07	2.04	2.06	2.03	2.08
Zn–L	1.92	1.97	2.07	2.07	2.04	2.07	2.06	2.09	1.99	2.02	1.99	2.06	2.09	2.15
Δ(Zn-Zn)	0.00		-0.03		0.05		0.02		-0.03		0.16		-0.07	
Δ(Zn-O(CBX))	-0.04		-0.03		-0.03		-0.03		-0.04		-0.02		-0.05	
Δ(Zn-L)	-0.05		0.00		-0.03		-0.02		-0.03		-0.07		-0.05	

The initial FF parameterization is based exclusively on first-principles DFT data. A previous DFT study of zinc and copper paddlewheel systems revealed some interesting structural features.[56] In particular, the ground state for an uncapped ZPW displays a large sliding distortion of D_{2d} symmetry consistent with the four-coordinate Zn centers trying to adopt a tetrahedral geometry. The higher symmetry D_{4h} structure is a transition state. To our knowledge, this feature has not been modelled with any previous FFs for ZPW systems although MOF-FF is formulated in a way which may

be able to reproduce the correct ground state.[22]. However, the use of an explicit angle-bending term in MOF-FF, even though based on a Fourier series which generates more than one reference angle,[57] is not as flexible as the current ZPW-FF approach which has no explicitly angle-bending term at the metal centers and uses instead a 1-3 interaction potential exclusively.[58,59] Our experience suggests, especially for coordination numbers greater than four, that this should be a better approach compared to methods like UFF4MOF[25] and BTW-FF[24] which have parameters which enforce a particular coordination geometry for a given coordination number. Moreover, the UFF4MOF implementation only considers the higher symmetry transition state structure for the 'bare' system plus an explicit Zn-Zn bond is employed which is not physically reasonable but required to generate better structures.

Experimentally, ZPWs all appear to have pentacoordinate metal centres so it is not surprising that no-one has considered a FF for four-coordinate zinc centres. However, this is quite significant for Cu paddlewheel analogues which often display 'naked' metal centres plus it also goes towards the inherent flexibility of the MOF. Therefore, Cu paddlewheel systems will be covered for comparison in chapters 5 and 6.

Given that the vast majority of ZPW MOFs have either pyridyl sp^2 or amine sp^3 nitrogen capping ligands, the required MMFF94 ligand parameter atom types are NPYD, N and OX, the latter referring to carboxylate oxygens. Three carboxylates are considered for the basic training species: formate, acetate and trifluoroacetate (R = H, CH_3 or CF_3) with zero, one or two capping groups, L, which are either pyridine (py) or ammonia (NH_3) (Figure 3.7). There are thus five complexes for each carboxylate with each species having a general formula ZnPR.nL, where ZnP represents the

$Zn_2(O_2C)_4$ core of the ZPW. The choice of carboxylates was motivated from a consideration of pK_a values. The pK_a of acetic acid (4.76) is among the higher values with trifluoroacetic acid (0.23) the lowest. Formate and benzoic acids are intermediate and hence the chosen acids span the relevant pK_a range. Benzoic acid is not in the training set but occurs frequently in the validation set.
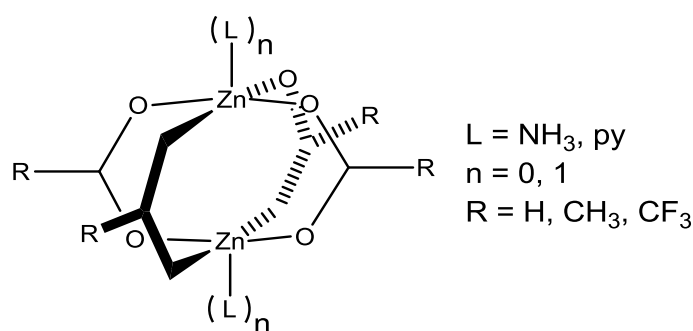
Figure 3.7; Schematic representation of the ZnPR.nL systems used for initial training.

Partial atomic charges were modified from the previously published FF for Mn(II) species[60] and are based on superimposing the change in Mulliken charges between uncoordinated and coordinated ligands onto the existing bond charge increment scheme from the Mn(II) FF. The new values are listed in Table 3.2 along with the standard MMFF94 values for comparison.

Table 3.2; New partial atomic charges for MMFF94 implementation of ZPW-FF. Standard MMFF94 charges in parentheses.

Atom type	Environment	New partial charges (Standard MMFF94 charge)
OX	All	-0.72 (-0.90)
N	NH_3	-0.90 (-1.08)
HN	NH_3	0.43 (0.36)
N	$N(Csp^3)_3$	-0.63 (-0.81)
C	Adjacent to $N(Csp^3)_3$	0.34 (0.27)
NPYD	All	-0.42 (-0.62)
Car	Adjacent to NPYD	0.23 (0.16)
HC	H-C-NPYD	0.23 (0.15)
CO2M	C of formate	0.74 (1.02)
CO2M	C connected to sp^3 carbon	0.626 (0.906)
Zn+2	four carboxylates	1.84
Zn+2	four carboxylates + N	1.45
Zn+2	four carboxylates + NPYD	1.34

Although there are no d-electron effects for Zn(II), we use the Ligand Field Molecular Mechanics (LFMM) method[46, 58] as implemented in DommiMOE,[44] our extended version of the Molecular Operating Environment (MOE).[61] LFMM parameters for M-L bond stretching (Morse function r_0 and α), ligand-ligand repulsion (A_{LL}), Zn-L-A angle bending (θ_0 and k_θ) and Zn-L-A-B torsional twisting (V_2 which favors torsions of 0 and 180 °) were manually optimized to minimize the rmsd in Zn-L bonds and heavy-atom (i.e. non-hydrogen) overlays.

The resulting ZPW-FF (see appendix 1) reproduces DFT very accurately as shown in Figure 3.8. The overall rmsd in Zn-L distances for all 15 systems is 0.02 Å with the highest value for any one complex being only 0.03 Å. The largest individual error in a single Zn-L bond length is 0.046 Å for two of the Zn-O contacts on the uncapped end of ZnPCF$_3$.NH$_3$.

The reproduction of the angular geometries is also excellent as evidenced by the overall average RMSD for heavy atom (i.e. non-hydrogen) overlays of only 0.16 Å. The FF successfully captures the broad variation in zinc coordination as well as a number of subtle structural features as illustrated for the formate species in Figure 3.8. MM tends to be a little more 'tetrahedral' than DFT, but the detailed variation in bond lengths and angles is remarkably well reproduced. This is especially apparent for the lower symmetry species where, for example, the Zn-O distances can vary substantially. In [Zn$_2$(O$_2$CH)$_4$], there are two symmetry independent types of oxygen donor with coordination distances differing by 0.16 Å in the DFT optimization. The ZPW-FF predicts a difference of 0.18 Å. The mono-capped species have an approximately trigonal bipyramidal five-coordinate zinc centre in conjunction with a flattened tetrahedral four-coordinate center. Again, the detailed agreement between DFT and ZPW-FF for both bond-length and bond angle variations is excellent.
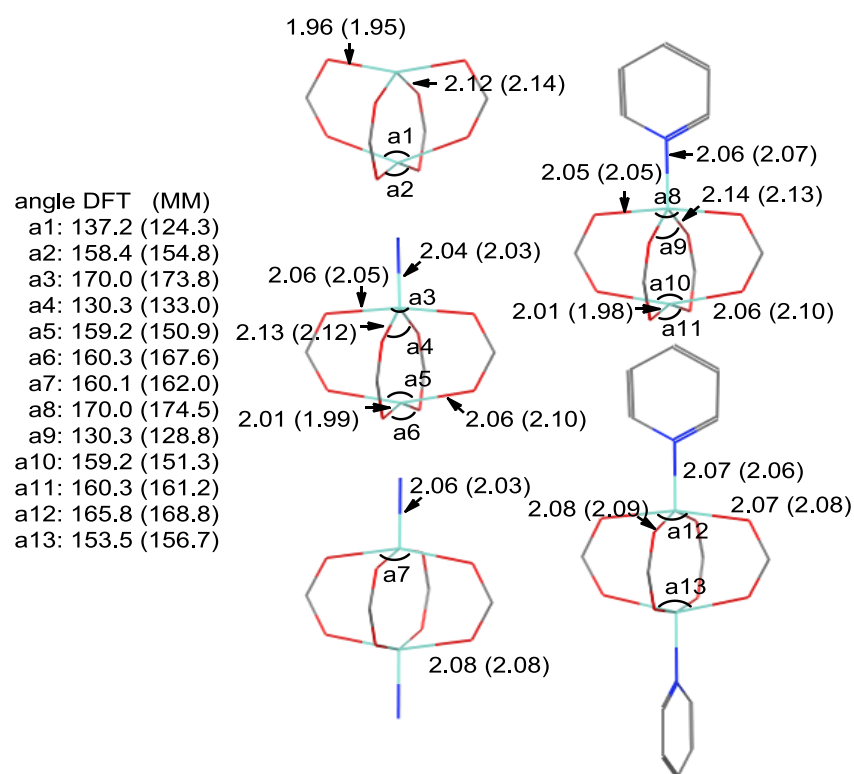
Figure 3.8; Comparison of optimized DFT and MM (in parentheses) structural parameters for ZnPH.nL, (n = 0, 1, 2; L = NH₃, py). Only unique Zn-L and L-Zn-L data shown. Distances in Å and angles in degrees. Hydrogens omitted for clarity. Depicted structures are from DFT-optimized coordinates.

Using the same ZPW-FF parameters, the structures and relative energies of the transition states for the uncapped species can be compared (Table 3.3). The structures were optimized using a simple in-house Newton-Raphson code which follows the largest negative eigenvalue. Good starting points for the TS search are needed and these can be conveniently generated by deleting the two capping groups from a ZnPR.2L system.

Table 3.3; Calculated Zn-O bond lengths (Å), activation energies (kcal mol^{-1}) and transition-state frequencies (cm^{-1}) for ZnPR transition state systems, R = H, CH$_3$ and CF$_3$.

R	r‡ (Zn-O):DFT	r‡ (Zn-O):MM	$\Delta E^{\ddagger}$:DFT[1]	$\Delta G^{\ddagger}$:DFT[2]	$\Delta E^{\ddagger}$:MM	$V^{\ddagger}$:DFT	$V^{\ddagger}$:MM
H	2.04	2.06	9.4	9.2	6.3	-87	-62
CH$_3$	2.03	2.07	10.8	10.3	7.6	-84	-57
CF$_3$	2.04	2.06	7.4	7.9	5.3	-60	-44

[1] Raw DFT electronic energy difference

[2] Free energy difference computed using standard statistical mechanics methods implemented in ORCA, P = 1 atm, T = 298 K.

The ZPW-FF barriers are about 30% lower than those from DFT but the overall agreement is satisfactory.

Recalling the systematic errors between experimental and DFT-optimized complexes, the current FF was retuned using experimental X-ray structural data of 32 ZPW complexes comprising 30 unique ligand combinations (Figure 3.9). The refinement was restricted to minor adjustments of Morse r_0 values to minimize the rmsd Zn-L deviations (see Appendix 1). The data in Table 3.4 shows that the adjusted FF delivers good structural accuracy. The average deviation in zinc-ligand distances is 0.04 Å (Table 3.4) while 92% of the individual deviations for all Zn-L distances are less than 0.05 Å and only 1% of all bond length deviations is larger than 0.1 Å with the largest error being 0.137 Å for XAYKOY. The overall shapes of the complexes are well reproduced with generally small heavy atom overlay rmsds (Table 3.4). The latter in particular will be subject to crystal packing influences so we cannot expect (nor want) exact agreement. However, overall, the results give us some confidence to carry on to modelling more complicated systems such as MOFs which contain multiple, interconnected ZPW units.

Table 3.4; Performance of ZPW-FF for molecules shown in Figure 3.9. Column 1 CSD refcodes. Column 2, root mean square deviation for Zn-L bond lengths. Column 3, root mean square deviation for heavy atom (i.e. non-hydrogen) overlay. Column 4, difference between experimental and computed Zn-Zn distance (a negative value implies a shorter computed value). All numerical data in Å.

Refcode	M-L(rmsd)	Heavy Atom rmsd	Zn-Zn diff
ABOWUL	0.03	0.62	-0.07
BOHXOM	0.02	0.30	-0.16
BOHXUS	0.01	0.45	-0.13
DAYNEX	0.01	0.95	-0.21
DOYZIA	0.02	0.45	-0.06
DUJVOU	0.01	0.57	-0.17
DUPXUI	0.04	0.47	-0.13
EBEPAC	0.03	0.87	-0.14
FACQOQ	0.02	1.37	-0.08
FOWLAF	0.04	0.55	-0.17
FOWLOT	0.02	0.75	-0.08
IJODOB	0.04	0.58	-0.15
INIBAJ	0.02	0.29	-0.15
INIZOU	0.02	0.32	-0.15
IRATAX	0.02	0.49	-0.16
IRATIF	0.02	0.59	-0.16
KIKXIM	0.04	0.36	0.05
KUSHIQ	0.03	0.90	-0.16
LIMWUZ	0.03	0.72	-0.12
NEHZUV	0.03	0.29	-0.03
NEHZUV01	0.02	0.13	-0.06
OGANIU	0.04	0.68	-0.12
ONASOM	0.03	0.35	-0.04
ONATAZ	0.03	0.52	-0.04
QATQAF	0.03	0.92	-0.09
QEIGAY	0.02	0.26	-0.15
RUDWUJ	0.02	0.75	-0.14
RUGVOF	0.02	0.92	-0.13
SADDUY	0.02	0.93	-0.15
TAHYEI	0.02	0.39	-0.05
TAYFIJ	0.04	0.83	-0.03
XAYKOY	0.05	0.35	-0.04
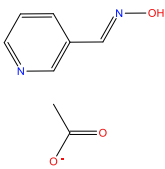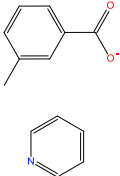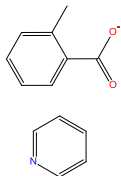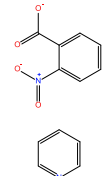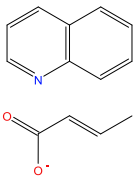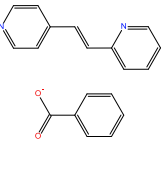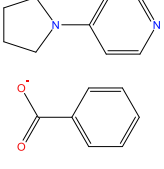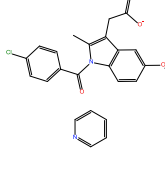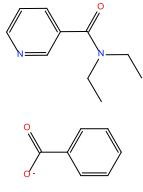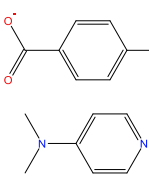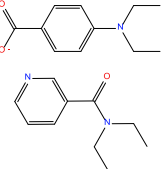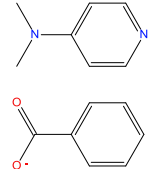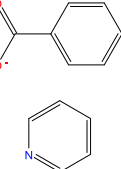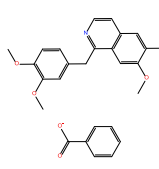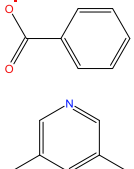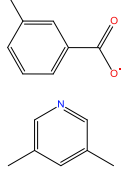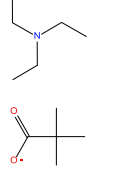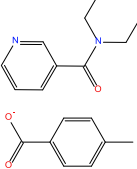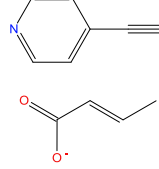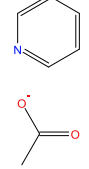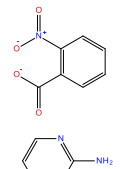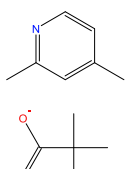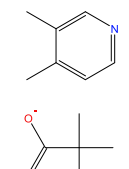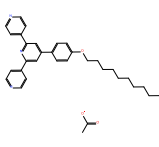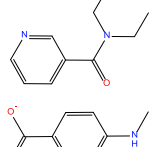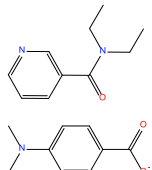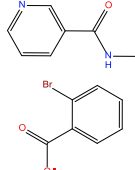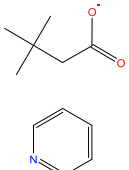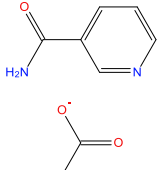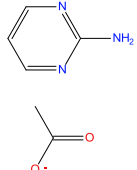
Figure 3.9; Structural diagrams of ligands for the ZPW systems listed by CSD refcode in Table 3.4. Only unique combinations displayed. (NEHZUV and NEHHUV01 are the same compound while INIBAJ and QETGAY have the same ligand set).

3.3.1 Flexible MOFs

Our preliminary investigations into flexible MOF materials focuses on models of individual pores and small grids of pores for $[Zn_2(bdc)_2(dabco)]_n$. We are motivated by the desire to explore the intimate inter- and intra-molecular interactions both within the framework and between the framework and adsorbed species to assess whether the flexible structures are an inherent feature of the pore. We recognize that many fundamental mechanical, thermal, and dielectric properties will not be available[24] and that care will be required when translating our findings into systems which, in reality, are fully periodic. Nevertheless, we believe the results reported in this chapter are significant both in their own right and in terms of a future development of a fully periodic implementation in our DL_POLY_LF platform.[62] Meanwhile, we consider the various ZPW systems highlighted in Figure 3.1.

A model for a single pore was constructed from the crystallographic CIF file. It comprises eight ZPW units at the pore corners with dabco pillars. Corner carboxylates are capped with hydrogen while corner zinc centers are capped with Me_3N groups. The X-ray structure shows significant disorder which results in the dabco groups not having 3-fold symmetry and the orientations of the DMF carbonyl oxygens is ambiguous. We have selected an arrangement such that the carbonyl oxygen of one DMF is directed towards the HC(O) hydrogen of a neighboring DMF. Water molecules are also identified in the crystal structure but their position at the face of the pore would make them susceptible to effects from adjoining pores. Also, preliminary calculations showed that they have strongly directional H-bonding effects and tend to migrate to the nearest ZPW unit causing significant local distortions. This is one of the shortcomings of using an aperiodic system and the water molecules have therefore not

been including in the subsequent MM optimizations. Also, given that there are now multiple ZPW units as opposed to the single ZPW systems considered so far, the standard 8 Å/10 Å electrostatic cut-offs are disabled and the default distance-dependent ($1/\varepsilon r^2$) dielectric model for electrostatics is replaced by the softer reaction field implemented in MOE. Both these changes have minimal effects on either the training systems or the refinement/validation set. The final single-pore model is shown in Figure 3.10.

[Zn$_2$(bdc)$_2$(dabco)] Pore Model

TOP   **SIDE**
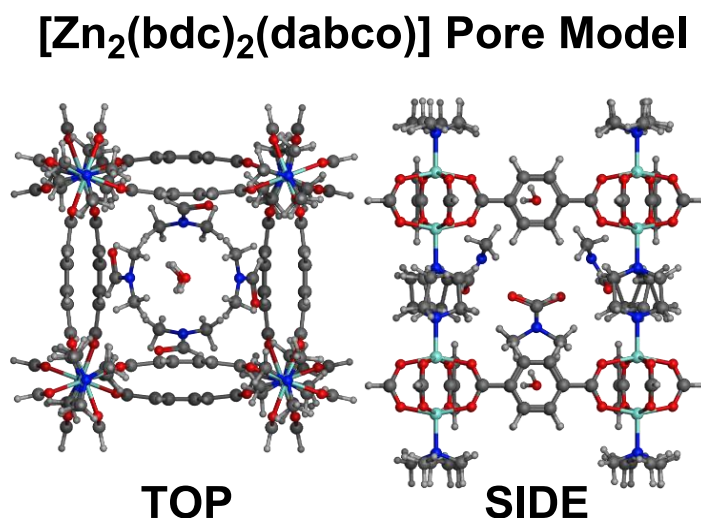
Figure 3.10; Starting pore model for MM optimizations derived from X-ray diffraction study. Positions of experimental water molecules are shown but waters are not included in the MM calculations.

MM optimizations of the single-pore model with four DMF molecules incorporated display a definite curvature of the pore edges (Figure 3.11, middle top). Removal of the DMF molecules leads to a regular 'cuboidal' geometry while replacement of the

DMF by benzene molecules gives a pronounced rhombohedral distortion. The MM-optimized pores are thus consistent with experiment but, apart from the vacant pore, the calculated distortions are underestimated. In practice, each pore vertex is connected to another pore and it is probably not surprising that a single-pore model is inadequate. Hence, we extended the model to a 3x3 grid of 9 pores so that the central one is connected on all sides.
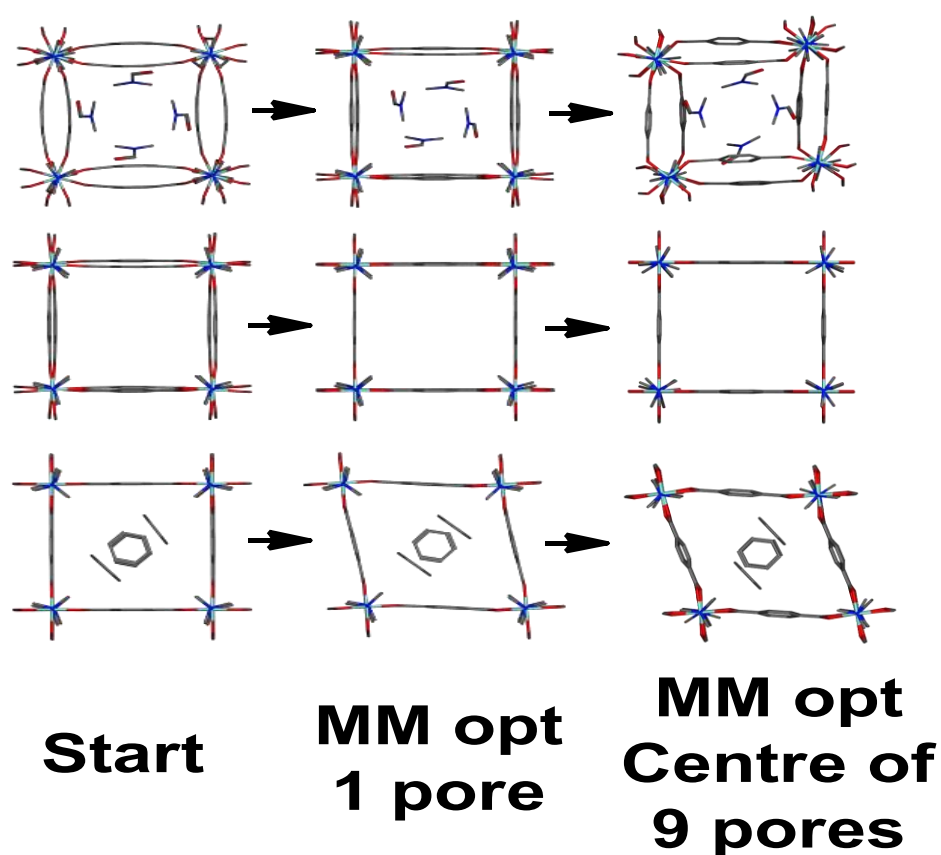
Figure 3.11; Development of the 'breathing' for $[Zn(bdc)_2(dabco)]_n$.solvate. Left column displays the single pore starting model for MM optimization. Central column shows the ZPW-FF optimized structure of the single pore model. The right column shows the ZPW-FF optimized structure of the central pore of the nine-pore 3x3 grid.

As shown on the right side of Figure 3.11, this leads to substantially better agreement with the reported X-ray structural data. The calculated unit cell dimensions of a = 11.0 Å and c = 9.6 Å for the empty pore are virtually identical to the experimental values of 10.9288(15) and 9.6084(12) while for the DMF adsorbate system, the dihedral twist between two ZPW groups connected by a dabco pillar increases from ~ 9 ° for the 1-pore model to ~30 ° for the 9-pore model compared to the experimental value of 40 °. This twist is accommodated in the modelling largely by a hinge movement along the O-O vector of the carboxylates which keeps the bdc unit flat as opposed to the X-ray structure which shows a smoother curved profile of the bdc bridge. For the benzene-solvated system, the acute angle formed from, for example, the top three zinc centres at the vertices of the pore changes from 81° for the 1-pore model to 75 ° for the 9-pore model compared to 77 ° from the X-ray structure.

The current FF thus appears to capture the breathing modes of this particular flexible MOF quite well using an aperiodic model system which we believe is a significant achievement given that only single-ZPW unit systems were employed in its construction. However, part of this success is undoubtedly due to the pillared structure, which means we only need to consider a single layer, plus the positions of the solvent molecules have been taken from experiment. A greater test would be to see whether the number and position of solvent molecules within the pore might be predicted.

We start with benzene since it is more symmetrical than DMF and the experimental structure is not disordered. A single benzene molecule was placed at the centre of an empty 1-pore model and energy minimized. It spontaneously migrated to the methylene units of a dabco pillar. Adding a second benzene to this structure, again

placed at the centre of the pore, and energy minimizing led to the second benzene spontaneously migrating to the opposite dabco pillar. Adding a third benzene to this model, which clearly generates a highly strained starting point, spontaneously leads to the third benzene migrating to the pore surface to form van der Waals contacts with bdc linker aromatic rings. So far, the benzene groups have positioned themselves exactly where experiment suggests and there is a clear visual indication of where the next benzene should go. However, following the same computational protocol, energy minimization once a fourth benzene is added leads to two results. Sometimes, the fourth benzene goes to the pore face opposite the third and the experimental solid-state packing is realized. Sometimes, the fourth benzene goes to the same face as the third and pushes the latter out such that it interacts with the NMe_3 groups on the pore periphery. In a periodic system, this benzene would be replicated near the 'vacant' face and, once again, we would deduce that this is the more favorable position and the experimental packing would be recovered once again. Visual inspection of a space-filling representation confirms that there is insufficient space to accommodate a fifth benzene. Finally, a number of short 300K MD annealing simulations were run which confirm that the four benzenes are located in reasonably stable positions.

A similar energy minimization procedure was followed for DMF and, to a large extent, the DMF molecules spontaneously migrated to their experimentally-observed positions. However, while in general, the DMF methyl groups are oriented towards the bdc phenyl rings with the carbonyl groups oriented towards dabco pillars, other orientations of DMF molecules have very similar energies and the barrier to rotation is low.

To test the modelling further, a fifth DMF molecule was added. Energy minimization leads to the fifth DMF being captured in a local minimum within the pore. However, a short MD simulated-annealing run shows that even the 1-pore model cannot sustain five DMF molecules and one is spontaneously pushed out through the relatively unrestricted face formed by bdc linkers. However, in the process, the 1-pore model becomes very badly distorted.

Consequently, we took the 9-pore model and removed the DMF molecules from all but the central pore. A fifth DMF was then added, the energy minimized and a short MD annealing run carried out. As for the 1-pore model, one of the DMFs is spontaneously ejected from the pore (Figure 3.12).
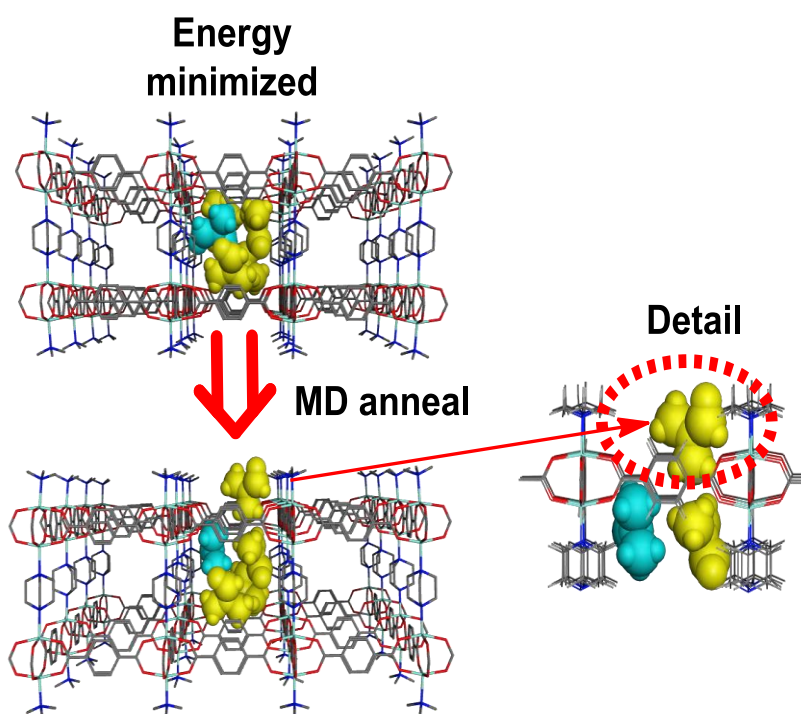
Figure 3.12; ZPW-FF simulated annealing starting from the energy-minimized, 9-pore model with the central pore containing the four original DMF molecules (in yellow) plus a fifth DMF (in cyan). After simulated annealing (bottom left), one of the DMF molecules exits the pore (right, highlighted by the dotted red ellipse).

The motions of the DMF molecules are displayed graphically in Figure 3.13 which shows the change in the distances between the amide N atoms of each DMF molecule and a nearby Zn atom. Three DMF molecules barely move while N1 is the one which is ejected. N2 adjusts its position to generate the approximately tetrahedral arrangement of DMF molecules in the pore, consistent with the experimental arrangement.
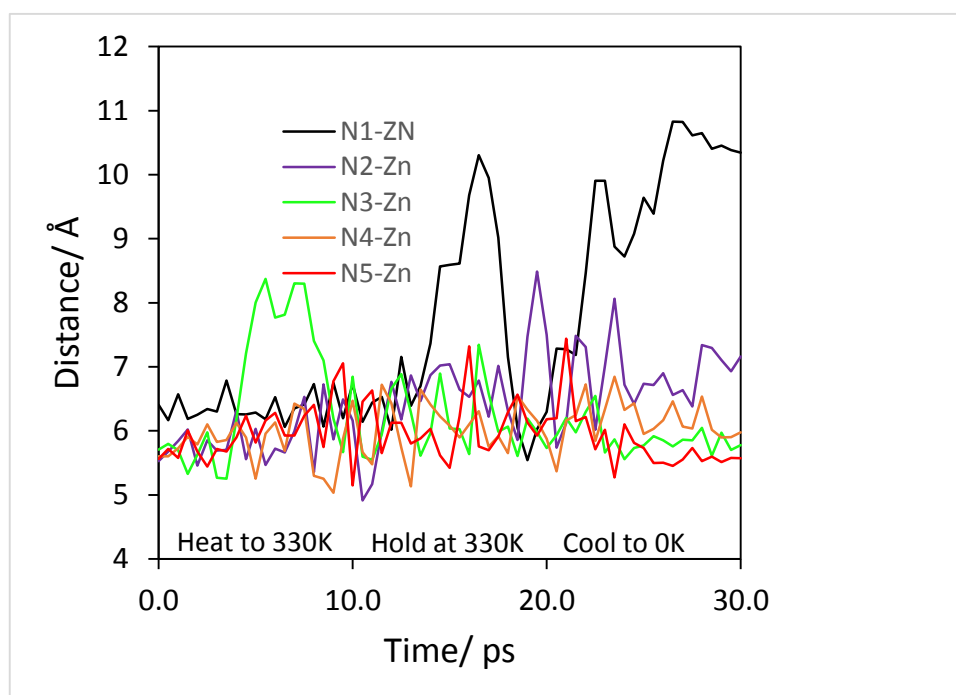
Figure 3.13; Plot of distances from a corner zinc centre to the N atom of the five DMF molecules in the central pore of the 3x3 grid during the simulated annealing MD run showing how one of the DMF molecules (N1) is spontaneously ejected from the central pore.

A shortcoming of the preceding series of calculations is the lack of any energetic information. Thus, while we can derive an idea of the maximum loading of adsorbate that an isolated pore can tolerate, we cannot predict the energetic consequences of this loading in the actual MOF since we do not include a full treatment of the pore surroundings. Thus, we cannot deal with the effect of, for example, the external

concentration of adsorbate. This requires a more sophisticated dynamics treatment along the lines of that reported by Grosh and Paesani.[63] However, the present study at least demonstrates that the underlying ZPW-FF should provide an excellent platform for such studies and we will report the results in due course.

3.4 Conclusions

A new experimentally-refined, first-principles force field has been developed for the zinc paddlewheel motif including pyridyl and amine capping groups. The ZPW-FF parameters are based on the Merck Molecular FF (MMFF) extended with additional Ligand Field Molecular Mechanics (LFMM) parameters as implemented in DommiMOE, our extended version of the Molecular Operating Environment. Given the absence of explicit d-electron effects for d^{10} Zn(II) centres, the parameters could easily be ported to other software codes which support the MMFF and LFMM potential energy functional forms.

The new ZPW-FF is based on a much larger set of training and validation systems than other MOF FFs. It accurately reproduces the DFT-computed structures for small model ZPW systems including uncapped, mono- and di-capped complexes. This includes the first ever empirical modelling of the high-symmetry transition state structures for the uncapped $[Zn_2(O_2CR)_4]$ systems. With a minor refinement of Morse function reference distances for Zn-O (carboxylate) and Zn-N bonds, excellent agreement with the structures of 32 crystallographically-characterized ZPW systems is also obtained.

The ZPW-FF is designed to accurately model the local structure of zinc centres coordinated to bridging carboxylate and monodentate N donor ligands and can be

applied equally well to isolated 'molecular' ZPW systems or to materials such as MOFs with multiple ZPW units. This permits us to construct aperiodic models of MOF pores and explore issues such as whether the behavior observed in the bulk is a function of an individual pore or a set of pores.

The new force field was therefore applied to pore models of the archetypal flexible MOF $[Zn_2(bdc)_2(dabco)]_n$. The dimensions of the calculated structure of an empty single pore are identical to the experimental unit cell parameters of the extended solid. The framework structure is also sensitive to adsorbed solvent and a 1-pore model already gives a qualitatively correct picture of the effect of including four DMF or four benzene molecules. The latter calculations start from the X-ray crystallographic coordinates but the number and orientation of solvent molecules is also predicted by systematically adding solvent molecules to the pore, energy minimizing and then, if necessary, carrying out short annealing MD runs. The four benzene molecules essentially occupy their experimental positions spontaneously. The DMF molecules show some variability in orientation but the energetic consequences are minor. MD simulations further show that any attempt to add a fifth DMF molecule to the pore will result in one being spontaneously ejected.

Overall, the ZPW-FF performs extremely well, at least for $[Zn(bdc)_2(dabco)]_n$, and is obviously many orders of magnitude more efficient than DFT. Our next goals are to extend the ZPW-FF to other more complicated MOFs and to develop our own version of a copper paddlewheel force field (CPW-FF) where the important d-electron effects arising from the strongly Jahn-Teller active d^9 copper(II) centres will be captured explicitly by the angular overlap model parameters of LFMM[58, 64] rather than via conventional FF parameters.[20] Also, while pore models may provide some useful

insights, the lack of periodicity means that many important mechanical, thermal and dielectric properties cannot be computed.[24] The LFMM methodology has recently been ported to Tinker.[65] The latter avoids the annual license fees associated with MOE and will hopefully lead to wider uptake by the academic community although there is much development work to be completed before the Tinker-LF implementation can match the functionality currently available in DommiMOE. On the other hand, the ability to model periodic systems in MOE is limited so it is worth noting that a LFMM is also available in DL_POLY, although our application involved Pt binding to DNA.[62] We will report on the performance of ZPW-FF for periodic systems in due course.

3.5 References

1.   L. R. MacGillivray, *Metal-Organic Frameworks: Design and Application*, John Wiley & Sons, Hoboken, New Jersey, 2010.

2.   A. U. Czaja, N. Trukhan and U. Mueller, *Chem. Soc. Rev.*, 2009, **38**, 1284-1293.

3.   S. Horike, S. Shimomura and S. Kitagawa, *Nat Chem*, 2009, **1**, 695-704.

4.   A. Schneemann, V. Bon, I. Schwedler, I. Senkovska, S. Kaskel and R. A. Fischer, *Chem. Soc. Rev.*, 2014, **43**, 6062-6096.

5.   L. Sarkisov, R. L. Martin, M. Haranczyk and B. Smit, *J. Am. Chem. Soc.*, 2014, **136**, 2228-2231.

6.   Q.-G. Zhai, N. Bai, S. n. Li, X. Bu and P. Feng, *Inorg. Chem.*, 2015, **54**, 9862-9868.

7.   S. Mukherjee, B. Joarder, A. V. Desai, B. Manna, R. Krishna and S. K. Ghosh, *Inorg. Chem.*, 2015, **54**, 4403-4408.

8.   B. Li, H.-M. Wen, W. Zhou and B. Chen, *J. Phys. Chem. Lett.*, 2014, **5**, 3468-3479.

9.   C. S. Hawes, Y. Nolvachai, C. Kulsing, G. P. Knowles, A. L. Chaffee, P. J. Marriott, S. R. Batten and D. R. Turner, *Chem. Commun.*, 2014, **50**, 3735-3737.

10.   D. Liu, K. Lu, C. Poon and W. Lin, *Inorg. Chem.*, 2013, **53**, 1916-1924.

11.   Y. Yue, J. A. Rabone, H. Liu, S. M. Mahurin, M.-R. Li, H. Wang, Z. Lu, B. Chen, J. Wang, Y. Fang and S. Dai, *J. Phys. Chem. C*, 2015, **119**, 9442-9449.

12.   D. N. Dybtsev, H. Chun and K. Kim, *Angew. Chem. Int. Ed.*, 2004, **43**, 5033-5036.

13.   S. O. Odoh, C. J. Cramer, D. G. Truhlar and L. Gagliardi, *Chem. Rev.*, 2015, **115**, 6051-6111.

14.   L. Chen, J. P. S. Mowat, D. Fairen-Jimenez, C. A. Morrison, S. P. Thompson, P. A. Wright and T. Düren, *J. Am. Chem. Soc.*, 2013, **135**, 15763-15773.

15.   Y. J. Colon and R. Q. Snurr, *Chem. Soc. Rev.*, 2014, **43**, 5735-5749.

16.   J. A. Gee and D. S. Sholl, *J. Phys. Chem. C*, 2015, **119**, 16920-16926.

17.   H. Wu, J. M. Simmons, Y. Liu, C. M. Brown, X.-S. Wang, S. Ma, V. K. Peterson, P. D. Southon, C. J. Kepert, H.-C. Zhou, T. Yildirim and W. Zhou, *Chem. Eur. J.*, 2010, **16**, 5205-5214.

18.   A. K. Rappe, C. J. Casewit, K. S. Colwell, W. A. Goddard and W. M. Skiff, *J. Am. Chem. Soc.*, 1992, **114**, 10024-10035.

19.   S. L. Mayo, B. D. Olafson and W. A. Goddard, *J. Phys. Chem.*, 1990, **94**, 8897-8909.

20.   M. Tafipolsky, S. Amirjalayer and R. Schmid, *J. Phys. Chem. C*, 2010, **114**, 14402-14409.

21.   E. Haldoupis, J. Borycz, H. Shi, K. D. Vogiatzis, P. Bai, W. L. Queen, L. Gagliardi and J. I. Siepmann, *J. Phys. Chem. C*, 2015, **119**, 16058-16071.

22. S. Bureekaew, S. Amirjalayer, M. Tafipolsky, C. Spickermann, T. K. Roy and R. Schmid, *Physica Status Solidi B-Basic Solid State Phys.*, 2013, **250**, 1128-1141.

23. M. Tafipolsky and R. Schmid, *J. Phys. Chem. B*, 2009, **113**, 1341-1352.

24. J. K. Bristow, D. Tiana and A. Walsh, *J. Chem. Theory. Comput.*, 2014, **10**, 4644-4652.

25. M. A. Addicoat, N. Vankova, I. F. Akter and T. Heine, *J. Chem. Theory. Comput.*, 2014, **10**, 880-891.

26. E. Garcia-Perez, P. Serra-Crespo, S. Hamad, F. Kapteijn and J. Gascon, *PCCP*, 2014, **16**, 16060-16066.

27. M. Ćendić, Z. D. Matović and R. J. Deeth, *J. Comput. Chem.*, 2013, **34**, 2687-2696.

28. C. M. Handley and R. J. Deeth, *J. Chem. Theory. Comput.*, 2012, **8**, 194-202.

29. R. Brodbeck and R. J. Deeth, *Dalton Trans.*, 2011, **40**, 11147-11155.

30. R. J. Deeth, A. E. Anastasi and M. J. Wilcockson, *J. Am. Chem. Soc.*, 2010, **132**, 6876–6877.

31. R. J. Deeth, A. Anastasi, C. Diedrich and K. Randell, *Coord. Chem. Rev.*, 2009, **253**, 795-816.

32. A. Anastasi and R. J. Deeth, *J. Chem. Theory. Comput.*, 2009, **5**, 2339–2352.

33. C. Diedrich and R. J. Deeth, *Inorg. Chem.*, 2008, **47**, 2494-2506.

34. A. Bentz, P. Comba, R. Deeth and E. Al., *Inorg. Chem.*, 2008, **47**, 9518-9527.

35. R. J. Deeth, *Inorg. Chem.*, 2007, **46**, 4492-4503.

36. F. Neese, U. Becker, D. Ganiouchine, S. Koßmann, T. Petrenko, C. Riplinger and F. Wennmohs, *Journal*, 2014.

37. A. D. Becke, *Phys. Rev. A*, 1988, **38**, 3098-3100.

38. J. P. Perdew and W. Yue, *Phys. Rev. B-Condensed Matter*, 1986, **33**, 8800-8802.

39. A. Schaefer, H. Horn and R. Ahlrichs, *J. Chem. Phys.*, 1992, **97**, 2571.

40. R. K. Hocking, R. J. Deeth and T. W. Hambley, *Inorg. Chem.*, 2007, **46**, 8238-8244.

41. A. Klamt and V. Jones, *J. Chem. Phys.*, 1996, **105**, 9972.

42. A. Klamt, *J. Phys. Chem.*, 1995, **99**, 2224.

43. A. Klamt and G. Schüürmann, *J. Chem. Soc., Perkin Trans.*, 1993, **2**, 799.

44. R. J. Deeth, N. Fey and B. J. Williams-Hubbard, *J. Comput. Chem.*, 2005, **26**, 123-130.

45. MOE, *Journal*, 2011.

46. R. J. Deeth and D. L. Foulis, *PCCP*, 2002, **4**, 4292-4297.

47. Users are responsible for obtaining a valid MOE licence from Chemical Computing Group.

48. P. Comba and R. Remenyi, *Coord. Chem. Rev.*, 2003, **238**, 9-20.

49. P. O. Norrby and P. Brandt, *Coord. Chem. Rev.*, 2001, **212**, 79-109.

50. R. J. Deeth and L. J. A. Hearnshaw, *Dalton Trans.*, 2006, 1092-1100.

51. X. Zhao, H. He, T. Hu, F. Dai and D. Sun, *Inorg. Chem.*, 2009, **48**, 8057-8059.

52. B. J. Houghton and R. J. Deeth, *Eur. J. Inorg. Chem.*, 2014, **2014**, 4573-4580.

53. E. J. Baerends, T. Ziegler, J. Autschbach, D. Bashford, A. Bérces, F. M. Bickelhaupt, C. Bo, P. M. Boerrigter, L. Cavallo, D. P. Chong, L. Deng, R. M. Dickson, D. E. Ellis, M. van Faassen, L. Fan, T. H. Fischer, C. Fonseca Guerra, A. Ghysels, A. Giammona, S. J. A. van Gisbergen, A. W. Götz, J. A. Groeneveld, O. V. Gritsenko, M. Grüning, S. Gusarov, F. E. Harris, P. van den Hoek, C. R. Jacob, H. Jacobsen, L. Jensen, J. W. Kaminski, G. van Kessel, F. Kootstra, A. Kovalenko, M. V. Krykunov, E. van Lenthe, D. A. McCormack, A. Michalak, M. Mitoraj, J. Neugebauer, V. P. Nicu, L. Noodleman, V. P. Osinga, S. Patchkovskii, P. H. T. Philipsen, D. Post, C. C. Pye, W. Ravenek, J. I. Rodríguez, P. Ros, P. R. T. Schipper, G. Schreckenbach, J. S. Seldenthuis, M. Seth, J. G. Snijders, M. Solà, M. Swart, D. Swerhone, G. te Velde, P. Vernooijs, L. Versluis, L. Visscher, O. Visser, F. Wang, T. A. Wesolowski, E. M. van Wezenbeek, G. Wiesenekker, S. K. Wolff, T. K. Woo and A. L. Yakovlev, *Journal*, 2012.

54. E. van Lenthe, A. E. Ehlers and E. J. Baerends, *J. Chem. Phys.*, 1999, **110**, 8943.

55. D. Nazarian, P. Ganesh and D. S. Sholl, *J. Mater. Chem. A.*, 2015, **3**, 22432-22440.

56. S. Bureekaew, S. Amirjalayer and R. Schmid, *J. Mater. Chem.*, 2012, **22**, 10249-10254.

57. V. S. Allured, C. M. Kelly and C. R. Landis, *J. Am. Chem. Soc.*, 1991, **113**, 1-12.

58. R. J. Deeth, *Coord. Chem. Rev.*, 2001, **212**, 11-34.

59. P. Comba and T. W. Hambley, *Molecular Modeling of Inorganic Compounds*, VCH, Weinheim, 1995.

60. R. J. Deeth, *Inorg. Chem.*, 2008, **47**, 6711-6725.

61. MOE, *Journal*, 2013.

62. H.-C. Tai, R. Brodbeck, J. Kasparkova, N. J. Farrer, V. Brabec, P. J. Sadler and R. J. Deeth, *Inorg. Chem.*, 2012, **51**, 6830–6841.

63. J. S. Grosch and F. Paesani, *J. Am. Chem. Soc.*, 2012, **134**, 4207-4215.

64. V. J. Burton, R. J. Deeth, C. M. Kemp and P. J. Gilbert, *J. Am. Chem. Soc.*, 1995, **117**, 8407-8415.

65. M. Foscato, R. J. Deeth and V. R. Jensen, *J. Chem. Inf. Mod.*, 2015, **55**, 1282-1290.

Chapter 4: The Extension of Zinc Paddlewheel Force Field (ZPW-FF) for Modelling a Flexible Metal Organic Framework with Apical Water Ligand.

4.1 Introduction

Metal-organic frameworks (MOFs), also known as coordination networks or coordination polymers, are now considered as one of the most promising classes of porous materials.[1-3] They consist of secondary building unites (SBUs) connected by well-designed linkers to form one-, two-, or three- dimensional networks. The SBUs are either transition metal complexes or small clusters, while the linkers are organic ligands (usually carboxylate) in combination with apical polytopic nitrogen-donor ligand such as, 1, 4-diazabicyclo(2.2.2)octane (dabco).

Although many MOFs have relatively rigid frameworks, other MOFs show a degree of flexibility or breathing such as, for example, $[Zn_2(bdc)_2(dabco)]_n$ (bdc = 1,4-benzenedicarboxylate) (Figure 4.1).[4, 5] This model displays a remarkable degree of flexibility depending on the adsorbed species which offers a variety of applications in separations[6-9] and sensing.[10-12] However, these interesting porous materials must be addressed and evaluated carefully before using them in the real-world systems. For example, one of the major concerns is the chemical stability of MOFs systems in gas storage and separations applications under the water vapor atmosphere.[13-15]

DMF/WATER **EMPTY** **BENZENE**
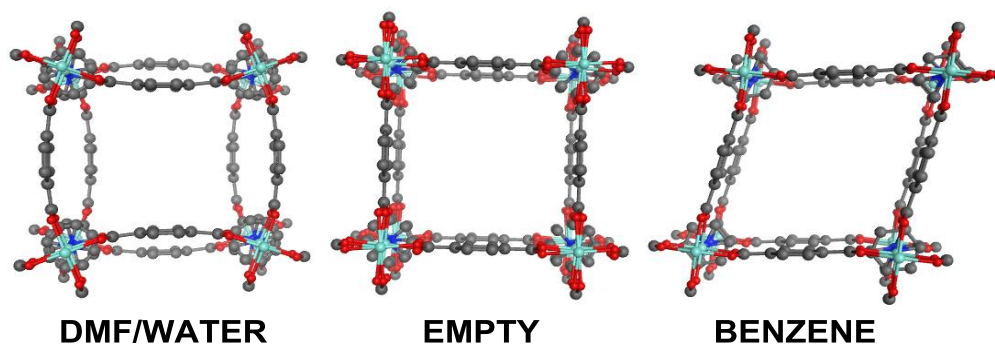
Figure 4.1; Pore framework structures for $[Zn_2(bdc)_2(dabco)]_n$ derived from published CIF files.[16] Hydrogens and encapsulated solvent removed. dabco and carboxylate disorder as per CIF file.

Computer modelling approaches can play an important role in investigating the properties and structures of MOFs at the atomic level. However, modelling the structural changes shown in Figure 4.1 are challenging and requires a sophisticated theoretical method.[17] Quantum chemical (QC) methods such as density functional theory (DFT) would be desirable, but the size and complexity of MOFs makes the application of QC methods extremely expensive, especially if the dynamical behaviour are of interest. In contrast, molecular mechanics (MM) methods offer an efficient alternative provided they can deliver a good agreement between the calculated structures of MOFs and experimental data.[18] However, MM require a flexible force field (FF) to represent the flexible modes shown in figure 4.1.

Our constructed first-principles force field (FF) for the bimetallic, four-bladed zinc paddlewheel (ZPW) motif, ZPW-FF, has successfully captured the breathing modes displayed by $[Zn_2(bdc)_2(dabco)]_n$ as a function of adsorbate.[19] However, ZPW-FF focuses solely on apical N donor ligand, while here the extension of ZPW-FF to apical water ligand will be considered. The extended version of ZPW-FF can then be used

for simulating and evaluating ZPW MOFs systems theoretically under the water vapor atmosphere.

In this chapter, we have followed the same methodology for constructing our original ZPW-FF.[19] However, here we focus on four-bladed zinc paddlewheel (ZPW) motif with capping water ligand. Therefore, the parameters between bonded and non-bonded interactions between water molecule (for both O and H atoms) and the ZPW motif have been carefully constructed. To achieve this, DFT calculations have been mainly considered to obtain further training data based on eight simple ZPW models with capping water ligand, including systems with one coordinated site such as $Zn_2(carboxylate)_4(H_2O)$. The reason for this is the lack of experimental reference data for ZPW systems with apical water. However, a further refinement of Zn-water bond length was based on available experimental data to reduce the systematic errors from our chosen DFT protocol.

Tan *et al*, state that exposing $Zn(bdc)(dabco)_{0.5}$ compound to condensed water vapor would simply replace the dabco ligand by water molecules through their oxygen atoms (Figure 4.2).[20] This study motivated us to modify the classical system shown in Figure 4.1 and replace the dabco top surface by water and use this model for preliminary investigation of our new version of ZPW-FF. Subsequently, the current force field was then employed on the two-dimensional (2D) microporous layer of MOF-2 system which comprise Zn (bdc)(H$_2$O).(dmf) building units.[21, 22] The successful MM data obtained from these investigations motivated us to model layer-by-layer stacking crystals of MOF-2 containing DMF guest molecules. At first sight the FF reproduced the model successfully. However, capturing the complicated hydrogen-bonding interactions between inter water ligands and carboxylate oxygens of an adjacent layer

(Figure 4.3) was not perfect. In addition, the positions and orientations of DMF guest molecules inside the MOF-2 cavities was not well reproduced. These shortcomings were fixed by modifying manually the charge schemes of inter water ligands and DMF guest molecules.[23] The final MM optimizations and MD simulations then reproduced the non-periodic model of MOF-2 packing systems successfully, based on our extended version of ZPW-FF.[24]
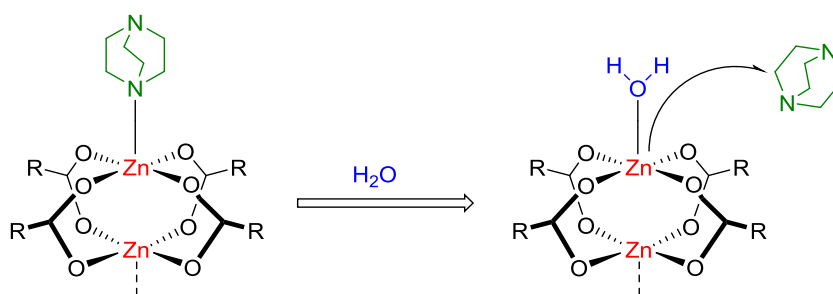
Figure 4.2; Schematic illustration of decomposition pathway of $Zn(bdc)(dabco)_{0.5}$ reacting with water molecules.
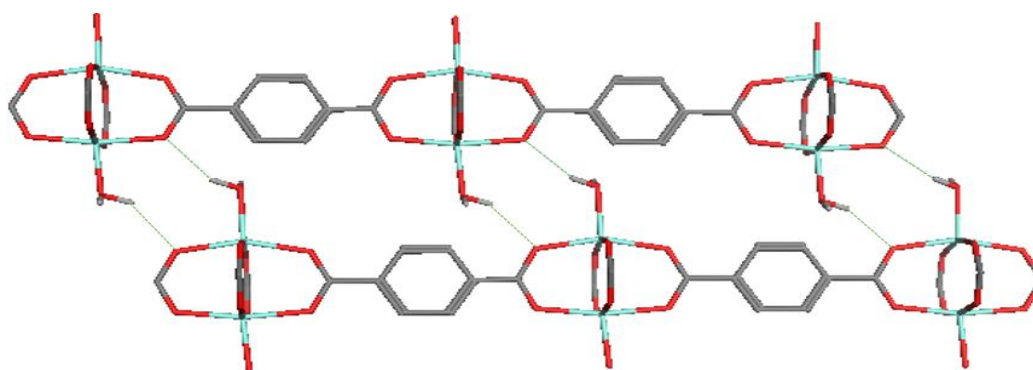
Figure 4.3; Horizontal viewing of the two layers stacking model in the crystals of MOF-2 showing H-bonding interactions (green dot line) between them.

4.2 Theoretical methods

All DFT calculations were carried out using ORCA version 3.0.1.[24] The Becke-Perdew BP86 functional [25, 26] and Ahlrichs' def2-SVP basis sets [27] were employed as a general protocol to construct a suitable and high quality training referencing data. Water was considered as a standard solvent in our calculation by employing the conductor like screening model (COSMO) as implemented in ORCA.[28-31]

Molecular mechanics, MM, calculations were carried out using DommiMOE [32], our extended version of the 2013 of the molecular operating environment.[33] The distributed version of Merck molecular force field, MMFF94 [34, 35] (mmff94x.ff), with additional terms such as Zn-L-A angle bend and Zn-L-A-B torsion, was used to capture the coordination environments around the zinc metal centers. These environments was defined using the ligand field molecular mechanics (LFMM)[36] parameters where the Zn-L interactions and the explicit angle bending around the metal center were described by Morse function (E_{Morse}) and a pure ligand-ligand repulsion (A_{LL}/d^n) respectively. As the d^{10} Zn^{2+} does not have ligand field stabilization energy, all spin-pairing and angular overlap model terms were set to zero. All of these terms and parameters are already available in our first-principal force field (ZPW-FF). However, the Zn-O (water) related parameters were augmented within ZPW-FF to capture the changes in behavior when the N-based ligand were substituted by water. The extended parameters files and partial-charge-setting scripts are available in the Appendix 1, and can also be requested from the author. The electrostatic interactions associated within our models are relaxed by a distance-dependent dielectric term where a cut-off starts at 8 Å and go to zero at 10 Å.

The Nosé-Poincaré-Anderson (NPA) algorithm method was used for molecular dynamics (MD) simulations with a 2 fs time step. The constant number of particles, volume, and temperature (NVT) ensemble annealing protocol was as follows: T0= 50 K; heat to 400 K in 10 ps, hold for 10 ps, and cool to 0 K in 10 ps. The light bond lengths, such as H atoms, were frozen. A 0.1 ps temperature relaxation time was used with configurations sampled every 0.5 ps.

4.3 Results and discussion

The original flexible and accurate all-atom first-principles force field, ZPW-FF, was based on a diverse set of training data. It relies on DFT studies of 15 simple ZPW systems with zero-, one-, and two apical N donor. The training data was then refined against 32 ZPW experimental complexes to reduce the systematic errors from the chosen DFT protocol (BP86/SVP/COSMO (water)). These steps have provided us a high quality sets of training data which can be used for developing our flexible version of ZPW-FF. However, the previous study focused only on the ZPW systems with apical N donor ligands, whereas in this chapter the ZPW systems with apical water ligand are considered.

Our previous study on 77 ZPW experimental systems, extracted from Cambridge Structural Database (CSD), regardless of apical ligands, shows that all the experimental data of central ZPW motif are remarkably similar, including parameters and the Zn geometries. However, the latter revealed some subtle variations of the local zinc geometries which were then captured successfully by ZPW-FF.

Despite the fact that the vast majority of ZPW systems have nitrogen capping ligands, we believe that extending our force field, ZPW-FF, for apical water donor is extremely important for future applications of ZPW MOFs systems. For example, it can play an important role in solving the limitation of the presence of water (moisture) in industrial scale development.[13-15] However, the lack of experimental data for ZPW systems with apical water donor has led us to exclusively develop the extended force field parametrization based solely on the DFT calculations with additional experimental refinement of Zn-O (water) bond length.

Our experimental searches using Cambridge Structural Database (CSD) yielded only three structures with apical water ligand. Although this search were restricted to a central ZPW motif and excludes the polymeric Zn-O (carboxylate) contacts, catena-(tetrakis(μ_6-1,1',1''-(1,3,5-triazine-2,4,6-triyl)tripiperidine-4-carboxylic acid)-hexaaqua-hexa-zinc[37] pyridine dimethyl sulfoxide solvate (CSD refcode WUHHEN) was obtained.[38] This compound is actually a MOF, and has a number of anomalous structural features as shown in Figure 4.4 (right). It is obvious that the carboxylate are oddly coordinated and the internal Zn-O and C-O distances are very asymmetric. Initially, we thought that the asymmetrical ZPW motif was caused by the apical water ligand. However, the overall R factor for the experimental refinement is relatively high (8.4 %), and the other two obtained structures (CSD refcode; HIQVUZ [39] and HOPTUC [40]) were ordered normally. This led us to do further DFT study on WUHHEN using high quality protocol (BP86/SVP/COSMO (water)). The resulting DFT-optimized structure has corrected the uncertainty parameters derived from experimental X-ray diffraction data as illustrated in Figure 4.4 (left).
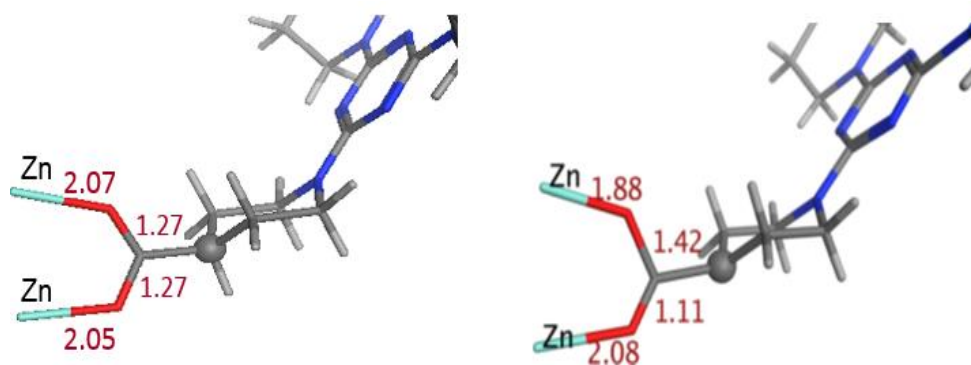
Figure 4.4; Local detail of carboxylate coordination in WUHHEN. Right structure shows the X-ray anomalously data and the left one shows the DFT-optimized structure. Bond length (Å) shown in dark red. One hydrogen is missing off the highlighted carbon (gray sphere).

The original ZPW-FF successfully reproduced the overall ZPW systems including their parameters and metal centers geometries, whether containing five- or four-coordinate zinc centres. The CSD examples and the DFT studies show that the five-coordinate zinc is approximately square pyramidal (SQP), especially when capped by nitrogen donor ligands. However, as there are no electronic effects in d^{10} Zn^{II}, they also should prefer adopting trigonal bipyramidal (TBP) structure. Unfortunately, there is no good experimental examples of TBP geometry. However, it is clearly observed computationally (DFT) when water is in the apical position (Figure 4.5). The energy differences between SQP and TBP coordination geometries is very small and readily undergo the Berry pseudorotation, which means that the transition from SQP to TBP or vice versa is relatively easy. Additionally, our previous DFT study on the four-coordinate Zn centres shows that the ground state geometry of uncapped ZPW systems is largely distorted and adopts a tetrahedral (TH) geometry. The SQP and TH

structures are already reproduced by our original ZPW-FF. However, as this work deals with ZPW systems containing water apical ligand, the TBP theoretical structures should be also reproduced by the ZPW-FF.
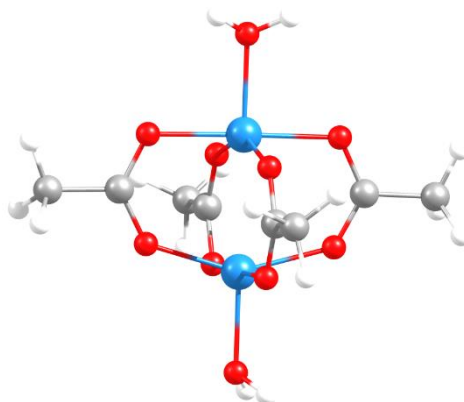
Figure 4.5; Optimized DFT structure of $Zn_2PCH_3.2H_2O$ system showing TBP geometry for zinc centres (Zn blue, O red, C gray and H white).

As the ZPW unit parameters are included already in the ZPW-FF, the Zn-O (water) relative parameters are required. Therefore, eight new ZPW systems containing one or two water capping groups, L, have been constructed with various carboxylates species, including formate, acetate, trifluroaoacetate, and benzoic acids (R= H, CH_3, CF_3 or benzene). Using these carboxylates species was motivated from a consideration of pK_a values ranging from the higher acetic acid (4.76) to the lowest trifluoroacetic acid (0.23). Benzoic and formate acids are intermediate which would contribute to span the relevant pK_a range. Benzoic acid was not in the training set of the original ZPW-FF. However, it is very important here as the validation experimental data is very lack. Therefore, there are two complexes for each carboxylate species represented by a general formula ZnPR.nL, where 'n' and 'ZnP' represent the number of apical water and the $Zn_2(O_2C)_4$ core of the ZPW respectively(Figure 4.6).
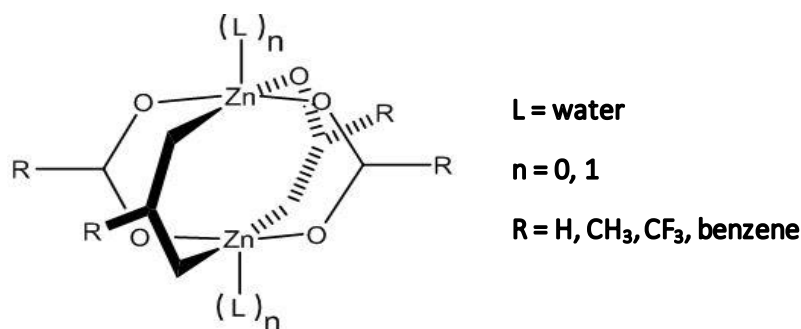
Figure 4.6; Schematic representation of the ZnPR.nL systems used for initial training.

The DFT calculations have revealed that the zinc centres with apical water sites prefer the TBP geometry. Moreover, the one capped site system shows that the five-coordinated zinc centre have adopted TBP geometry while the bare zinc centre is approximately tetrahedral. Nevertheless, we notice that the bond lengths and angles bending values of ZPW units, including the explicit Zn-Zn bond, do not vary very much from the previous N capping ZPW systems training sets. Hence, we focused only on the relative LFMM parameters between zinc metal centres and apical water ligands.

Despite there being no d-electron effects for Zn [37], the ligand field molecular mechanics (LFMM) method [36] as implemented within DommiMOE [32], our extended version of the molecular operating environment, [33] was used. The parameters for the ZPW unit, such as Zn-L-A angle bending (θ_0 and k_θ) and Zn-L-A-B torsional twisting (V_2 which favors torsions of 0 and 180 °) are already available in ZPW-FF. Thus, the required MMFF94 ligand parameters atom types are OH2 and HOH which refer to oxygen and hydrogen atoms in water respectively. The LFMM parameters for Zn-water bond stretching (Morse function r_0 and α) and ligand-ligand repulsion (A_{LL}) were manually optimized based on the training data to minimize the RMSD in Zn-O bonds

and heavy-atom (i.e. non-hydrogen) overlays. In addition, the partial atomic charges for Zn [37] attached to water (Zn+2), OH2, and HOH atoms type were augmented to ZPW-FF and set to 1.68, -0.71 and 0.43 respectively. These atomic charges were based on the Mulliken charge changes between coordinated and uncoordinated water ligand onto the existing bond charge increment (bci) scheme from the previously published Mn [37] FF.[41] The partial atomic charge values for the current ZPW-FF are listed in Table 4.1 along with the standard MMFF94 values for comparison.

Table 4.1; The partial atomic charges for MMFF94 implementation of ZPW-FF. Standard MMFF94 charges in parentheses.

Atom type	Environment	New partial charges (Standard MMFF94 charge)
OX	All	-0.72 (-0.90)
N	NH_3	-0.90 (-1.08)
HN	NH_3	0.43 (0.36)
OH2	O (water)	-0.71 (-0.86)
HOH	H (water)	0.43 (0.43)
N	$N(Csp^3)_3$	-0.63 (-0.81)
C	Adjacent to $N(Csp^3)_3$	0.34 (0.27)
NPYD	All	-0.42 (-0.62)
Car	Adjacent to NPYD	0.23 (0.16)
HC	H-C-NPYD	0.23 (0.15)
CO2M	C of formate	0.74 (1.02)
CO2M	C connected to sp^3 carbon	0.626 (0.906)
Zn+2	four carboxylates	1.84
Zn+2	four carboxylates + N	1.45
Zn+2	four carboxylates + NPYD	1.34
Zn+2	four carboxylates + OH2	1.68

The new version of ZPW-FF (shown in Appendix 1) reproduced successfully the DFT-optimized structures for all eight models, including their ZPW motif parameters and the TBP distortion behavior of the zinc metals coordinated to water. However, the distance values between zinc and water required further refinement based on the available experimental X-ray structural data, where the Zn-O (water) bond lengths average is 1.97 Å. After a minor adjustment on the Zn-O (water) bond distance parameter, the ZPW-FF delivers better structural accuracy, and the systematic error for the Zn-O (water) bond lengths (~ 2.06 Å) arising from DFT was corrected. It also reduces the TBP distortion behavior of some zinc centers which lead to increase the overall RMSD for Zn-L distances and heavy atom (i.e., non-hydrogen) overlays to be 0.03 Å and 0.22 Å respectively. However, the detailed variation in bond lengths, angles, and the metals geometries for all models are remarkably well reproduced by the ZPW-FF.

The highest RMSD value of Zn-L distance is 0.048 Å for the $Zn_2PCH_3.2H_2O$ model which also has the largest individual error for a single Zn-O (water) bond length at 0.09 Å. In addition, the MM optimizations revealed that both metal centres of this complex adopt approximately SQP geometry while all other models prefer TBP structure. We note that the reason behind adapting these geometries, in both DFT and ZPW-FF, is the orientation of the apical water molecule as illustrated in Figure 4.7. This has convinced us to employ the current ZPW-FF on real experimental complexes.

SQP   **TBP**
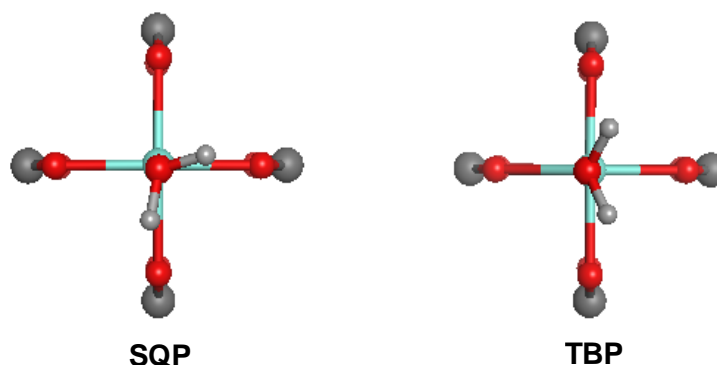
Figure 4.7; The possible rotations of the apical water ligand those identify the ZPW motif geometries. These models are obtained by MM optimization which are clearly revealed both geometries based on the rotations of water.

For more validation, the current ZPW-FF was employed on the DFT-optimized structures of Catena(tetrakis(m2-Benzoato-O,O')-diaqua-di-zinc[37] tetrakis(m2-1,2-bis(4-pyridyl)ethane-N,N')-octakis(benzoato-O)-tetra-zinc[37])complex (CSD refcode; HOPTUC) and WHHHEN (see Figure 4.8 for overlaid structures). The chosen DFT methodology enforces Zn [37] metal centres to adopt TBP geometry and overestimates the Zn-O (water) distance by around 0.07 Å. In addition, the Zn-Zn distance is underestimated by around 0.16 Å. The ZPW-FF has corrected these distance errors and reproduces the metal centre geometries related to the apical water possible orientations very well. The above results give us confidence to use ZPW-FF for modelling more complicated ZPW MOFs systems with capping water ligands, or modify existing systems with capping dabco ligand.
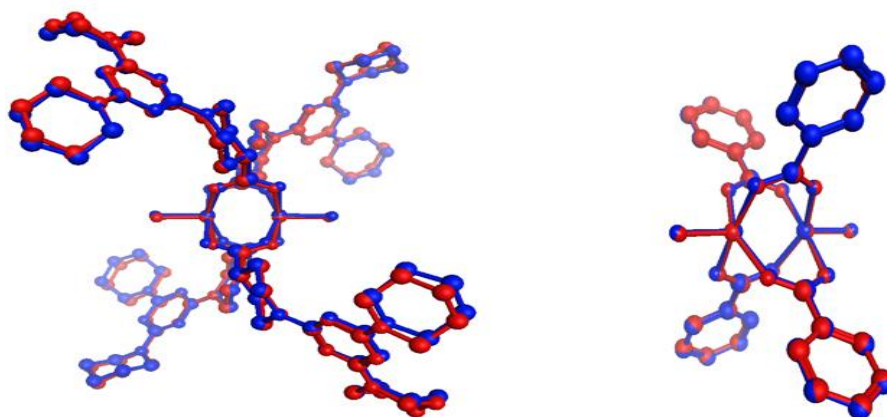
Figure 4.8; Overlays of DFT (blue) and MM-optimised [42] structures for the available ZPW systems. Hydrogens omitted for clarity.

4.3.1 Modelling MOFs with a water surface

Our original ZPW-FF has reproduced the flexible model $[Zn_2(bdc)_2(dabco)]_n$ (Figure 4.1) very well, including inter- and intra-molecular interactions both within the framework and between the framework and adsorbed species.[19] Therefore, extending ZPW-FF for ZPW systems with apical water ligand motivated us to modelling more ZPW MOFs systems under humid conditions, which could help in evaluating them before used in the real-world.

Our preliminary investigation was to replace the top surface dabco molecules of $[Zn_2(bdc)_2(dabco)]_n$ model by water ligands to assess the effects of the water vapor on this model. All the possible distortions shown in Figure 4.1 were considered, including 1 and 9-pores models. The MM-optimized pores are not effected too much and consistent with our previous results with dabco top surface model. However, MD annealing simulation on 1 and 9- pores models shows that each pore has lost one adsorbed molecule (whether for benzene or DMF adsorbate models) when the

temperature exceed 165 K. A further loss is observed by increasing the temperature to 330 K. We notice that benzene molecule left the pore from the water surface side without any interactions with the framework functional groups. However, the DMF adsorbate model observed two possible evacuating mechanisms. Sometimes the DMF molecule forms H-bonding interaction with the water ligand and sometimes left the pore without any interactions (Figure 4.9). These mechanisms were favor by the arrangement of both DMF adsorbed molecules and water ligands on the top surface. This observation has motivated us to run our ZPW-FF on real ZPW MOFs systems containing apical water ligand. Unfortunately, there is no existing systems with benzene adsorbate spices.
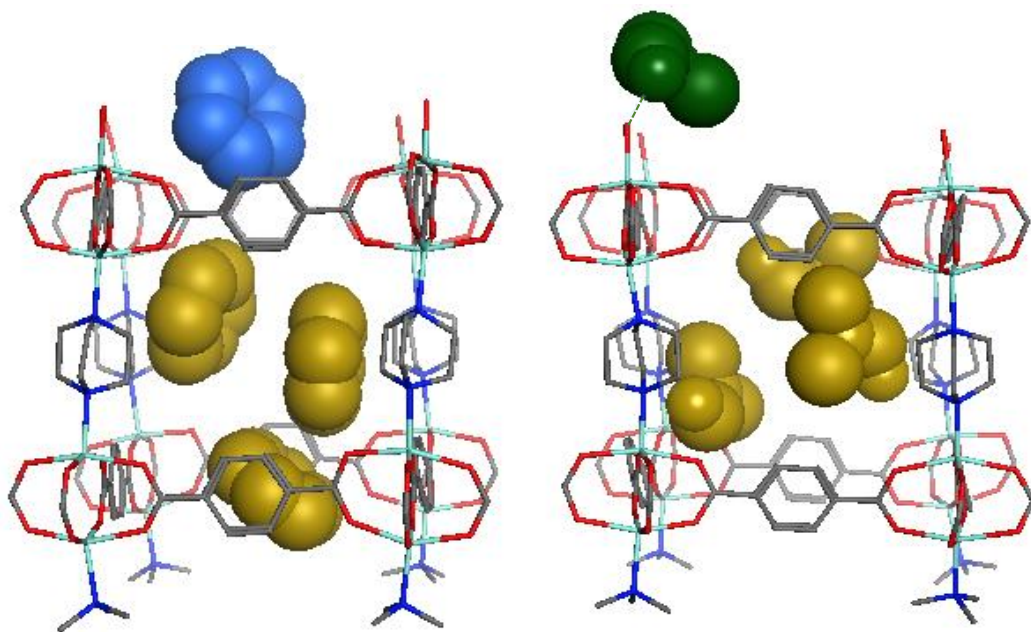
Figure 4.9; ZPW-FF simulated annealing starting from the energy-optimized, 1 pore model showing that of the guest molecules (benzene blue, left and DMF dark green, right) ejected the pore from the water top surface side. The DMF model has shown H-bonding between water molecule and the DMF (highlighted by dotted green line).

4.3.2 Modeling MOF-2

One of the most common MOFs systems is MOF-2, which comprises Zn (bdc)(H_2O).(dmf) building units. However, we considers here only (4,4) net packing model of MOF-2. Although, many fundamental thermal, mechanical, and dielectric properties are not available in this study, the results reported below can be useful in future development of fully periodic MOF-2, using our DL_POLY_LF_ platform.[43]

The current ZPW-FF has reproduced the building block unite accurately and overestimated the H-bonding interaction between water and DMF molecules. The atomic charges and the orientation of the DMF molecules were modified manually to reproduce the experimental structure and strength the interactions between inter water and DMF.[23] Figure 4.10 shows the new charge scheme for DMF molecule in modelling MOF-2 systems.[21, 22] We recognize that changing DMF atomic charges would effects the total energy of whole system. However, this study considers only the pore size/shape and the behavior of DMF guest molecules inside MOF-2 voids. The acetic acids on bdc were replaced by hydrogen atoms to facilitate MM optimization. Subsequently, the MM optimized structure was in good agreement with experimental data. However, the H-bonding interaction between water ligand and the DMF guest molecule are underestimated by 0.12 Å. Nevertheless, these findings permit us to model two-dimensional layered framework and layer-by-layer stacking model of MOF-2.
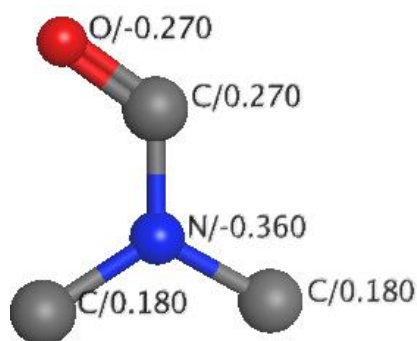
Figure 4.10; The new charge scheme for DMF guest molecules inside MOF-2 cavities.

The builder tool available in the MOE software was used for constructing a neutral 2D layer of MOF-2 without DMF molecules. The pore size/shape of the MM optimized model was in excellent agreement with the experimental model (Figure. 4.11).[22] However, filling each void by 2 DMF molecules leads to deviation in the main plane of the 2D model.[39] This is favored by the interactions between water and DMF adsorbate species. Other DMF molecules were held in the pores by van der Waals interactions with the framework. These results were sufficient to move on and modelling three-dimensional model of MOF-2 system.
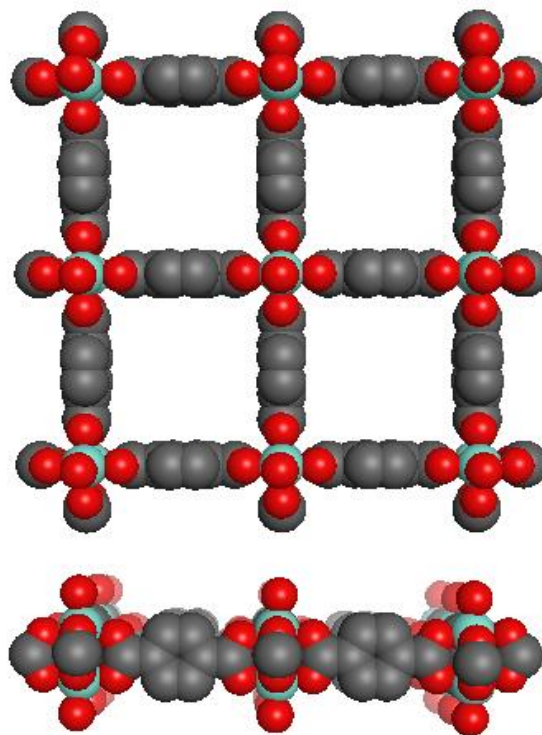
Figure 4.11; The MM-optimized neutral two-dimensional layered framework of MOF-2 without DMF quest molecules. The top represents the optimized structure along the vertical direction, while the down along the horizontal direction.

Constructing a layer-by-layer stacking 3D model of MOF-2 was quite challenge. In this system, the layers are held together along *a* axis by H-bonding interactions between the inter coordinated water ligands of one layer and carboxyl groups of adjacent layer. Thus, the orientations of water ligands between layers were identified carefully considering all possible H-bonding interactions, either with carboxylate oxygens from adjacent layer or with DMF guest molecules. Then, we stacked two layers together carefully and run MM optimization. At first sight, the size/shape of pores and the orientation of DMF species of MM-optimized structure were in good agreement with experimental data. However, the complicated interactions between

two layers result in some disagreement, particularly for the H-bonding lengths and the unit cell dimensions.[21] In addition, the MD simulations studies could not successfully represent the movement behavior of DMF guest molecules inside the cavities. These shortcomings required a little systematic modifications on the atomic charges of the inter water ligands.

The atomic charges of the inter water ligands were modified with O and H atom charges set at -0.31 and 0.23 respectively. Subsequently, the MM-optimized structure was in good agreement with the experimental structural data, including the H-bonding lengths. In addition, the calculated unit cell dimension (*Triclinic*) of a= 6.85 Å of (4,4) nets pack model are sufficiently close to experiment (6.97 Å).[39] In addition, the position of DMF guest molecules are also reproduced well compared to the experimentally-suggested position, where some DMF molecules are held by water ligand and others by van der Waals interactions with the bdc framework as shown in Figure 4.12. The average of the H-bonding length between water and DMF is 2.64 Å which is close to the experimental value 2.60 Å.[21] The MD simulations show that each MOF-2 pore contains only 2 DMF molecules held by the inter water ligands via H-bonding. Others DMF species pushed out through top and/or down surfaces of the model.
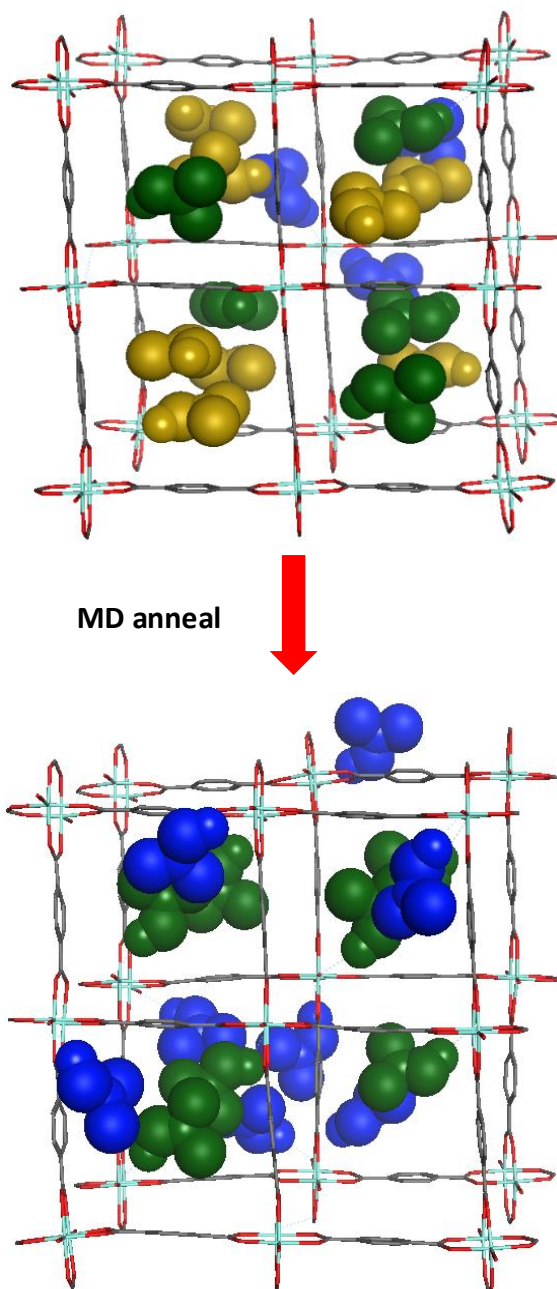
Figure 4.12; MM calculations of 3D layer-by-layer model in the crystal of MOF-2. The top model is the MM-optimized structure, the bottom is MD annealing of the top. The DMF guest molecules are represented with space-filling spheres. The yellow spheres for the DMF molecules held in voids by vdW interaction with bdc linker, dark blue spheres for ejected DMF molecules, and the green spheres for the DMF molecules held by inter water ligand. Almost Each voids held 2 DMF guest molecules.

However, these new charges sets are only for modelling the complicated layer-by-layer stacking model of MOF-2 and are not included in the current ZPW-FF. In addition, we recognize that these changes may give an issue in the future development of MOF-2 system especially when mechanical, thermal and dielectric properties are of interest. This situation can be fixed in future by creating new atomic types in our ZPW-FF for the water ligand atoms (O and H) connected to carboxylate oxygen atoms by H-bonding. However, at this stage we believe that modifying the atomic charge of inter water ligand manually is sufficient for two reasons. The first is that our charge scheme within ZPW-FF has successfully reproduced all ZPW complexes with apical water ligand very well, whether for the simple systems model we made or the experimental systems extracted from CSD. Thus, modifying the whole charge scheme will absolutely affect our previous results for ZPW systems, including systems with apical nitrogen donor. The second reason is that these new atomic charges sets for inter water ligand atoms are only required for modeling specific layer stacking models of MOF-2. This includes the inherent feature of the pore and DMF guest behaviors inside the voids which could help developing the system itself or modelling others MOFs systems based on our findings.

Finally, a number of short 450 K MD simulations were run on the final MM-optimized (4,4) net MOF-2 model for further comparison between our findings and experimental data.[22] Again, we notice that each void accommodates only 2 DMF held by H-bonding interaction between inter water and DMF guest molecules. In addition, all others DMF guest molecules were leaving the voids at about 150 K. The distance between inter water ligands and carboxylates groups form the adjacent layer was increased by about 1 Å at 450 K. These observations are quite close to the experimental data which

revealed that the weight of MOF-2 is reduced by increasing the temperature above 160 K. In addition, increasing the distance between layers represents the decomposition process of the MOF-2 framework at 400 K.

All of these results can drive some ideas for developing ZPW MOFs systems in the presence of water vapor. Modelling MOF-2 system and the arrangement of the DMF adsorbate spices inside its voids can also be used as a base for more dynamics studies in the future. However, this study can at least demonstrate that the new version of our ZPW-FF should provide an excellent platform for modelling more ZPW MOFs systems, whether capping by nitrogen-donor ligands or water.

4.4 Conclusion

An extended version of the first-principles ZPW-FF has been developed for the zinc paddlewheel motif including water capping group. The training data was based on DFT-computed structures of various ZPW simple models containing mono- and di-capped water ligands. A minor refinement of Morse function reference distances for Zn-O(water) bond was based on three experimental complexes. The new ZPW-FF reproduces accurately the DFT-computed models and the available crystallographically-characterized ZPW complexes with apical water ligand.

These findings permit us to apply the new ZPW-FF to isolated ZPW systems or to materials such as MOFs with ZPW multiple building units capped by N-based ligands or water. This can also be used for constructing aperiodic ZPW MOFs pores or modifying existing systems by replacing nitrogen ligands by water and vice versa.

Consequently, the current FF can be useful for solving many industrial issues of MOFs under water atmosphere.

The pore model of flexible $[Zn_2(bdc)_2(dabco)]_n$ was modified by replacing the top dabco surface by water. The new FF was applied to the modified model to assess the effects of water vapor on this model. The MM and MD calculations have revealed that the number and the positions of benzene and DMF guest molecules are affected too much in presence of water. A further MM/MD studies have been done on (4,4) net packing crystal of MOF-2 which comprises $Zn (bdc)(H_2O).(dmf)$ building units. After a little modification on DMF atomic charges and inter water ligands, the ZPW-FF reproduces aperiodic model of MOF-2 very well. In addition, the MD simulations show that the MOF-2 sustain only two DMF molecules held by inter water ligands via hydrogen-bonding interactions. The bond length distances and unite cell dimensions of MOF-2 are well reproduced by the new version of ZPW-FF.

Overall, the performance of ZPW-FF is extremely good and more efficient than DFT, at least for isolated ZPW complexes. It also provides a sufficient results for complicated MOFs such as MOF-2 and can be extended to other more complicated systems comprising ZPW units. Since the ability of modelling periodic systems in MOE software is limited, our next goal is to transfer the current FF to DL_POLY software. The latter has already LFMM functions which would facilitate the transformation process. Thus, we will be able to use our ZPW-FF for more studies of fully periodic systems in the near future.

4.5 References

1. L. R. MacGillivray, *Metal-organic frameworks: design and application*, John Wiley & Sons, 2010.

2. S. Horike, S. Shimomura and S. Kitagawa, *Nat. Chem.*, 2009, **1**, 695-704.

3. A. U. Czaja, N. Trukhan and U. Müller, *Chem. Soc. Rev.*, 2009, **38**, 1284-1293.

4. L. Sarkisov, R. L. Martin, M. Haranczyk and B. Smit, *J. Am. Chem. Soc.*, 2014, **136**, 2228-2231.

5. A. Schneemann, V. Bon, I. Schwedler, I. Senkovska, S. Kaskel and R. A. Fischer, *Chem. Soc. Rev.*, 2014, **43**, 6062-6096.

6. C. S. Hawes, Y. Nolvachai, C. Kulsing, G. P. Knowles, A. L. Chaffee, P. J. Marriott, S. R. Batten and D. R. Turner, *Chem. Commun.*, 2014, **50**, 3735-3737.

7. B. Li, H.-M. Wen, W. Zhou and B. Chen, *J. Phys. Chem. Lett.*, 2014, **5**, 3468-3479.

8. S. Mukherjee, B. Joarder, A. V. Desai, B. Manna, R. Krishna and S. K. Ghosh, *Inorg. Chem.*, 2015, **54**, 4403-4408.

9. Q.-G. Zhai, N. Bai, S. n. Li, X. Bu and P. Feng, *Inorg. Chem.*, 2015, **54**, 9862-9868.

10. M. Drobek, J.-H. Kim, M. Bechelany, C. Vallicari, A. Julbe and S. S. Kim, *ACS Appl. Mater. Interfaces.*, 2016, **8**, 8323-8328.

11. S.-m. Hyun, J. H. Lee, G. Y. Jung, Y. K. Kim, T. K. Kim, S. Jeoung, S. K. Kwak, D. Moon and H. R. Moon, *Inorg. Chem.*, 2016, **55**, 1920-1925.

12. Y. Yue, J. A. Rabone, H. Liu, S. M. Mahurin, M.-R. Li, H. Wang, Z. Lu, B. Chen, J. Wang and Y. Fang, *J. Phys. Chem. C*, 2015, **119**, 9442-9449.

13. L. Huang, H. Wang, J. Chen, Z. Wang, J. Sun, D. Zhao and Y. Yan, *Micropor. Mesopor. Mat.*, 2003, **58**, 105-114.

14. Y. Li and R. T. Yang, *Langmuir*, 2007, **23**, 12937-12944.

15. M. P. Suh, H. J. Park, T. K. Prasad and D.-W. Lim, *Chem. Rev.*, 2011, **112**, 782-835.

16. D. N. Dybtsev, H. Chun and K. Kim, *Angew. Chem.*, 2004, **116**, 5143-5146.

17. S. O. Odoh, C. J. Cramer, D. G. Truhlar and L. Gagliardi, *Chem. Rev.*, 2015, **115**, 6051-6111.

18. Q. Yang, D. Liu, C. Zhong and J.-R. Li, *Chem. Rev.*, 2013, **113**, 8261-8323.

19. K. A. Alzahrani and R. J. Deeth, *J. Mol. Model.*, 2016, **22**, 1-13.

20. K. Tan, N. Nijem, P. Canepa, Q. Gong, J. Li, T. Thonhauser and Y. J. Chabal, *arXiv preprint arXiv:1209.2564*, 2012.

21. H. Li, M. Eddaoudi, T. L. Groy and O. Yaghi, *J. Am. Chem. Soc.*, 1998, **120**, 8571-8572.

22. P.-Z. Li, Y. Maeda and Q. Xu, *Chem. Commun.*, 2011, **47**, 8436-8438.

23. V. Vasudevan and S. H. Mushrif, *J. Mol. Liq.*, 2015, **206**, 338-342.

24. F. Neese, U. Becker, D. Ganiouchine, S. Koßmann, T. Petrenko, C. Riplinger and F. Wennmohs, *Journal*, 2014.

25. A. D. Becke, *Phys. Rev. A*, 1988, **38**, 3098.

26. J. P. Perdew and W. Yue, *Phys. Rev. B.*, 1986, **33**, 8800.

27. A. Schäfer, H. Horn and R. Ahlrichs, *J. Chem. Phys*, 1992, **97**, 2571-2577.

28. R. K. Hocking, R. J. Deeth and T. W. Hambley, *Inorg. Chem.*, 2007, **46**, 8238-8244.

29. A. Klamt and V. Jonas, *J. Chem. Phys*, 1996, **105**, 9972-9981.

30. A. Klamt, *J. Phys. Chem.*, 1995, **99**, 2224-2235.

31. A. Klamt and G. Schüürmann, *J. Chem. Soc. Perkin. Trans. 2*, 1993, 799-805.

32. R. J. Deeth, N. Fey and B. Williams–Hubbard, *J. Comput. Chem.*, 2005, **26**, 123-130.

33. M. O. Environment, *Journal*, 2007.

34. T. A. Halgren, *J. Comput. Chem.*, 1999, **20**, 720-729.

35. T. A. Halgren, *J. Comput. Chem.*, 1999, **20**, 730-748.

36. R. J. Deeth and D. L. Foulis, *PCCP*, 2002, **4**, 4292-4297.

37. W. Lu, Z. Wei, Z.-Y. Gu, T.-F. Liu, J. Park, J. Park, J. Tian, M. Zhang, Q. Zhang and T. Gentle III, *Chem. Soc. Rev.*, 2014, **43**, 5561-5593.

38. X. Zhao, H. He, T. Hu, F. Dai and D. Sun, *Inorg. Chem.*, 2009, **48**, 8057-8059.

39. F.-K. Wang, S.-Y. Yang, R.-B. Huang, L.-S. Zheng and S. R. Batten, *CrystEngComm*, 2008, **10**, 1211-1215.

40. H. Kwak, S. H. Lee, S. H. Kim, Y. M. Lee, B. K. Park, Y. J. Lee, J. Y. Jun, C. Kim, S.-J. Kim and Y. Kim, *Polyhedron*, 2009, **28**, 553-561.

41. R. J. Deeth, *Inorg. Chem.*, 2008, **47**, 6711-6725.

42. V. S. Allured, C. M. Kelly and C. R. Landis, *J. Am. Chem. Soc.*, 1991, **113**, 1-12.

43. H.-C. Tai, R. Brodbeck, J. Kasparkova, N. J. Farrer, V. Brabec, P. J. Sadler and R. J. Deeth, *Inorg. Chem.*, 2012, **51**, 6830-6841.

Chapter 5: Density Functional Calculations Reveal a Flexible Version of the Copper Paddlewheel Unit: Implications for Metal Organic Frameworks

5.1 Introduction

Metal Organic Frameworks (MOFs) are porous materials with many potential applications in gas storage, separations and catalysis.[1] They consist of nodes, either transition metal centres or small clusters, connected by organic linkers, often polytopic carboxylates. The resulting frameworks are often sufficiently rigid to allow molecules adsorbed in the pores to be removed or replaced without the framework collapsing.

Flexible MOFs are an interesting development.[2] The pore size and/or shape responds to the adsorbed species, a property which suggests applications in selectivity and separations. An early example of such flexible MOFs was $[Zn(bdc)_2(dabco)]_n$ (bdc = 1,4-benzenedicarboxylate; dabco = 1,4-diazabicyclo- (2.2.2) octane) which contains layers of four-bladed paddlewheel $\{Zn_2(O_2CR)_4\}$ units connected by dabco pillars.[3] The unit cell of this material is sensitive to adsorbed species (Figure 5.1).

The paddle-wheel motif (Figure 5.2) is common in flexible MOFs with many zinc and copper examples. Zn^4-based systems are considered to be more flexible than comparable Cu^4 paddlewheel (CPW) MOFs and this has been attributed to their respective electronic structures.[5] The d^{10} Zn^4 centres have no particular electronic preference so a pentacoordinated Zn^4 would be expected to adopt a trigonal bipyramidal (TBP) structure. This occurs when the axial group is a water ligand (as shown in Chapter 4) but N donors favour a square pyramidal (SQP) structure.[6]

However, the TBP and SQP coordination geometries have similar energies (cf. the Berry pseudorotation) and the transition from TBP to SQP or vice versa is relatively easy. Hence, the zinc paddlewheel (ZPW) unit is relatively flexible.
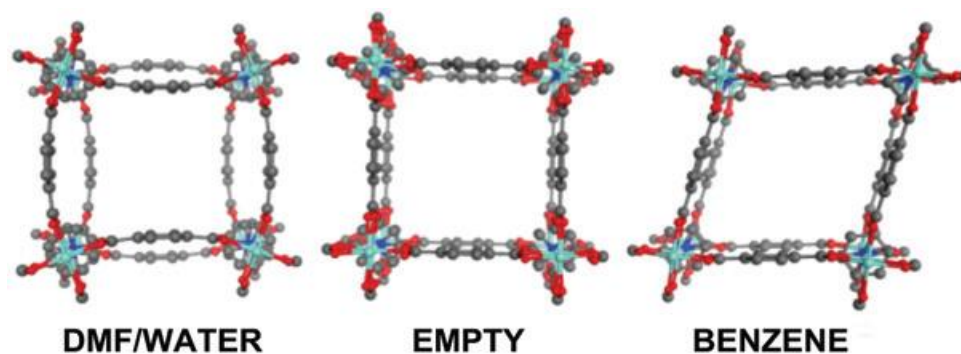
Figure 5.1; Unit cell of $[Zn(bdc)_2(dabco)]_n$. Left: as-synthesised material with four dimethylformamides and a water molecule; centre: after evacuation; right: after uptake of four benzene molecules. (Adsorbed species and H atoms omitted for clarity.)
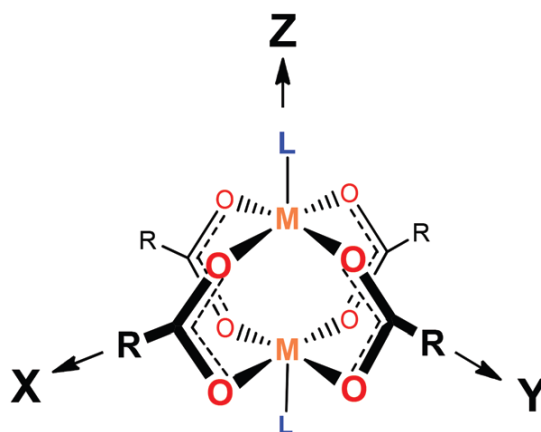
Figure 5.2; Schematic representation of four-bladed paddlewheel complex.

In contrast, d^9 Cu^4 CPW centres show a preference for planar CuO_4 coordination with the unpaired electron being in the $d_{x^2-y^2}$ orbitals on each metal. We will call this state T_0 since geometry optimisations are carried out on the ferromagnetic spin triplet surface. We note that while the true ground states are the anti-ferromagnetically coupled singlet states, the structures of CPWs are not sensitive to this coupling (see Appendix 2).

For T_0, the 'hole' in the otherwise filled d shell on each metal is localised in the equatorial plane leading to a 'stereochemical activity' which shortens the Cu–O distances and concomitantly lengthens the bond to the axial ligand.[7] This is the same mechanism by which the Jahn–Teller elongation of six-coordinate Cu^4 complexes may be rationalised.[8]

These observations also lead to a dilemma. Since pentacoordinate species are inherently flexible and Cu^4 centres are strongly Jahn–Teller active, CPW units should be more flexible than their zinc counterparts. Density functional theory calculations on $[Cu_2(O_2CR)_4L_2]$ systems reveal a change in ground state with increasing Cu–L bond strength. For L = N-heterocyclic carbene (NHC), the Jahn–Teller axis switches from parallel to orthogonal to the Cu–Cu vector and the copper coordination geometry becomes highly flexible. While the calculated dimer/monomer equilibrium for isolated complexes slightly favours monomers, the preformed paddlewheel units embedded in many metal organic frameworks are potential targets for developing novel materials.

5.2 Theoretical methods

Most calculations used ORCA version 3.0.3.[9] A typical geometry optimisation/frequency calculation employed the Becke-Perdew functional, def2-SVP basis sets, a COSMO solvation field with water as the solvent and, for the NHC systems, the Grimme D3 dispersion corrections. For copper species, a spin-unrestricted formalism was employed with a total spin $S = 1$.

Magnetic coupling constants employed the broken-symmetry [10] scheme implemented in ORCA (FlipSpin) and used the B3LYP functional with def2-TZVP basis sets and the COSMO(water) solvation field. BS geometry optimisations included Grimme's D3 correction.

The structural studies were based on the spin triplet potential energy surface rather than the BS surface for two reasons. Firstly, we found no significant geometry change between the structure optimised on the (ferromagnetic) triplet state and the BS solution. The effect on the magnetic coupling was noticeable but does not change our conclusions. For the symmetric TBP NHC system, $[Cu_2(acetate)_4(Me_2NHC)_2]$, the computed J value for the $S = 1$ geometry is -139.55 cm^{-1} and for the BS geometry, $J = -166.35$ cm^{-1}. Secondly, while geometry optimisations were possible on the BS surface, numerical frequency calculations (necessary since we were using a COSMO field) were unstable. We thus opted to use the triplet surface throughout.

The high-symmetry (constrained) optimisations used the Amsterdam Density Functional 2014 code[11-13] since, in our hands, we find it more convenient than ORCA when specifying particular electronic configurations. Geometry optimisations employed the Becke-Perdew functional with DZP basis sets on all atoms apart from

the metals for which TZP bases were employed. Small frozen cores were selected and a COSMO(water) correction, as implemented in ADF, was used. Given the qualitative nature of the high-symmetry study, we did not bother with any dispersion corrections nor were vibrational frequencies computed.

5.3 Results and discussion

In mononuclear CuL_6 complexes, the first-order Mexican hat potential energy surface shows that all the structures in the circular minimum have the same energy despite the large bond length fluctuations associated with the change from a tetragonal elongation along one Cartesian axis through a series of rhombic distortions to a tetragonally compressed structure along a different axis.[14]

Evidently, the copper centres in the CPW moiety behave differently to a typical CuL_6 system. The first indication of this was the anomalously low magnetic moment for the archetypal CPW $[Cu_2(acetate)_4(OH_2)_2]$.[15] The structure of copper acetate dihydrate was unknown but when its dinuclear nature was revealed,[16] the magnetic behaviour could be correlated with anti-ferromagnetic coupling between the two unpaired $d_{x^2-y^2}$ electrons. All subsequent studies on copper acetate and related CPW systems have concentrated on characterising the details of this coupling. There does not appear to have been any previous attempt to locate other local minima.

Our first step was to search for a 'compressed' CPW form. Using the spin triplet surface of $[Cu_2(formate)_4(OH_2)_2]$ as a model, all our DFT optimisations collapsed back to the elongated form. However, for $[Cu_2(formate)_4(NH_3)_2]$ a second stable configuration was located (Figure 5.3). Interestingly, this does not correspond to a fully compressed structure which would have d_{z^2} as the singly occupied d orbital on

each copper. Instead, the spin density distribution corresponds to a mixed $d_x^2-y^2/d_z^2$ configuration. We call this state T_M (Figure 5.3, right).
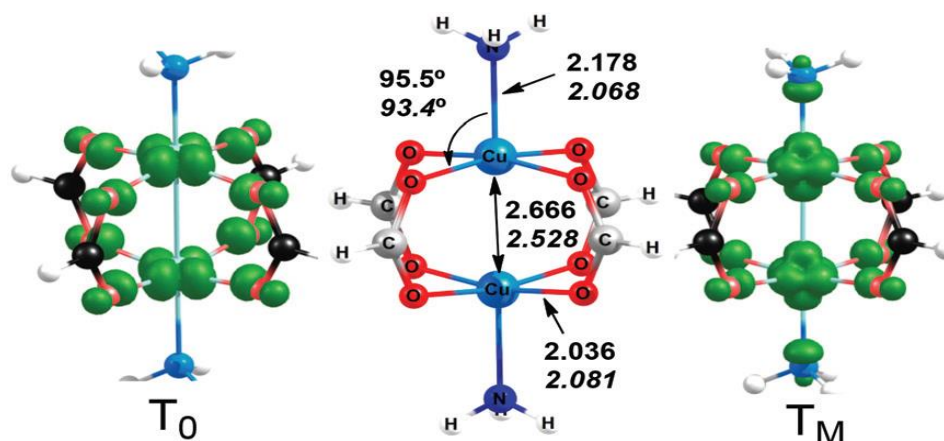
Figure 5.3; Centre: selected calculated geometrical data for $[Cu_2(formate)_4(NH_3)_2]$. Normal text for elongated $d_x^2-y^2/d_x^2-y^2$ state (T_0) structure; italics for mixed $d_x^2-y^2/d_z^2$ state (T_M) structure. Spin density plots to left and right.

Qualitatively, the presence of this new state is easy to understand. Following Hay, Thibeault and Hoffmann's analysis,[17] the 'normal' (i.e. elongated) CPW electronic structure arises from joining two isolated square pyramidal copper species where the apical direction lies parallel to the Cu–Cu vector. This leads to $d_x^2-y^2$ lying above d_z^2 as shown on the left of Figure 5.4. Focusing on the valence, mainly-d orbitals, we generate symmetric (S) and antisymmetric (A) combinations in the dimer. Since the 'equatorial' orbitals $d_x^2-y^2$ are oriented for metal–metal δ-bonding which is, at best, very weak, the splitting of the symmetric (S_{Eq}) and antisymmetric (A_{Eq}) molecular orbitals is relatively small, the triplet and anti-ferromagnetic singlet states are close in energy and, at least from a structural perspective, the two ends of the CPW behave like

isolated pentacoordinate SQP copper complexes with comparatively short $Cu-O_{eq}$ bond lengths and a relatively long $Cu-L_{ax}$ bond.

With a stronger axial field generated by shortening the $Cu-NH_3$ and lengthening the $Cu-O$ bonds, d_z^2 becomes the highest energy d orbital for the isolated pentacoordinate system (Figure 5.4, right). In the dimer, these orbitals are oriented for metal-metal σ-bonding and the splitting between the S and A combinations is no longer small. The more one tries to force a stronger axial ligand field, the more stabilised the symmetric d_z^2 MO (S_{Ax}) becomes while the antisymmetric d_z^2 MO (A_{Ax}) is increasingly destabilised. The system becomes trapped in an intermediate 'mixed' state in which one unpaired electron occupies the A_{Ax} d_z^2 MO and the other the higher of the two $d_x^2{-}_{y^2}$ combinations which turns out to be S_{Eq}.
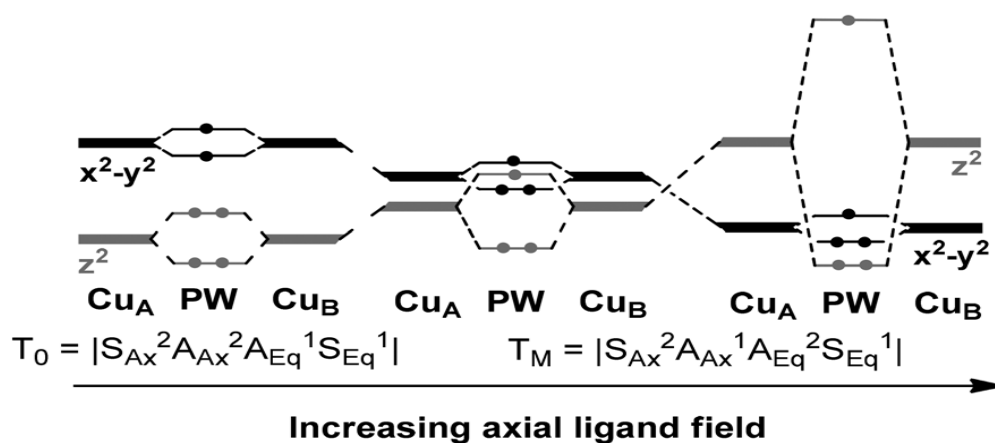
Figure 5.4; Schematic partial valence molecular orbital (MO) energy level diagram for copper paddlewheel systems as a function of increasing the axial ligand field. For the MOs, S refers to a symmetric (in-phase) combination of d orbitals, A to an asymmetric combination, Ax = d_z^2 and Eq = $d_x^2{-}_{y^2}$.

This new mixed $d_{x^2-y^2}/d_{z^2}$ state, T_M, is interesting in that the unpaired electron on each copper centre is shared between the $d_{x^2-y^2}$ and d_{z^2} orbitals. In the localised picture, we have a resonance mixing of two configurations, one with an unpaired electron in the d_{z^2} orbital on Cu_A and the other unpaired electron in the $d_{x^2-y^2}$ orbital on Cu_B, and vice versa.

For $[Cu_2(formate)_4(NH_3)_2]$, the mixed state is a local minimum but some 5–6 kcal mol^{-1} higher than the elongated state. However, it provides the clue that using stronger axial donors may eventually favour the mixed state.

In order to maintain strict control over the electronic states, we carried out a series of symmetry-restricted optimisations. These structures are only local minima with respect to the applied point group so the calculated values of $\Delta E(T_M - T_0)$ serve only as an approximate guide.

Table 5.1; Energy differences (kcal mol^{-1}) between T_M and T_0 states for symmetry restrained optimised CPW systems.

Complex	Point Group	BP86/DZP $\Delta E(T_M - T_0)$	B3LYPD/TZVP $\Delta E(T_M - T_0)$
CuPH.2H$_2$O	D$_{2h}$	16.42	
CuPCH$_3$.2H$_2$O	D$_2$	18.38	
CuPCH$_3$.2NH$_3$	C$_{2h}$	6.73	
CuPCH$_3$.2py	D$_2$	7.07	
CuPCH$_3$.2CN	D$_2$	4.46	
CuPCH$_3$.2NHC	C$_{2v}$	0.03	
CuPCF$_3$.2NHC	C$_{2v}$	-6.17	-2.42

Table 5.1 shows that $\Delta E(T_M - T_0)$ decreases with decreasing electronegativity of the axial donor, L, and decreasing pKa of the equatorial carboxylate. The former corresponds to increasing the covalency (and hence strength) of the axial ligand field while the latter corresponds to a progressive weakening of the equatorial field. The calculations suggest that the combination of a strong carboxylic acid (hence weak conjugate base) and a highly covalent axial group such as an N heterocyclic carbine (NHC) may be sufficient to make the T_M (i.e. mixed) state the lowest energy spin triplet.

To explore this possibility, we relaxed all symmetry constraints and carried out full optimisations and frequency calculations for N-methyl NHC complexes. The structures changed significantly compared to the symmetry-constrained cases and the T_M state becomes the lowest triplet state already for the acetato species.

The presence of the strong-field NHC groups completely change the coordination geometry compared to copper acetate dihydrate. The lowest-energy NHC structure has a 'symmetric' TBP geometry but with relatively long equatorial carboxylate bond lengths (2.14 Å) and short 'axial' carboxylate contacts of 2.01 Å (Figure 5.5, left). At almost the same energy is an 'asymmetric' TBP geometry (Figure 5.5, right) where the NHC moiety tilts towards an equatorial oxygen resulting in a lengthening of that Cu–O bond by ~0.1 Å while the other 'equatorial' Cu–O distance shortens by 0.07 Å. This type of structural change is well known for pentacoordinate Cu^4 species such as [Cu(bipy)$_2$Cl]$^+$ where the Cu–Cl distance increases from 2.26 Å to 2.36 Å as the equatorial N–Cu–N angle opposite opens up from ~97° to ~124°. Here, the energy difference between 'symmetric' and 'asymmetric' TBP-like structures is less than 1 kcal mol^{-1} which now mirrors simple mononuclear Cu^4 complexes where the d_z^2 and

$d_{x^2-y^2}$ orbitals mix freely. The shape of the 'hole' in the d shell, and its stereochemical activity, is thus highly variable resulting in significant changes in structure for almost no change in energy.

The structural change destroys the nominal tetragonal symmetry assumed in the construction of Figure 5.4 and thus muddies the distinction between Ax and Eq with regard to the d orbitals containing the unpaired spin. The dominant axis is now aligned along the shorter Cu–O$_{eq}$ bonds (Figure 5.6). Broken symmetry B3LYP calculations still show that the ground state is antiferromagnetically coupled ($J = -140$ cm^{-1}). The J value should be compared to $J = -240$ cm^{-1} calculated for copper acetate using the same protocol versus an experimental value of 286 cm^{-1}.

Figure 5.5; Optimised geometries for [Cu$_2$(acetate)$_4$(Me$_2$NHC)$_2$]. Top: complete structures; Middle and bottom: local geometrical detail around the metal centres. Numbers with two decimal places are distances in Å; those to one decimal place are angles in °.
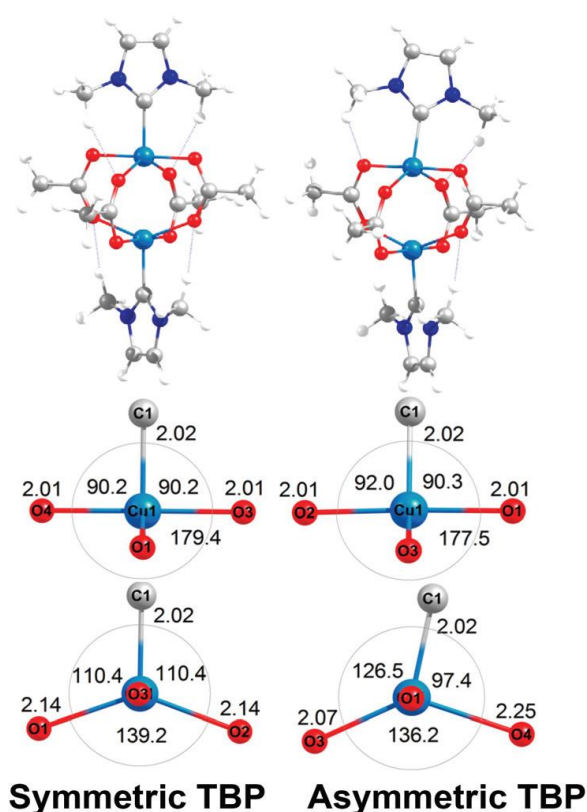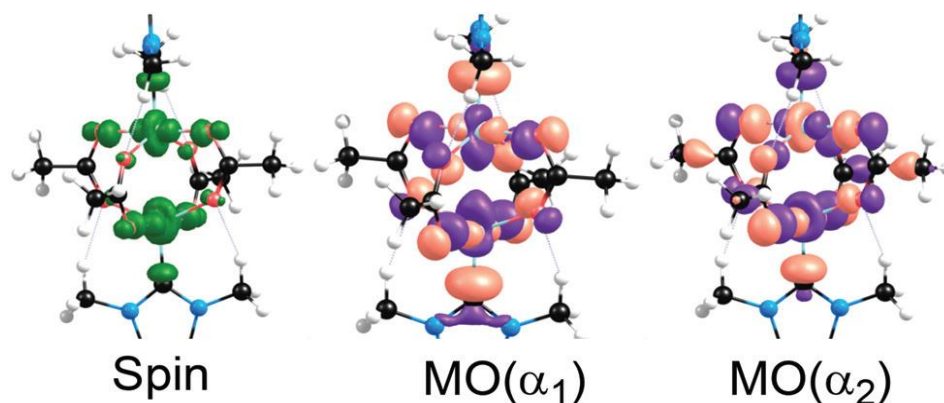
Figure 5.6; Spin density (left) and plots of the molecular orbital housing the two unpaired electrons for the symmetric TBP structure shown in Figure 5.5, left.

The change in electronic structure thus has a significant effect on the geometric structure and flexibility of the CPW. As shown schematically in Figure 5.7, the tilting of the NHC causes significant structural changes more, so when we consider that there is an equivalent tilting motion at right angles to that shown at the bottom of Figure 5.7.
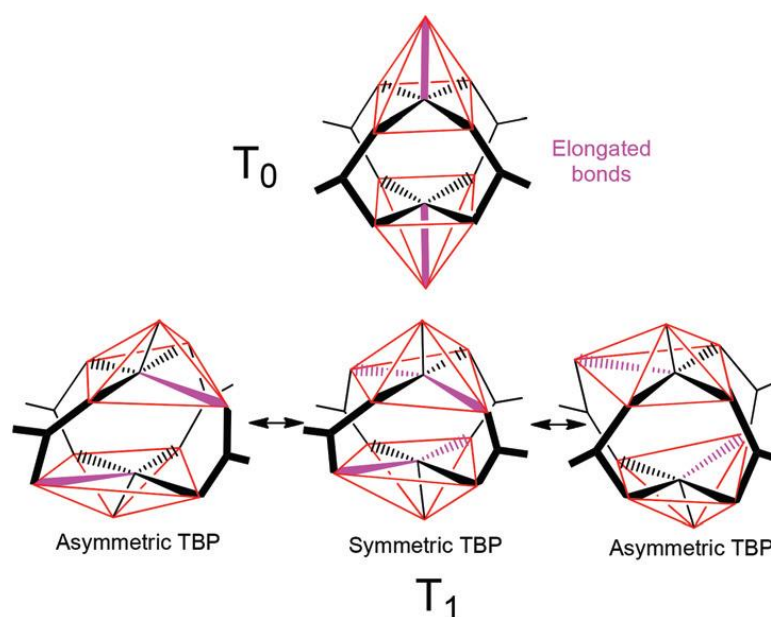
Figure 5.7; Schematic diagram of the sense of Jahn–Teller elongation (highlighted in pink) for CPW–NHC systems.

We believe these computational results might have significant implications for CPW MOFs. Given the existence of zinc paddlewheel complexes with NHC axial groups [18] (e.g. Cambridge Structural Database recode AZOGOL, Figure 5.8, top) plus an example of a Cu_4–carboxylate–NHC complex[19] (refcode QAXKAC, Figure 5.8, bottom), it appears that synthesising a CPW with NHC groups might be feasible. Computational support for this assertion is, firstly, that the NHC CPWs are true local minima on the potential energy surface. Secondly, the estimated ΔG values for acetato CPW complexes with three carbenes which span a range of pKa values[20] (see Appendix 2) is comparable to that for two corresponding QAXKAC-like monomers, being ∼8 to 10 kcal mol^{-1} in favour of the CPW at the BP86/SVP/D3 level and ∼1–2 kcal mol^{-1} less favourable at the B3LYP/TZVP/D3 broken symmetry level. Thus, while the thermodynamics may seem to favour monomers, a higher calculated free energy does not preclude the formation of the dimer and both monomer and dimer can be stable entities just as is observed for copper acetate hydrate where both the 'unexpected' monomer[21] and the 'normal' dimer [16] exist. However, obtaining the species with the higher free energy may require clever synthetic strategies. The formation of an NHC CPW directly from its components may fail but introducing the NHC to pre-formed CPWs, such as those often encountered in MOFs, may succeed.
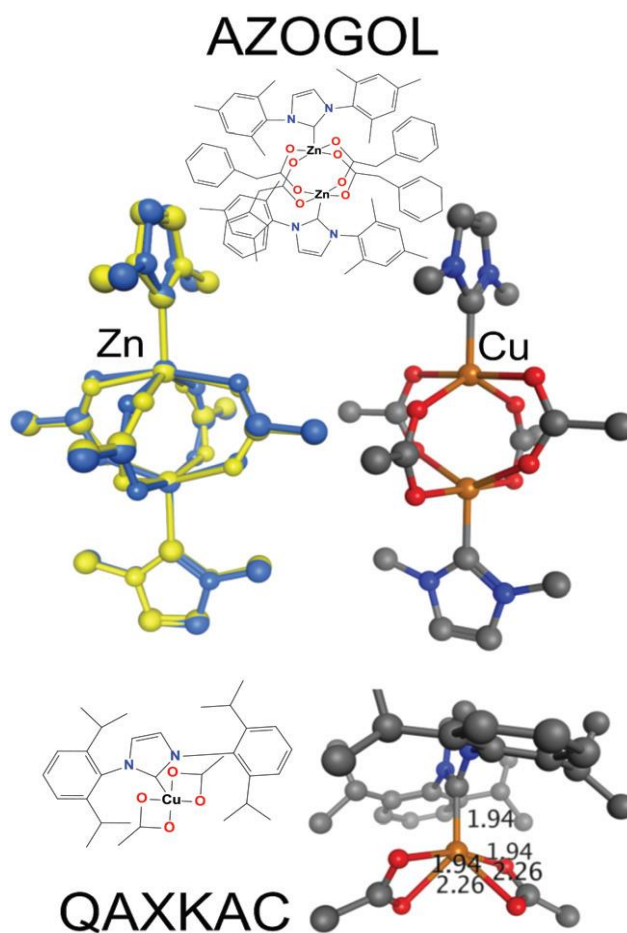
Figure 5.8; Illustrative metal–NHC complexes. AZOGOL is a zinc–NHC paddlewheel [$Zn_2(OC_2CH_2Ph)_4$(N-MesitylNHC)$_2$] while QAXKAC is Cu^4–{bis- (2,5-iPrPh)NHC}(acetate)$_2$. For the Zn complex, yellow corresponds to the X-ray structure, blue to the DFT optimisation. The CPW is also the computed geometry (BP86/SVP/D3/COSMO).

Several CPW MOFs have large enough pores to accommodate NHC capping groups.[22,] [23] The question will be whether the NHCs will coordinate to the copper sites and whether any barriers to dissociation are high enough. Simply increasing the Cu–Cu separation in an isolated NHC CPW rapidly increases the energy (As shown in Appendix 2) so the system is at least stable with respect to this dissociation route. Partial capping should also help keep the framework stable. If synthetic strategies to generate CPW NHC MOFs can be developed, the comparison of the structures of

AZOGOL with its copper analogue (Figure 5.8) suggests that a Cu–NHC MOF could behave quite differently to existing CPW MOFs.

5.4 Conclusion

Flexible MOFs are interesting[24] and while NHCs have been incorporated into MOFs,[25] simply attaching NHCs to the copper paddlewheel centres has, to our knowledge, not yet been reported. Given the predicted effects on the structures and the fact that the Cu[4]–NHC–carboxylate complex is a hydrosilylation precatalyst,[19] the properties of partially- or fully-capped NHC CPW MOFs, if they can be synthesised, are certain to be different and may potentially be very interesting compared to current systems. Chapter 6 explains our attempts for extending our first-principles ligand field molecular mechanics[26, 27] force field for zinc paddlewheels[28] to CPWs in order to model such systems.

5.5 references

1. D. Farrusseng, *Metal-organic frameworks: applications from catalysis to gas storage*, John Wiley & Sons, 2011.

2. A. Schneemann, V. Bon, I. Schwedler, I. Senkovska, S. Kaskel and R. A. Fischer, *Chem. Soc. Rev.*, 2014, **43**, 6062-6096.

3. D. N. Dybtsev, H. Chun and K. Kim, *Angew. Chem.*, 2004, **116**, 5143-5146.

4. W. Lu, Z. Wei, Z.-Y. Gu, T.-F. Liu, J. Park, J. Park, J. Tian, M. Zhang, Q. Zhang and T. Gentle III, *Chem. Soc. Rev.*, 2014, **43**, 5561-5593.

5. S. Bureekaew, S. Amirjalayer and R. Schmid, *J. Mater. Chem.*, 2012, **22**, 10249-10254.

6. S. Vagin, A. K. Ott and B. Rieger, *Chem. Ing. Tech.*, 2007, **79**, 767-780.

7. R. Deeth and M. Gerloch, *Inorg. Chem.*, 1985, **24**, 4490-4493.

8. R. J. Deeth and M. A. Hitchman, *Inorg. Chem.*, 1986, **25**, 1225-1233.

9. F. Neese, U. Becker, D. Ganiouchine, S. Koßmann, T. Petrenko, C. Riplinger and F. Wennmohs, *Journal*, 2014.

10. B. Hoskins and R. Robson, *J. Am. Chem. Soc.*, 1990, **112**, 1546-1554.

11. G. T. te Velde, F. M. Bickelhaupt, E. J. Baerends, C. F. Guerra, S. J. A. Van Gisbergen, J. G. Snijders and T. Ziegler, *J. Comput. Chem.*, 2001, **22**, 931-967.

12. C. Fonseca Guerra, J. G. Snijders, G. te Velde and E. J. Baerends, *Theor. Chem. Acc.*, 1998, **99**, 391.

13. E. J. Baerends, T. Ziegler, J. Autschbach, D. Bashford, A. Bérces, F. M. Bickelhaupt, C. Bo, P. M. Boerrigter, L. Cavallo, D. P. Chong, L. Deng, R. M. Dickson, D. E. Ellis, M. van Faassen, L. Fan, T. H. Fischer, C. Fonseca Guerra, A. Ghysels, A. Giammona, S. J. A. van Gisbergen, A. W. Götz, J. A. Groeneveld, O. V. Gritsenko, M. Grüning, S. Gusarov, F. E. Harris, P. van den Hoek, C. R. Jacob, H. Jacobsen, L. Jensen, J. W. Kaminski, G. van Kessel, F. Kootstra, A. Kovalenko, M. V. Krykunov, E. van Lenthe, D. A. McCormack, A. Michalak, M. Mitoraj, J. Neugebauer, V. P. Nicu, L. Noodleman, V. P. Osinga, S. Patchkovskii, P. H. T. Philipsen, D. Post, C. C. Pye, W. Ravenek, J. I. Rodríguez, P. Ros, P. R. T. Schipper, G. Schreckenbach, J. S. Seldenthuis, M. Seth, J. G. Snijders, M. Solà, M. Swart, D. Swerhone, G. te Velde, P. Vernooijs, L. Versluis, L. Visscher, O. Visser, F. Wang, T. A. Wesolowski, E. M. van Wezenbeek, G. Wiesenekker, S. K. Wolff, T. K. Woo and A. L. Yakovlev, *Journal*, 2014.

14. R. J. Deeth and L. J. Hearnshaw, *Dalton Trans*, 2006, 1092-1100.

15. B. Bleaney and K. Bowers, 1952.

16. J. N. van Niekerk and F. Schoening, *Acta Crystallogr.*, 1953, **6**, 227-232.

17. P. J. Hay, J. C. Thibeault and R. Hoffmann, *J. Am. Chem. Soc.*, 1975, **97**, 4884-4899.

18. D. Wang, K. Wurst and M. R. Buchmeiser, *J. Organomet. Chem.*, 2004, **689**, 2123-2130.

19. J. Yun, D. Kim and H. Yun, *Chem. Commun.*, 2005, 5181-5183.

20. A. M. Magill, K. J. Cavell and B. F. Yates, *J. Am. Chem. Soc.*, 2004, **126**, 8717-8724.

21. X.-Y. Wang, X.-T. Deng and C.-G. Wang, *Acta Crystallogr. Sect. Sect. E: Struct. Rep. Online*, 2006, **62**, m3578-m3579.

22. Y. Yan, M. Juricek, F. o.-X. Coudert, N. A. Vermeulen, S. Grunder, A. Dailly, W. Lewis, A. J. Blake, J. F. Stoddart and M. Schröder, *J. Am. Chem. Soc.*, 2016, **138**, 3371-3381.

23. Y. Yan, S. Yang, A. J. Blake and M. Schröder, *Acc. Chem. Res.*, 2013, **47**, 296-307.

24. T. D. Bennett, A. H. Fuchs, A. K. Cheetham and F.-X. Coudert, *Dalton Trans*, 2016, **45**, 4058-4059.

25. C. I. Ezugwu, N. A. Kabir, M. Yusubov and F. Verpoort, *Coord. Chem. Rev.*, 2016, **307**, 188-210.

26. R. J. Deeth, *Coord. Chem. Rev.*, 2001, **212**, 11-34.

27. M. Foscato, R. J. Deeth and V. R. Jensen, *J. Chem. Inf. Model*, 2015, **55**, 1282-1290.

28. K. A. Alzahrani and R. J. Deeth, *J. Mol. Model.*, 2016, **22**, 80.

Chapter 6: Molecular Modelling of the Copper Paddlewheel Unit: Implications for Metal Organic Frameworks.

6.1 Introduction

As has been covered many times in this thesis, metal organic frameworks (MOFs) are nonporous materials with many potential industrial applications in gas storage, separations, and catalysis. The framework composes secondary building units (SBUs) connected by linkers to generate 3-dimensional networks.[1-4] The SBUs are based on transition metal centres often connected to organic linkers in combination with axial ligands such as, for example, 1,4-diazabicyclo (2.2.2) octane (dabco) or pyrazine.

One type of SBU is based on the copper paddle wheel (CPW) motif which consists of two copper cations bridged by four carboxylate anions giving a local square planar (SQP) coordination geometry (Figure 6.1). In contrast to the zinc paddle wheel (ZPW) motif, CPWs can be synthesised easily even without axial ligand which is advantageous in these systems for gas storage and catalysis applications.[5] Therefore, the CPW structure has been used extensively as a building unit for many existing metal organic frameworks (Figure 6.1).[6-8] For example, HKUST-1 $[Cu_3(btc)_2]$ (btc = 1,3,5-benzenetricarboxylate) is one of the earliest and most investigated MOF systems based on the CPW unit.[9] This system has been widely used for gas storage,[10] gas separations,[11-13] and heterogeneous catalysis applications.[14-16] However, HKUST-1 is a rigid system while this work highlights the possibilities for flexible copper paddle wheel complexes in isolation and incorporated into MOF systems.
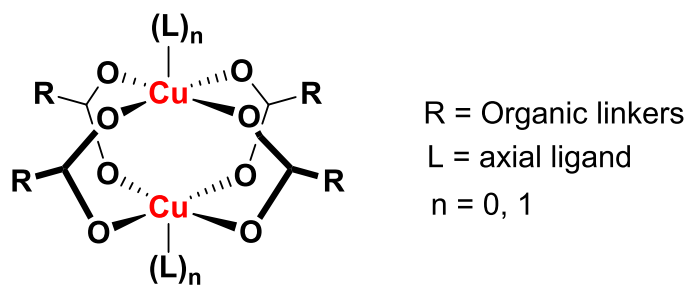
Figure 6.1; Schematic representation of CPWs building units within MOFs.

In the past decade, well-designed flexible carboxylate organic linkers have played an important role in producing many flexible CPW MOFs.[17-19] However, to our knowledge, there is no reported flexible CPW system. In addition, the CPW unit is often considered to be less flexible than the comparable zinc paddle wheel (ZPW) unit and this has been attributed to the electronic structure of CPW.[20]

However, our DFT calculations (Chapter 5) have revealed that CPW units can be more flexible than their ZPW counterparts. In addition, the calculations suggest that other local minima structures of CPWs can be located when using strong axial ligands field, such as N-heterocyclic carbine (NHC) and strong carboxylic acids (hence weak equatorial field), such as trifluoroacetic acid.[21] Modelling very large systems, such as MOFs, remains the province of fully atomistic molecular mechanics/molecular dynamic (MM/MD) simulations. Although there are bespoke FFs designed for MOF systems based on CPW unit such as MOF-FF [22] and UFF4MOF [23] , none of them considers this observation and in general they deal with the CPW as a rigid motif.

Reproducing the DFT studies revealed in Chapter 5 requires a sophisticated and flexible copper paddle wheel force field, CPW-FF, which can consider the effects

associated with axial and equatorial ligands fields. The following sections will explain our initial attempts at extending our first-principles ligand field molecular mechanics (LFMM) force field for zinc paddlewheels, ZPW-FF,[24] to CPW-FF in order to model flexible CPW units regardless the combination of equatorial and apical ligands.

6.2 Theoretical methods

Most of the DFT calculations reported here used ORCA version 3.0.3.[25] The general protocol for geometry optimisation and frequencies employed the Becke-Perdew BP86 functional[26] with def2-SVP basis sets.[27] A COSMO solvation field with water, as implemented in ORCA, was used as the solvent.[28, 29] For the NHC systems, the Grimme D3 dispersion corrections was also employed. A spin-unrestricted formalism (UKS) for copper species was employed with a total spin $S = 1$.

We find that the Amsterdam Density Functional 2014 code [30, 31] is more convenient than ORCA particularly for high-symmetry optimisation of CPW units. The Becke-Perdew functional, TZP basis sets for metals, and DZP basis sets for all other atoms were employed for geometry optimisations. A COSMO (water) solvation field, as implemented in ADF, was used with selected small frozen cores. Given the qualitative nature of the high-symmetry study, we did not bother with any dispersion corrections nor were vibrational frequencies computed.

Molecular mechanics (MM) calculations were carried out using DommiMOE,[32] our extended version of the 2013 of the molecular operating environment.[33] The distributed version of the Merck molecular force field, MMFF94, (mmff94x.ff)[34, 35] with additional terms such as Cu-L-A angle bend and Cu-L-A-B torsion was used to

capture the coordination environments around the copper metal centers. These environments were defined using ligand field molecular mechanics (LFMM)[36, 37] parameters where the Cu-L interactions and the explicit angle bending around the metal center were described by Morse functions (E_{Morse}) and pure ligand-ligand repulsion (A_{LL}/d^n) respectively. The Cu-L σ and π interactions are modelled by the angular overlap model (AOM) with M-L bonding interaction described by e_σ, $e_{\pi\chi}$ and $e_{\pi y}$ respectively (Figure 6.3). In addition, the AOM parameter, e_{ds}, for treating the so-called d-s mixing interactions between s and d orbitals on the copper and some ligands are also considered in this work. The preliminary parameter file and partial-charge-setting script are available and can be requested from the author. However, these initial parameters are only good for reproducing relatively rigid CPWs. Further work will be needed to capture flexible CPWs. The electrostatic interactions are treated by a distance-dependent dielectric term with a cut-off starting at 8 Å and going to zero at 10 Å.

6.3 Results and discussion

Constructing a good and transferable force field (FF) for coordination compounds relies on a diverse set of training data.[38, 39] Previous experience with copper force field shows that the inherent plasticity of Jahn-Teller active d^9 centre can yield sufficient diversity that an accurate FF can be constructed using structural data derived solely from experimental X-ray diffraction studies.[40] The Cambridge Structural Database (CSD) is a rich source of experimental data. Our initial searches were restricted to a

central copper paddle wheel (CPW) motif such that none of the Cu-O(carboxylate) bonds were coded as 'polymeric'. However, this search yielded more than one thousand CPW complexes with various axial and equatorial ligands.

Therefore, we decided to follow the same methodology for constructing the ZPW-FF and modelled 21 CPW systems for developing our initial training set based only on DFT data. Our preliminary investigations considers only three carboxylates species: formate, acetate and trifluoroacetate (R = H, CH_3 or CF_3) with zero, one or two capping groups, L, which are either pyridine (py), ammonia (NH_3) or water (H_2O) (Figure 6.2). Thus, there are seven complexes for each carboxylate represented by the general formula CuPR.nL, where CuP represents the $Cu_2(O_2C)_4$ core of the CPW, R is the carboxylate substituted, L the capping group and 'n' the number of such groups. The choice of carboxylates was motivated from a consideration of pK_a values. The pK_a of trifluoroacetic acid (0.23) is among the lowest while that for acetic acid (4.76) is much higher. Formate is intermediate and hence the chosen acids span the relevant pK_a range.

R = H, CH_3, CF_3
L = NH_3, py, water
n = 0, 1
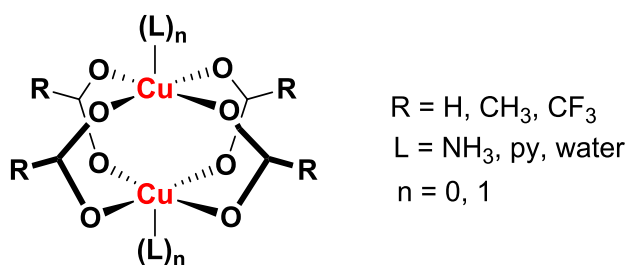
Figure 6.2; Schematic representation of the CuPR.nL systems used for initial training data.

Our initial DFT studies (using only ORCA) on these simple models revealed that the CPWs prefer an elongated form where the axial bonds are longer than the equatorial bonds. In addition, it is known that the CuO_4 moiety is approximately square planar (SQP). However, the trifluoroacetate models sometimes prefer a TBP geometry. Although there were some small negative frequencies (less than 40 cm^{-1}), this observation has motivated us to do a further theoretical investigations on CPWs.

A high quality ADF protocol was then employed on some CPW models (Figure 6.3) to locate other local minimum structures of CPWs. These models were modelled carefully with various ligands based on the strength of the interaction fields with copper centres. The reason for using ADF here is that we find it more convenient than ORCA when specifying particular electronic configurations of CPWs.

(A)   (B)

(C)   (D)
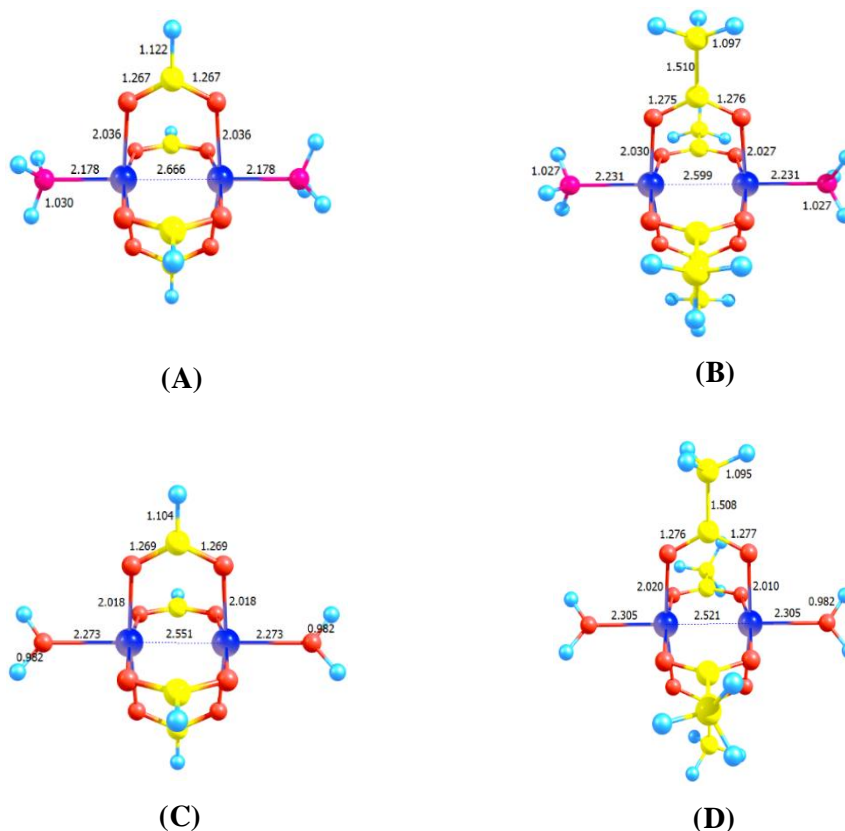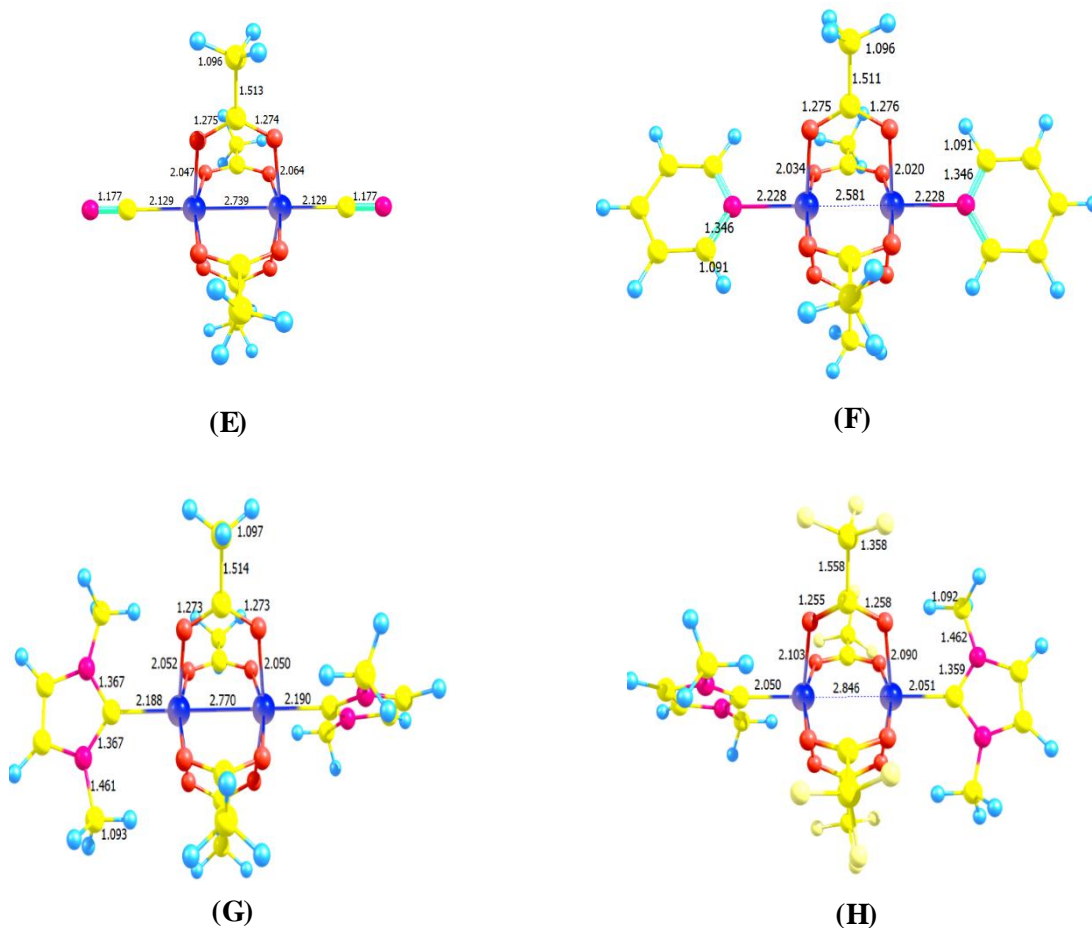
Figure 6.3; DFT optimized structures of some CPWs models. It is clear that the CPWs units are usually elongated structure. However, (H) forms compressed structure because the presence of strong axial ligand filed (NHC) in combination with weak carboxylate specie (trifluoroacetate). The atoms are coloured for clarity (Cu = dark blue, O = red, N = pink, and C = yellow, F = white-yellow, and H = blue)

As described in Chapter 5, our DFT studies have revealed that using a stronger axial ligand field, such as an N-heterocyclic carbene (NHC), in combination with weak equatorial ligands, such as trifluoroacetate, would locate the compressed CPW as the

local minimum structure (Figure 6.3, H). Hence, the local minimum structure of CuPCF$_3$.2NHC has equatorial bonds lengths that are longer than the axial bonds. We called this mixed state, T$_M$, where the unpaired electron on each copper centre is shared between the $d_x{}^2{}_{-y}{}^2$ and $d_z{}^2$ orbitals (Figure 6.4). In addition, the [Cu$_2$(acetate)$_4$(Me$_2$NHC)$_2$] has revealed that the copper coordination geometry could adopt a TBP geometry instead of SQP with almost no change in energy (Figure 6.5). These findings have revealed that the CPW units are more flexible than comparable ZPW units.
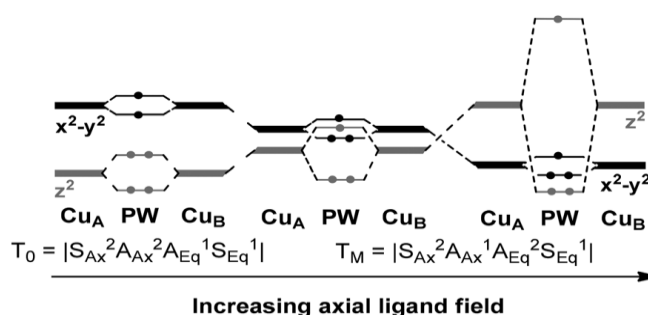
Figure 6.4; Schematic partial valence molecular orbital (MO) energy level diagram for copper paddlewheel systems as a function of increasing the axial ligand field. For the MOs, S refers to a symmetric (in-phase) combination of d orbitals, A to an asymmetric combination, Ax = $d_z{}^2$ and Eq = $d_x{}^2{}_{-y}{}^2$.
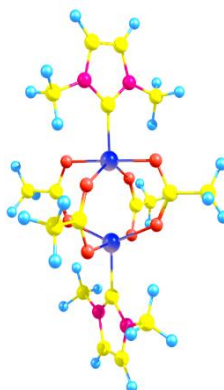
Figure 6.5; DFT optimized geometry for [Cu$_2$(acetate)$_4$(Me$_2$NHC)$_2$] showing that the Copper centres adopt TBP structure.

Modelling flexible CPWs required a sophisticated force field (FF) based on high quality training sets obtained from theoretical DFT studies. Then further refinements would be based on the X-ray diffraction experimental data of some CPW complexes. However, it is clear that the DFT data for the CPW models, as shown in figure 6.3, are not identical and the Cu-O(carboxylate) distances vary very much ranging almost from 2.01 to 2.10 Å. As mentioned previously, the bond distances variations are affected by the axial and equatorial ligands fields coordinated to the copper centers.

Fortunately, the ligand field molecular mechanics (LFMM) model has been applied previously to copper systems for developing a reasonable treatment of four-, five- and six-coordinated structures.[41-44] In addition, the LFMM performs well in capturing Jahn-teller effects and the associated energies of mononuclear CuL_6 complexes, where L here refers to N-based ligands.[40] Thus, a good basis of FF parameters for copper based systems is already available in the LFMM force field. However, the dinuclear copper centres and their anomalous magnetic behaviour between the two unpaired $d_{x^2-y^2}$ electrons require specific FF parameters for reproducing the complicated electronic structure associated with CPWs.[21]

In addition, our previous experience with the ZPW-FF has proven that the LFMM method is very flexible for capturing the angle-bending terms around the metal centres. This is because the LFMM model uses a 1-3 interaction potential exclusively.[36, 45] However, the d^{10} Zn (II) has no d-electron effects, while the d^9 Cu (II) metal centre is strongly affected by the d-electron orbitals interactions.[20] Hence, developing a generic CPW-FF must consider all the Cu-L interaction potential carefully.

Based on the available DFT data, our first attempt at developing the CPW-FF has shown that the rigid CPWs can be easily reproduced, while the flexible CPWs require

specific parameters for each carboxylates species. Therefore, transferable Cu-O(carboxylate) parameters will require a lot more works and further DFT studies to be able to reproduce all forms of CPW motif by CPW-FF. Unfortunately, since our time is limited, we decided to leave this for future work. Here, we restrict ourselves to identifying the main LFMM parameters responsible for controlling the ligand field' interactions in CPWs.

In the LFMM method, the Morse function, the ligand–ligand repulsion term, A_{LL}, and AOM parameters will all have a strong influence on the Cu-L bond distance.[46] The AOM parameters can be derived from spectroscopic data of d-d splittings or theoretical studies to describe separate σ and π interactions, as shown in Figure 6.6. However, since DFT studies show that each carboxylate species has different Cu-L values (Figure 6.3), the CPW-FF must deal with these variations and consider each ligand field individually, including the carboxylates species.
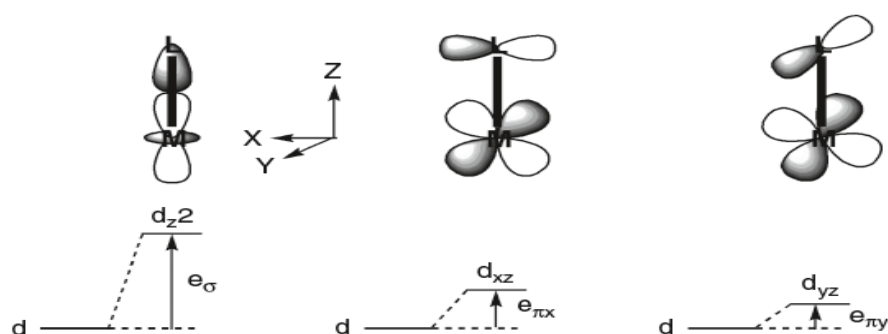
Figure 6.6; Introduction of AOM parameters of local M-L bonding showing the differences between σ and π interactions.

After a lot of attempts, we noticed while that by modifying the AOM parameters manually and increasing the axial field strength, L, with decreasing the equatorial carboxylate field strength, the mixed state (T_M) can be located as LFMM optimized structures. In addition, increasing the axial donor strength more enforces the pentacoordinate TBP copper complexes with comparatively long Cu-O(carboxylate) bond lengths and a relatively short axial bond (Figure 6.7). These preliminary observations demonstrate that the LFMM is able to reproduce the DFT-optimized structures those shown in figure 6.3.

(a)   **(b)**   **(c)**
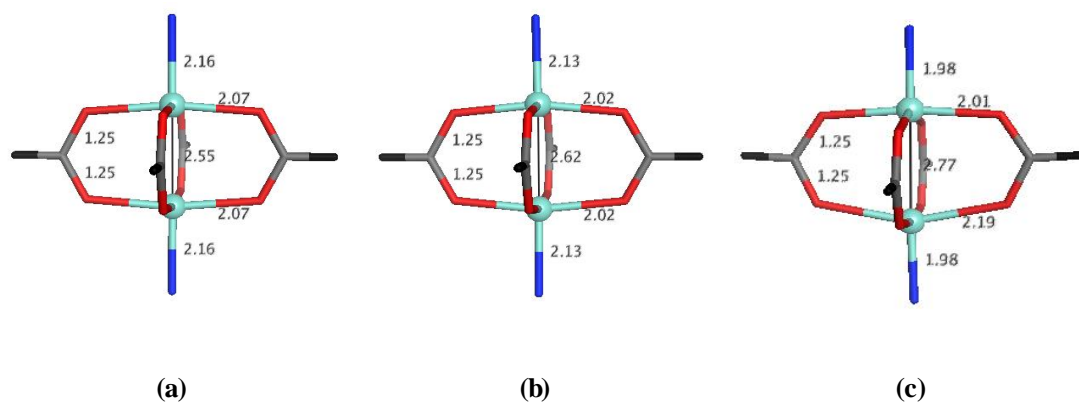
Figure 6.7; the LFMM optimized structure for various axial and equatorial ligands (carboxylates) fields. (a) Represents the DFT-optimized structure of CuPH.$2NH_3$ model. (b) Represents the LFMM-optimized structure before modifying the previous values of e_σ for equatorial and axial ligands (OX = 250000 cm^{-1} and N= 100000 cm^{-1}). (c) Represents the LFMM-optimized structure comprises of strong axial e_σ interaction and weak equatorial ligand field (OX = 100000 cm^{-1} and N= 650000 cm^{-1}). Dark blue stick represents axial field (N) whereas black sticks for equatorial field (OX). Copper metals are highlighted and adopt SQP geometry in (a) and (b), while adopt TBP in (c). Bond lengths are in grey numbers.

Although the bonds lengths are not in complete not agreement with the DFT-optimized structures, the differences could be fixed by specifying special parameters for each carboxylate type in the future. For example, one suggested solution is to construct special parameters for each carboxylate species based on their pK_a values. In addition, the current CPW-FF should consider the effects associated with the combination of axial and equatorial ligand fields. Therefore, based on our findings in this chapter, constructing a generic CPW-FF for reproducing CPWs seems possible. In addition, these findings could be a good starting point for further investigations either by our group or by any other groups who are interested in modelling CPWs in isolation and incorporated into MOF systems.

6.4 Conclusion

In this chapter, our preliminary data for constructing a generic CPW-FF are reported. The DFT studies have shown that the parameters for CPWs vary a lot based on the axial and equatorial ligand fields. The LFMM method has proven its ability in producing these variations of carboxylate parameters and geometries around the Cu(II) centres. However, constructing a generic CPW-FF for all CPWs complexes requires a more comprehensive set of quantum mechanical studies. Unfortunately, we did not have sufficient time to build a general training set for each carboxylate species in conjunction with the apical ligands. This remains a task for the future.

6.5 References

1. Y. Cui, B. Li, H. He, W. Zhou, B. Chen and G. Qian, *Acc. Chem. Res*, 2016, **49**, 483-493.
2. D. Farrusseng, *Metal-organic frameworks: applications from catalysis to gas storage*, John Wiley & Sons, 2011.
3. T. Islamoglu, S. Goswami, Z. Li, A. J. Howarth, O. K. Farha and J. T. Hupp, *Acc. Chem. Res.*, 2017, **50**, 805-813.
4. B. Li, M. Chrzanowski, Y. Zhang and S. Ma, *Coord. Chem. Rev.*, 2016, **307**, 106-129.
5. L. J. Murray, M. Dincă and J. R. Long, *Chem. Soc. Rev.*, 2009, **38**, 1294-1314.
6. X. Lin, I. Telepeni, A. J. Blake, A. Dailly, C. M. Brown, J. M. Simmons, M. Zoppi, G. S. Walker, K. M. Thomas and T. J. Mays, *J. Am. Chem. Soc.*, 2009, **131**, 2159-2171.
7. L. Ma and W. Lin, *J. Am. Chem. Soc.*, 2008, **130**, 13834-13835.
8. Y. Yan, M. Juricek, F. o.-X. Coudert, N. A. Vermeulen, S. Grunder, A. Dailly, W. Lewis, A. J. Blake, J. F. Stoddart and M. Schröder, *J. Am. Chem. Soc.*, 2016, **138**, 3371-3381.
9. S. S.-Y. Chui, S. M.-F. Lo, J. P. Charmant, A. G. Orpen and I. D. Williams, *Science*, 1999, **283**, 1148-1150.
10. J. A. Mason, M. Veenstra and J. R. Long, *Chem. Sci.*, 2014, **5**, 32-51.
11. L. Ge, W. Zhou, V. Rudolph and Z. Zhu, *J. Mater. Chem. A*, 2013, **1**, 6350-6358.
12. L. Hamon, E. Jolimaître and G. D. Pirngruber, *Ind. Eng. Chem. Res.*, 2010, **49**, 7497-7503.
13. Q. M. Wang, D. Shen, M. Bülow, M. L. Lau, S. Deng, F. R. Fitch, N. O. Lemcoff and J. Semanscin, *Micropor. Mesopor. Mat.*, 2002, **55**, 217-230.
14. E. Pérez-Mayoral and J. Čejka, *ChemCatChem*, 2011, **3**, 157-159.
15. L. H. Wee, N. Janssens, S. R. Bajpe, C. E. Kirschhock and J. A. Martens, *Catal. Today*, 2011, **171**, 275-280.
16. J.-y. Ye and C.-j. Liu, *Chem. Commun.*, 2011, **47**, 2167-2169.
17. F. Dai, H. He, D. Gao, F. Ye, X. Qiu and D. Sun, *CrystEngComm*, 2009, **11**, 2516-2522.
18. Y. Yan, S. Yang, A. J. Blake and M. Schröder, *Acc. Chem. Res.*, 2013, **47**, 296-307.
19. Q. Yang, X. Chen, Z. Chen, Y. Hao, Y. Li, Q. Lu and H. Zheng, *Chem. Commun.*, 2012, **48**, 10016-10018.

20. S. Bureekaew, S. Amirjalayer and R. Schmid, *J. Mater. Chem.*, 2012, **22**, 10249-10254.

21. K. Alzahrani and R. J. Deeth, *Dalton Trans*, 2016, **45**, 11944-11948.

22. S. Bureekaew, S. Amirjalayer, M. Tafipolsky, C. Spickermann, T. K. Roy and R. Schmid, *physica status solidi (b)*, 2013, **250**, 1128-1141.

23. M. A. Addicoat, N. Vankova, I. F. Akter and T. Heine, *J. Chem. Theory Comput.*, 2014, **10**, 880-891.

24. K. A. Alzahrani and R. J. Deeth, *J. Mol. Model.*, 2016, **22**, 80.

25. F. Neese, *Inorg. Chem*, 2014, **50**, 7460.

26. A. D. Becke, *J. Chem. Phys*, 1988, **88**, 2547-2553.

27. J. P. Perdew and W. Yue, *Phys. Rev. B.*, 1986, **33**, 8800.

28. A. Klamt, *J. Phys. Chem.*, 1995, **99**, 2224-2235.

29. A. Klamt and V. Jonas, *J. Chem. Phys*, 1996, **105**, 9972-9981.

30. S. ADF, *Theoretical Chemistry, Vrije Universiteit, Amsterdam, The Netherlands, 2014*.

31. G. t. Te Velde, F. M. Bickelhaupt, E. J. Baerends, C. Fonseca Guerra, S. J. van Gisbergen, J. G. Snijders and T. Ziegler, *J. Comput. Chem.*, 2001, **22**, 931-967.

32. R. J. Deeth, N. Fey and B. Williams–Hubbard, *J. Comput. Chem.*, 2005, **26**, 123-130.

33. moe, *Chemical Computing Group (2013) Molecular operating environment,(MOE) 2013 edn. Chemical Computing Group, Montreal*, 2013.

34. T. A. Halgren, *J. Comput. Chem.*, 1999, **20**, 720-729.

35. T. A. Halgren, *J. Comput. Chem.*, 1999, **20**, 730-748.

36. R. J. Deeth, *Coord. Chem. Rev.*, 2001, **212**, 11-34.

37. R. J. Deeth and D. L. Foulis, *PCCP*, 2002, **4**, 4292-4297.

38. P. Comba and R. Remenyi, *Coord. Chem. Rev.*, 2003, **238**, 9-20.

39. P.-O. Norrby and P. Brandt, *Coord. Chem. Rev.*, 2001, **212**, 79-109.

40. R. J. Deeth and L. J. Hearnshaw, *Dalton Trans*, 2006, 1092-1100.

41. V. J. Burton and R. J. Deeth, *J. Chem. Soc., Chem. Commun.*, 1995, 573-574.

42. V. J. Burton, R. J. Deeth, C. M. Kemp and P. J. Gilbert, *J. Am. Chem. Soc.*, 1995, **117**, 8407-8415.

43. I. W. Davies, R. J. Deeth, R. D. Larsen and P. J. Reider, *Tetrahedron Lett.*, 1999, **40**, 1233-1236.

44. R. J. Deeth and L. J. Hearnshaw, *Dalton Trans*, 2005, 3638-3645.

45. P. Comba, T. W. Hambley and B. Martin, *Molecular modeling of inorganic compounds*, John Wiley & Sons, 2009.

46. R. J. Deeth, *Adv. Inorg. Chem.*, 2010, **62**, 1-39.

Chapter 7: Conclusions and Future Work

The aim of the work presented in this thesis was to develop computational approaches to the modelling of zinc and copper paddlewheel complexes both in isolation and when incorporated into metal organic frameworks (MOFs). We considered both 'ab initio' and empirical force field methods based mainly on DFT and ligand field molecular mechanics (LFMM) respectively.

Chapter 3 described a new, experimentally-refined, first-principles force field, ZPW-FF, that was developed for the zinc paddlewheel (ZPW) motif, including pyridyl and amine axial groups. The ZPW-FF accurately reproduced the DFT-computed structures for isolated zinc paddlewheel systems for a range of simple carboxylates spanning uncapped, mono-, and di-capped complexes. In addition, the ZPW-FF was applied to pore models of the archetypal flexible MOF $[Zn_2(bdc)_2(dabco)]_n$ and using a 3x3 9-pore grid provided good agreement with the observed pronounced structural changes upon adsorption of either dimethylformamide or benzene.

In Chapter 4, the ZPW-FF was extended successfully to reproduce mono- and di-capped ZPW complexes with axial water ligands. The extended version of ZPW-FF was then used to investigate the flexible MOF $[Zn_2(bdc)_2(dabco)]_n$ systems under water vapour where surface dabco groups were replaced by water ligands. It was also applied to 2D and 3D crystal systems of MOF-2 which comprises ZPW units capped by water ligands. The performance of the ZPW-FF was extremely good and more efficient than DFT, at least for isolated ZPW complexes capped by N- and water- based

ligands. The ZPW-FF looks promising for modelling other complicated MOFs containing ZPW building units in the future.

In the second part of this thesis, the development of a copper paddlewheel force field, CPW-FF, for copper paddlewheel (CPW) motifs in isolation and incorporated into MOFs was highlighted. It was shown in Chapter 5 that the electronic structure of the CPW motif is significantly affected by the axial and equatorial ligands. The DFT investigations on various CPW systems revealed that the local minimum structures were usually elongated. However, the local minimum structure of CPW systems comprising a strong axial ligand, such as an N heterocyclic carbene (NHC), and a weak carboxylic acid, such as trifluoroacetate, was compressed. These findings have revealed that the CPW systems can be more flexible than comparable ZPW systems giving the possibility of using modelling to discover new flexible CPW MOFs.

Chapter 6 concerned a preliminary attempt to develop a generic CPW-FF for all CPW complexes. However, reproducing the variations with different carboxylates and the associated changes in electronic structures of CPW systems using LFMM requires a general training set based on more comprehensive quantum mechanical studies for each carboxylate species in conjunction with the apical ligands. Therefore, since we did not have sufficient time, we restricted ourselves to identifying the main LFMM parameters responsible for controlling the ligand field interactions in CPWs. The preliminary observations demonstrated that the LFMM is able to reproduce the DFT-optimized structures revealed in Chapter 5. Thus, our preliminary LFMM parameters for constructing a generic CPW-FF were reported in Chapter 6. However, a definitive version of the CPW-FF remains a task for the future.

Overall, there are some future goals based on this thesis. The most important are to extend the ZPW-FF to other more complicated MOF systems and to develop a better version of the CPW-FF. These improved force fields can then be used for modelling new MOF systems based on zinc or copper paddlewheel units. However, many important mechanical, thermal and dielectric properties cannot be computed in the molecular operating environment (MOE) software. This is because the ability to model periodic systems in MOE is limited. Therefore, another future goal is to transfer our FF parameters to the DL-POLY simulation software which already has the LFMM methodology incorporated although its performance with periodic boundary conditions has not yet been assessed. DL_POLY_LF may help researchers to make further theoretical investigations on existing MOF systems or even to model their own new MOFs theoretically and assess them before introducing them to the real world. In addition, as the LFMM method has proven its ability in reproducing the flexibility of paddlewheel complexes and the geometries around metal centres, it could be extended to more paddlewheel complexes such as those comprising different transition metal elements such as Co, Fe, Mn, and Cr.

Appendix 1 - MOE and LFMM Parameter Files for Training Set and SVL Script for Setting Partial Atomic Charges for ZPW Systems.

MOE and LFMM parameter files for initial training set (Chapter 3)

```
# LFMM parameters for MMFF94 Zinc Paddlewheels

[Morse]
#T1   T2    dist         D            a
Zn+2  OX    1.95          50.7         1.65         0.0   0.0
Zn+2  N     1.99          58.0         1.40         0.0   0.0
Zn+2  NPYD  1.98          60.0         1.40         0.0   0.0

%

[ll]
#M    L     A     n
Zn+2  OX    6700  6
Zn+2  N     5500  6
Zn+2  NPYD  3000  6

%

[esig]
#M    L     esig0 esig1 esig2 esig3 esig4 esig5 esig6
Zn+2  OX    0     0     0     0     0     0     0
Zn+2  NPYD  0     0     0     0     0     0     0
Zn+2  N     0     0     0     0     0     0     0
%

[epix]
#M    L     epix0 epix1 epix2 epix3 epix4 epix5 epix6
Zn+2  OX    0     0     0     0     0     0     0
Zn+2  N     0     0     0     0     0     0     0
Zn+2  NPYD  0     0     0     0     0     0     0
%

[epiy]
#M    L     epiy0 epiy1 epiy2 epiy3 epiy4 epiy5 epiy6
Zn+2  OX    0     0     0     0     0     0     0
Zn+2  N     0     0     0     0     0     0     0
Zn+2  NPYD  0     0     0     0     0     0     0
%

[exds]
#M    L     exds0 exds1 exds2 exds3 exds4 exds5 exds6
Zn+2  OX    0     0     0     0     0     0     0
Zn+2  N     0     0     0     0     0     0     0
Zn+2  NPYD  0     0     0     0     0     0     0
%
```

```
[pair]
#M     L     P0    P1    P2    P3    P4    P5    P6
Zn+2  OX    0     0     0     0     0     0     0
Zn+2  N     0     0     0     0     0     0     0
Zn+2  NPYD  0     0     0     0     0     0     0
%
```

Refined ZPW-FF LFMM parameters after recalibration using crystallographic structural data. Only the Morse function α values have been changed relative to the training set parameters. (Chapter 3 and 4)

```
[Morse]
#T1    T2    dist          D             alpha
# X-ray fit
Zn+2  OX    1.90          50.7          1.65          0.0   0.0
Zn+2  N     1.99          58.0          1.40          0.0   0.0
Zn+2  NPYD  1.92          60.0          1.40          0.0   0.0
Zn+2  OH2   1.95          53.0          1.0           0.0   0.0

%


[ll]
#M     L     A     n
Zn+2  OX    6300  6
Zn+2  N     5300  6
Zn+2  NPYD  5000  6
Zn+2  OH2   2100  6
%


[esig]
#M     L     esig0  esig1  esig2  esig3  esig4  esig5  esig6
Zn+2  N     0      0      0      0      0      0      0
Zn+2  NPYD  0      0      0      0      0      0      0
Zn+2  OX    0      0      0      0      0      0      0
Zn+2  OH2   0      0      0      0      0      0      0

%


[epix]
#M     L     epix0  epix1  epix2  epix3  epix4  epix5  epix6
Zn+2  N     0      0      0      0      0      0      0
Zn+2  NPYD  0      0      0      0      0      0      0
Zn+2  OX    0      0      0      0      0      0      0
Zn+2  OH2   0      0      0      0      0      0      0

%


[epiy]
#M     L     epiy0  epiy1  epiy2  epiy3  epiy4  epiy5  epiy6
Zn+2  N     0      0      0      0      0      0      0
Zn+2  NPYD  0      0      0      0      0      0      0
Zn+2  OX    0      0      0      0      0      0      0
Zn+2  OH2   0      0      0      0      0      0      0

%
```

```
[exds]
#M     L      exds0  exds1  exds2  exds3  exds4  exds5  exds6
Zn+2   N      0      0      0      0      0      0      0
Zn+2   NPYD   0      0      0      0      0      0      0
Zn+2   OX     0      0      0      0      0      0      0
Zn+2   OH2    0      0      0      0      0      0      0


%


[pair]
#M     L      P0     P1     P2     P3     P4     P5     P6
Zn+2   N      0      0      0      0      0      0      0
Zn+2   NPYD   0      0      0      0      0      0      0
Zn+2   OX     0      0      0      0      0      0      0
Zn+2   OH2    0      0      0      0      0      0      0
```

Additional MMFF94x MOE force field parameters for ZPW systems.

```
type   Zn+2   Zn     'Zn+2 (d10)'


[rules]
#transition series metal cations, by row
#first row
Zn+2   match    '[Zn+2]'                        #Zn+2
#if matching fails, use atom names
Zn+2   atom-name 'Zn+2'                         #Zn+2
#rjd: match bonded ligand types to free ligand types
OH2    match '[OX3]([#T])([#1])([#1])'          # water ligand
HOH    match '[#1]O([#T])([#1])'                # hydrogens of water ligand
N      match '[NX4][#T]'                        # amine ligand
HN     match '[#1][NX4][#T]'                    # H of amine ligand
NPYD   match 'n([#T])(c)(c)'                    # pyridyl nitrogen


[ang] # ----------------------- TM ANGLE PARAMETERS ------------------------
ang-function  angle
#code  T1     T2     T3     angle     k2       k3    k4
*      Zn+2   OX     CO2M   125.0    24.0    0.0    0.0
*      Zn+2   N      HN     120.0            60.0         0.0          0.0
*      Zn+2   NPYD   Car    120.0            10.0         0.0          0.0
*      OX     CO2M   OX     125.000  100.    0.0    0
*      Zn+2   OH2    HOH    123.0            30.0         0.0


[stb] # ----------------- stretch-bend parameters ---------------------
#code  T1     T2     T3     kbIJK    kbKJI
*      OX     CO2M   Car    0.0      0.0
*      Car    Car    CO2M   0.0      0.0
*      Zn+2   OX     CO2M   0.0      0.0
*      Zn+2   N5B    C5A    0.0      0.0
*      NPYD   Zn+2   OX     0.0          0.0
*      OX     Zn+2   OX     0.0          0.0
*      N      Zn+2   OX     0.0          0.0
*      Zn+2   NPYD   Car    0.0          0.0
*      Zn+2   N      C      0.0          0.0
*      Zn+2   OH2    HOH    0.0          0.0
```

```
[ptor] # ----------------- PROPER TORSIONS ----------------------------
#code   T1     T2     T3     T4      V1/2    V2/2    V3/2   V4/2    V5/2
*       Zn+2   OX     CO2M   HC      0.000   -2.500  0.000  0.000   0.000
*       Zn+2   OX     CO2M   OX      0.000   -2.500  0.000  0.000   0.000
*       Zn+2   OX     CO2M   Car     0.000   -1.000  0.000  0.000   0.000
*       Zn+2   OX     CO2M   C       0.000   -2.500  0.000  0.000   0.000
*       Zn+2   OX     CO2M   Csp2    0.000   -2.500  0.000  0.000   0.000
*       Zn+2   OX     CO2M   Car     0.000   -1.000  0.000  0.000   0.000
*       Zn+2   NPYD   Car    Car     0.000   -5.000  0.000  0.000   0.000
*       OH2    Zn+2   OX     CO2M    0.000   -2.000  0.000  0.000   0.000


[oop] # ----------------- out of plane parameters -----------------------
#T1    T2*    T3     T4     koop
Zn+2   NPYD   Car    Car    2.00

[nonbonded] # ---------- nonbonded atomic parameters ----------------------
#type  radius well   apol   Neff   mass   DA    q0      fcadj  pbci
Zn+2   1.620  0.106  0.400  6.000  -      -     2.0000  0.0000 0.0000
```

SVL script for setting partial atomic charges (Chapter 3 and 4)

```
function PartialCharge;

function fix_carboxylates[]

// Detect mononuclear carboxylate, make sure it's not in a chelate ring
// join up both oxygens and check carbon charge
write ['Start of carboxylate fix\n'];

local metkeys = Atoms[] | sm_Match [ '[Zn]', Atoms[] ];
//pr metkeys;

// Set metal names to correct value
aSetName [ metkeys, 'Zn+2'];
aSetIon [ metkeys, 2];

// Fix donor N ionisation states while we're at it...
local n_keys = Atoms[] | sm_Match [ '[#7][Zn]', Atoms[] ];
aSetIon [n_keys, 0];
aSetHintLP [ n_keys, 1];

// Find coordinated bridging carboxylates

local ligkeys = split [ cat sm_MatchAtoms [ 'C(O[#T])(O[#T])', Atoms[] ], 5 ];

local n_carb = length ligkeys;

write ['>>> {n:} bridging carboxylate ligands found\n', length ligkeys ];

// Set HintLP on oxygens, and ionisation states
local il;
for il = 1, length ligkeys loop
        aSetHintLP [ ligkeys(il)(2), 1];
        aSetHintLP [ ligkeys(il)(4), 1];
        aSetIon [ ligkeys(il)(1), 1];   // Carbon
//      aSetIon [ ligkeys(il)(2), -1];  // Oxygen
```

```
//      aSetIon [ ligkeys(il)(4), -1];  // Oxygen
endloop;

// Set force field charges to current FF - CAUTION: only MMFF94_tm seems to work
local [q, pos] = PartialCharge [Atoms[], 'FF'];

aSetCharge [ Atoms[], q ];

local tot_chg = pr (add aCharge Atoms[] - n_carb); // adjust total charge for no.
carboxylates

//Adjust carbon and oxygen charges
// Automatic charges make carboxylate charge one unit too positive
local c_alter = -0.78; // rjd 0.22 derived from Khalid's DFT calculations
local o_alter = -0.15; // rjd O charge based on bci

local c_keys = (tr ligkeys)(1);
local o_keys = cat [(tr ligkeys)(2),(tr ligkeys)(4)];
//pr o_keys; exit[];

local c_charge = aCharge c_keys;
local o_charge = aCharge o_keys;

aSetCharge [ c_keys, c_charge + c_alter ];
aSetCharge [ o_keys, o_charge + o_alter ];

// Find bidentate carboxylates
ligkeys = split [ cat sm_MatchAtoms [ 'C1O[#T]O1', Atoms[] ], 4 ];
for il = 1, length ligkeys loop
        aSetHintLP [ ligkeys(il)(2), 1];
        aSetHintLP [ ligkeys(il)(4), 1];
        aSetIon [ ligkeys(il)(1), 1];   // Carbon
        aSetIon [ ligkeys(il)(2), -1];  // Oxygen
        aSetIon [ ligkeys(il)(4), -1];  // Oxygen
endloop;
c_keys = (tr ligkeys)(1);
o_keys = cat [(tr ligkeys)(2),(tr ligkeys)(4)];

c_charge = aCharge c_keys;
o_charge = aCharge o_keys;

aSetCharge [ c_keys, c_charge + c_alter ];
aSetCharge [ o_keys, o_charge + o_alter ];

// Find water bridges and set H charges to 0.54
ligkeys = split [ cat sm_MatchAtoms [ '[OH2]([#1])([#1])([#T])([#T])', Atoms[] ],
5 ];

o_keys = cat [(tr ligkeys)(1)];
local h_keys = cat [(tr ligkeys)(2),(tr ligkeys)(3)];
o_charge = aCharge o_keys;

local h_charge = first aCharge h_keys;
o_alter = 2* (0.54 - h_charge);

aSetCharge [ h_keys, 0.54 ];
aSetCharge [ o_keys, o_charge - o_alter ];

// Find Zn-NR3 units and make the R atoms 0.07 more positive
```

```
//ligkeys = split [ cat sm_MatchAtoms [ 'N([#1])([#1])([#1])([#T])', Atoms[] ], 5
];
ligkeys = split [ cat sm_MatchAtoms [ 'N(*)(*)(*)([#T])', Atoms[] ], 5 ];

h_keys = cat [(tr ligkeys)(2),(tr ligkeys)(3),(tr ligkeys)(4)];

//h_charge = first aCharge h_keys;
h_charge = aCharge h_keys;

aSetCharge [ h_keys, h_charge + 0.07 ];

// Find Zn-py and adjust C/H charges next to N
ligkeys = split [ cat sm_MatchAtoms [ 'n(c[#1])(c[#1])([#T])', Atoms[] ], 6 ];
h_keys = cat [(tr ligkeys)(3),(tr ligkeys)(5)];
h_charge = first aCharge h_keys;
aSetCharge [ h_keys, h_charge + 0.08 ];

//aSetSelected [ h_keys, 1 ]; exit[];
c_keys = cat [(tr ligkeys)(2),(tr ligkeys)(4)];
c_charge = first aCharge c_keys;
aSetCharge [ c_keys, c_charge + 0.07 ];

// Adjust Zinc charges
local chg_diff = tot_chg - (add aCharge Atoms[]);

// Four coord: rho(Zn) = 1.84
// Five coord: ammonia: rho(Zn) = 1.45
// Five coord: pyridine: rho(Zn) = 1.34

local mkey, bkeys;

for mkey in metkeys loop
   bkeys = cat aBonds mkey;
   if (length bkeys) == 4 then
      aSetCharge [ mkey, 1.84 ];
   elseif add (aMMType bkeys == 'NPYD' ) == 1 then // !!! MMFF94 specific !!!
         aSetCharge [ mkey, 1.34 ];
   elseif add (aMMType bkeys == 'N' ) == 1 then
         aSetCharge [ mkey, 1.45 ];
   elseif add (aMMType bkeys == 'OH2' ) == 1 then
         aSetCharge [ mkey, 1.68 ]; // based on bci of 0.15
   endif;
endloop;
//pr chg_diff; exit[];

//aSetCharge [ metkeys, (aCharge metkeys) + (chg_diff/(length metkeys)) ];

write ['>>> Total molecular charge: {n:5.1f}\n', add aCharge Atoms[] ];

endfunction
```

Appendix 2 - Cartesian coordinates, energies and lowest 12 vibrational frequencies to confirm local minimum achieved (Chapter 5)

Complexes are listed in the order in which they appear in Chapter 5 and 6. Nomenclature: $[Cu_2(O_2CR)_4L_n]$ → CuPR.nL

The electronic energy is included in parentheses after the name of the appropriate computer code and is a total electronic energy for ORCA and a binding energy for ADF.

The necessary MO occupations to generate the desired energy state in ADF are included. If no occupation specified, that geometry corresponds to the automatically located Aufbau state.

```
CuPH.2NH3: 'elongated': ORCA (-4150.49254046 Eh)
Cu     -0.005099000      0.000448000      1.333207000
O       1.428995000     -1.432605000      1.143311000
O      -1.437377000      1.433604000      1.136557000
O      -1.437409000     -1.432899000      1.136845000
O       1.428860000      1.433661000      1.142840000
C       1.824657000     -1.824503000      0.005025000
C      -1.824692000     -1.824725000     -0.004415000
Cu      0.004855000     -0.000205000     -1.333202000
O      -1.429092000      1.432959000     -1.143223000
O       1.437207000     -1.433393000     -1.136411000
O       1.437112000      1.433051000     -1.136973000
O      -1.429218000     -1.433338000     -1.142925000
C      -1.824659000      1.824857000     -0.004894000
C       1.824302000      1.824970000      0.004288000
H      -2.618582000     -2.618218000     -0.007027000
H      -2.618060000      2.618827000     -0.007916000
H       2.617823000      2.618832000      0.006838000
H       2.618221000     -2.618302000      0.008049000
N      -0.002564000     -0.001223000     -3.511452000
H       0.938875000     -0.027108000     -3.928611000
H      -0.502895000     -0.808032000     -3.911396000
H      -0.458704000      0.830474000     -3.913239000
N       0.002372000      0.000300000      3.511455000
H      -0.939083000     -0.024187000      3.928665000
H       0.501719000     -0.806913000      3.911813000
H       0.459563000      0.831647000      3.912774000

    0:        0.00 cm**-1
    1:        0.00 cm**-1
    2:        0.00 cm**-1
    3:        0.00 cm**-1
```

```
      4:           0.00 cm**-1
      5:           0.00 cm**-1
      6:          33.46 cm**-1
      7:          49.39 cm**-1
      8:          60.80 cm**-1
      9:          70.58 cm**-1
     10:          77.27 cm**-1
     11:          84.80 cm**-1
     12:          89.56 cm**-1
```

CuPH.2NH3: 'mixed': ORCA (-4150.48497904 Eh)
```
Cu      -0.007629000      0.000505000      1.263830000
O        1.461325000     -1.468174000      1.142750000
O       -1.475998000      1.469546000      1.133177000
O       -1.476126000     -1.468539000      1.133442000
O        1.461353000      1.469495000      1.142442000
C        1.860290000     -1.860146000      0.007301000
C       -1.860515000     -1.860372000     -0.006812000
Cu       0.007343000      0.000023000     -1.263803000
O       -1.461288000      1.469057000     -1.142753000
O        1.475966000     -1.468734000     -1.133089000
O        1.475721000      1.469116000     -1.133488000
O       -1.461724000     -1.468736000     -1.142414000
C       -1.860043000      1.861135000     -0.007265000
C        1.859961000      1.861134000      0.006765000
H       -2.654933000     -2.655089000     -0.011970000
H       -2.654208000      2.656105000     -0.012771000
H        2.654160000      2.656071000      0.011823000
H        2.654830000     -2.654735000      0.012791000
N       -0.004030000     -0.001473000     -3.332069000
H        0.944262000     -0.029843000     -3.731978000
H       -0.514195000     -0.815776000     -3.702314000
H       -0.466483000      0.839236000     -3.705886000
N        0.003768000     -0.000090000      3.332077000
H       -0.944544000     -0.027217000      3.732024000
H        0.513070000     -0.814727000      3.702768000
H        0.467130000      0.840337000      3.705406000
```

```
      0:           0.00 cm**-1
      1:           0.00 cm**-1
      2:           0.00 cm**-1
      3:           0.00 cm**-1
      4:           0.00 cm**-1
      5:           0.00 cm**-1
      6:           8.79 cm**-1
      7:          12.51 cm**-1
      8:          84.42 cm**-1
      9:          86.70 cm**-1
     10:          87.12 cm**-1
     11:          89.28 cm**-1
     12:          91.19 cm**-1
```

CuPH.2H2O: T$_0$(D$_{2h}$): ADF (-5.10539471 a.u.)
```
Cu       0.000000000      0.000000000     -1.275396000
Cu       0.000000000      0.000000000      1.275396000
O        1.426069000      1.421853000     -1.140404000
```

```
O        1.426069000      -1.421853000     -1.140404000
O       -1.426069000       1.421853000     -1.140404000
O       -1.426069000      -1.421853000     -1.140404000
C        1.821355000       1.815160000      0.000000000
C        1.821355000      -1.815160000      0.000000000
O        1.426069000       1.421853000      1.140404000
O       -1.426069000      -1.421853000      1.140404000
C       -1.821355000      -1.815160000      0.000000000
O        1.426069000      -1.421853000      1.140404000
O       -1.426069000       1.421853000      1.140404000
C       -1.821355000       1.815160000      0.000000000
O        0.000000000       0.000000000     -3.548713000
H        0.783560000       0.000000000     -4.141379000
H       -0.783560000       0.000000000     -4.141379000
O        0.000000000       0.000000000      3.548713000
H        0.783560000       0.000000000      4.141379000
H       -0.783560000       0.000000000      4.141379000
H       -2.602677000       2.595139000      0.000000000
H       -2.602677000      -2.595139000      0.000000000
H        2.602677000      -2.595139000      0.000000000
H        2.602677000       2.595139000      0.000000000
```

CuPH.2H2O: $T_M(D_{2h})$: ADF (-5.07922654 a.u.)
```
Cu       0.000000000       0.000000000     -1.227489000
Cu       0.000000000       0.000000000      1.227489000
O        1.467907000       1.463810000     -1.136654000
O        1.467907000      -1.463810000     -1.136654000
O       -1.467907000       1.463810000     -1.136654000
O       -1.467907000      -1.463810000     -1.136654000
C        1.863957000       1.859658000      0.000000000
C        1.863957000      -1.859658000      0.000000000
O        1.467907000       1.463810000      1.136654000
O       -1.467907000      -1.463810000      1.136654000
C       -1.863957000      -1.859658000      0.000000000
O        1.467907000      -1.463810000      1.136654000
O       -1.467907000       1.463810000      1.136654000
C       -1.863957000       1.859658000      0.000000000
O        0.000000000       0.000000000     -3.316186000
H        0.793920000       0.000000000     -3.894232000
H       -0.793920000       0.000000000     -3.894232000
O        0.000000000       0.000000000      3.316186000
H        0.793920000       0.000000000      3.894232000
H       -0.793920000       0.000000000      3.894232000
H       -2.644802000       2.641828000      0.000000000
H       -2.644802000      -2.641828000      0.000000000
H        2.644802000      -2.641828000      0.000000000
H        2.644802000       2.641828000      0.000000000
```

CuPCH3.2H2O: $T_0(D_2)$: ADF (-7.51870373 a.u.)
```
Cu       0.000000000       0.000000000      1.260700000
Cu       0.000000000       0.000000000     -1.260700000
O        1.421500000      -1.427700000      1.114200000
O        1.427400000       1.411100000      1.158400000
O       -1.427400000      -1.411100000      1.158400000
O       -1.421500000       1.427700000      1.114200000
C        1.837100000      -1.829800000     -0.023600000
```

```
C       1.837100000      1.829800000      0.023600000
O       1.427400000     -1.411100000     -1.158400000
O      -1.427400000      1.411100000     -1.158400000
C      -1.837100000      1.829800000     -0.023600000
O       1.421500000      1.427700000     -1.114200000
O      -1.421500000     -1.427700000     -1.114200000
C      -1.837100000     -1.829800000      0.023600000
O       0.000000000      0.000000000      3.566200000
H       0.780500000      0.051300000      4.160500000
H      -0.780500000     -0.051300000      4.160500000
O       0.000000000      0.000000000     -3.566200000
H       0.780500000     -0.051300000     -4.160500000
H      -0.780500000      0.051300000     -4.160500000
C      -2.905900000      2.893200000     -0.019000000
H      -2.528700000      3.782700000      0.504900000
H      -3.199200000      3.161700000     -1.039700000
H      -3.781300000      2.525900000      0.534900000
C       2.905900000      2.893200000      0.019000000
H       2.528700000      3.782700000     -0.504900000
H       3.199200000      3.161700000      1.039700000
H       3.781300000      2.525900000     -0.534900000
C       2.905900000     -2.893200000     -0.019000000
H       3.199200000     -3.161700000     -1.039700000
H       3.781300000     -2.525900000      0.534900000
H       2.528700000     -3.782700000      0.504900000
C      -2.905900000     -2.893200000      0.019000000
H      -3.199200000     -3.161700000      1.039700000
H      -3.781300000     -2.525900000     -0.534900000
H      -2.528700000     -3.782700000     -0.504900000

CuPCH3.2H2O: T_M(D_2): ADF (-7.48941290 a.u.)
Cu      0.000000000      0.000000000     -1.215677000
Cu      0.000000000      0.000000000      1.215677000
O      -1.481625000      1.457362000     -1.089093000
O       1.434060000      1.479642000     -1.174149000
O      -1.434060000     -1.479642000     -1.174149000
O       1.481625000     -1.457362000     -1.089093000
C      -1.870641000      1.883397000      0.046860000
C       1.870641000      1.883397000     -0.046860000
O      -1.434060000      1.479642000      1.174149000
O       1.434060000     -1.479642000      1.174149000
C       1.870641000     -1.883397000      0.046860000
O       1.481625000      1.457362000      1.089093000
O      -1.481625000     -1.457362000      1.089093000
C      -1.870641000     -1.883397000     -0.046860000
O       0.000000000      0.000000000     -3.323139000
H       0.258406000      0.749214000     -3.902544000
H      -0.258406000     -0.749214000     -3.902544000
O       0.000000000      0.000000000      3.323139000
H      -0.258406000      0.749214000      3.902544000
H       0.258406000     -0.749214000      3.902544000
C       2.937418000     -2.953322000      0.048672000
H       3.828996000     -2.577179000     -0.472533000
H       3.203094000     -3.246280000      1.070325000
H       2.572242000     -3.829425000     -0.505396000
C       2.937418000      2.953322000     -0.048672000
H       3.828996000      2.577179000      0.472533000
H       3.203094000      3.246280000     -1.070325000
H       2.572242000      3.829425000      0.505396000
```

```
C        -2.937418000         2.953322000         0.048672000
H        -3.203094000         3.246280000         1.070325000
H        -2.572242000         3.829425000        -0.505396000
H        -3.828996000         2.577179000        -0.472533000
C        -2.937418000        -2.953322000        -0.048672000
H        -3.203094000        -3.246280000        -1.070325000
H        -2.572242000        -3.829425000         0.505396000
H        -3.828996000        -2.577179000         0.472533000
```

CuPCH3.2NH3: T$_0$(C$_{2h}$): ADF (-7.92078556 a.u.)
```
Cu       -1.299400000         0.000900000         0.000000000
O        -1.135100000         1.426500000         1.431000000
O        -1.137000000        -1.433100000        -1.427000000
O        -1.137000000        -1.433100000         1.427000000
O        -1.135100000         1.426500000        -1.431000000
C         0.000600000         1.843200000         1.835500000
C        -0.000600000        -1.843200000         1.835500000
Cu        1.299400000        -0.000900000         0.000000000
O         1.135100000        -1.426500000        -1.431000000
O         1.137000000         1.433100000         1.427000000
O         1.137000000         1.433100000        -1.427000000
O         1.135100000        -1.426500000         1.431000000
C        -0.000600000        -1.843200000        -1.835500000
C         0.000600000         1.843200000        -1.835500000
C        -0.002900000         2.944000000         2.869200000
H         0.911300000         2.913900000         3.473900000
H        -0.039200000         3.911700000         2.345400000
H        -0.889200000         2.870100000         3.511000000
C         0.002900000        -2.944000000         2.869200000
H         0.889200000        -2.870100000         3.511000000
H        -0.911300000        -2.913900000         3.473900000
H         0.039200000        -3.911700000         2.345400000
C         0.002900000        -2.944000000        -2.869200000
H        -0.911300000        -2.913900000        -3.473900000
H         0.889200000        -2.870100000        -3.511000000
H         0.039200000        -3.911700000        -2.345400000
C        -0.002900000         2.944000000        -2.869200000
H        -0.889200000         2.870100000        -3.511000000
H        -0.039200000         3.911700000        -2.345400000
H         0.911300000         2.913900000        -3.473900000
N         3.530100000        -0.007200000         0.000000000
H         3.932400000         0.937700000         0.000000000
H         3.917600000        -0.486600000         0.821600000
H         3.917600000        -0.486600000        -0.821600000
N        -3.530100000         0.007200000         0.000000000
H        -3.917600000         0.486600000        -0.821600000
H        -3.932400000        -0.937700000         0.000000000
H        -3.917600000         0.486600000         0.821600000
```

CuPCH3.2NH3: T$_M$(C$_{2h}$): ADF (-7.91005747 a.u.)
symmetry C(2h)
occupations
A.g   21.0   //   21.0
B.g   16.0   //   15.0
A.u   16.0   //   16.0
B.u   21.0   //   20.0
end

```
Cu        -1.249700000      -0.001100000       0.000000000
O         -1.141500000       1.472100000       1.469300000
O         -1.126300000      -1.469100000      -1.473200000
O         -1.126300000      -1.469100000       1.473200000
O         -1.141500000       1.472100000      -1.469300000
C         -0.007700000       1.881300000       1.880700000
C          0.007700000      -1.881300000       1.880700000
Cu         1.249700000       0.001100000       0.000000000
O          1.141500000      -1.472100000      -1.469300000
O          1.126300000       1.469100000       1.473200000
O          1.126300000       1.469100000      -1.473200000
O          1.141500000      -1.472100000       1.469300000
C          0.007700000      -1.881300000      -1.880700000
C         -0.007700000       1.881300000      -1.880700000
C         -0.006000000       2.977000000       2.926300000
H          0.876800000       2.895700000       3.572000000
H          0.035500000       3.947800000       2.409000000
H         -0.922600000       2.945500000       3.527300000
C          0.006000000      -2.977000000       2.926300000
H          0.922600000      -2.945500000       3.527300000
H         -0.876800000      -2.895700000       3.572000000
H         -0.035500000      -3.947800000       2.409000000
C          0.006000000      -2.977000000      -2.926300000
H         -0.876800000      -2.895700000      -3.572000000
H          0.922600000      -2.945500000      -3.527300000
H         -0.035500000      -3.947800000      -2.409000000
C         -0.006000000       2.977000000      -2.926300000
H         -0.922600000       2.945500000      -3.527300000
H          0.035500000       3.947800000      -2.409000000
H          0.876800000       2.895700000      -3.572000000
N          3.328300000      -0.020800000       0.000000000
H          3.728200000       0.925200000       0.000000000
H          3.692200000      -0.508800000       0.827600000
H          3.692200000      -0.508800000      -0.827600000
N         -3.328300000       0.020800000       0.000000000
H         -3.692200000       0.508800000      -0.827600000
H         -3.728200000      -0.925200000       0.000000000
H         -3.692200000       0.508800000       0.827600000
```

CuPCH3.2py: T$_0$(D$_2$): ADF (-11.62463259 a.u.)
```
Cu         1.290700000       0.000000000       0.000000000
Cu        -1.290700000       0.000000000       0.000000000
O          1.121000000      -1.438200000      -1.428600000
O          1.152000000       1.403400000      -1.446600000
O          1.152000000      -1.403400000       1.446600000
O          1.121000000       1.438200000       1.428600000
C         -0.018000000      -1.819100000      -1.856900000
C          0.018000000       1.819100000      -1.856900000
O         -1.152000000      -1.403400000      -1.446600000
O         -1.152000000       1.403400000       1.446600000
C         -0.018000000       1.819100000       1.856900000
O         -1.121000000       1.438200000      -1.428600000
O         -1.121000000      -1.438200000       1.428600000
C          0.018000000      -1.819100000       1.856900000
C         -0.016000000       2.861300000       2.950700000
H          0.495500000       3.765600000       2.591600000
H         -1.036400000       3.113500000       3.259800000
```

```
H           0.549500000          2.481200000          3.813400000
C           0.016000000          2.861300000         -2.950700000
H          -0.495500000          3.765600000         -2.591600000
H           1.036400000          3.113500000         -3.259800000
H          -0.549500000          2.481200000         -3.813400000
C          -0.016000000         -2.861300000         -2.950700000
H          -1.036400000         -3.113500000         -3.259800000
H           0.549500000         -2.481200000         -3.813400000
H           0.495500000         -3.765600000         -2.591600000
C           0.016000000         -2.861300000          2.950700000
H           1.036400000         -3.113500000          3.259800000
H          -0.549500000         -2.481200000          3.813400000
H          -0.495500000         -3.765600000          2.591600000
N           3.518700000          0.000000000          0.000000000
C           4.209800000         -0.143700000          1.146200000
C           4.209800000          0.143700000         -1.146200000
C           5.602000000         -0.151200000          1.190800000
C           5.602000000          0.151200000         -1.190800000
C           6.312200000          0.000000000          0.000000000
H           3.615200000         -0.261600000          2.053600000
H           3.615200000          0.261600000         -2.053600000
H           6.116200000         -0.273400000          2.145100000
H           6.116200000          0.273400000         -2.145100000
H           7.403700000          0.000000000          0.000000000
N          -3.518700000          0.000000000          0.000000000
C          -4.209800000         -0.143700000         -1.146200000
C          -4.209800000          0.143700000          1.146200000
C          -5.602000000         -0.151200000         -1.190800000
C          -5.602000000          0.151200000          1.190800000
C          -6.312200000          0.000000000          0.000000000
H          -3.615200000         -0.261600000         -2.053600000
H          -3.615200000          0.261600000          2.053600000
H          -6.116200000         -0.273400000         -2.145100000
H          -6.116200000          0.273400000          2.145100000
H          -7.403700000          0.000000000          0.000000000
```

CuPCH3.2py: T_M(D₂): ADF (-11.61336618 a.u.)
symmetry D(2)
occupations
A   24.0 1.0 // 24.0 1.0
B1 23.0   // 23.0
B2 23.0   // 23.0
B3 23.0 1.0 1.0 // 23.0 0.0 0.0
end
```
Cu          1.244300000          0.000000000          0.000000000
Cu         -1.244300000          0.000000000          0.000000000
O           1.136100000         -1.546600000         -1.399300000
O           1.121700000          1.387500000         -1.537900000
O           1.121700000         -1.387500000          1.537900000
O           1.136100000          1.546600000          1.399300000
C           0.003800000         -1.878500000         -1.876600000
C          -0.003800000          1.878500000         -1.876600000
O          -1.121700000         -1.387500000         -1.537900000
O          -1.121700000          1.387500000          1.537900000
C           0.003800000          1.878500000          1.876600000
O          -1.136100000          1.546600000         -1.399300000
O          -1.136100000         -1.546600000          1.399300000
C          -0.003800000         -1.878500000          1.876600000
```

```
C      0.004800000      2.958200000      2.939400000
H      0.439000000      3.877100000      2.520000000
H     -1.009200000      3.163200000      3.300000000
H      0.641600000      2.643900000      3.778300000
C     -0.004800000      2.958200000     -2.939400000
H     -0.439000000      3.877100000     -2.520000000
H      1.009200000      3.163200000     -3.300000000
H     -0.641600000      2.643900000     -3.778300000
C      0.004800000     -2.958200000     -2.939400000
H     -1.009200000     -3.163200000     -3.300000000
H      0.641600000     -2.643900000     -3.778300000
H      0.439000000     -3.877100000     -2.520000000
C     -0.004800000     -2.958200000      2.939400000
H      1.009200000     -3.163200000      3.300000000
H     -0.641600000     -2.643900000      3.778300000
H     -0.439000000     -3.877100000      2.520000000
N      3.318500000      0.000000000      0.000000000
C      3.997000000     -0.082100000      1.157900000
C      3.997000000      0.082100000     -1.157900000
C      5.387800000     -0.083100000      1.198000000
C      5.387800000      0.083100000     -1.198000000
C      6.096000000      0.000000000      0.000000000
H      3.395700000     -0.152600000      2.064600000
H      3.395700000      0.152600000     -2.064600000
H      5.900600000     -0.149500000      2.158000000
H      5.900600000      0.149500000     -2.158000000
H      7.187300000      0.000000000      0.000000000
N     -3.318500000      0.000000000      0.000000000
C     -3.997000000     -0.082100000     -1.157900000
C     -3.997000000      0.082100000      1.157900000
C     -5.387800000     -0.083100000     -1.198000000
C     -5.387800000      0.083100000      1.198000000
C     -6.096000000      0.000000000      0.000000000
H     -3.395700000     -0.152600000     -2.064600000
H     -3.395700000      0.152600000      2.064600000
H     -5.900600000     -0.149500000     -2.158000000
H     -5.900600000      0.149500000      2.158000000
H     -7.187300000      0.000000000      0.000000000


CuPCH3.2CN: T0(D2): ADF (-7.95330195)
Cu     0.000000000     -1.369530000      0.000000000
Cu     0.000000000      1.369530000      0.000000000
O     -1.430383000     -1.110928000      1.465270000
O     -1.460366000     -1.162540000     -1.419503000
O      1.460366000     -1.162540000      1.419503000
O      1.430383000     -1.110928000     -1.465270000
C     -1.855029000      0.027527000      1.846892000
C     -1.855029000     -0.027527000     -1.846892000
O     -1.460366000      1.162540000      1.419503000
O      1.460366000      1.162540000     -1.419503000
C      1.855029000      0.027527000     -1.846892000
O     -1.430383000      1.110928000     -1.465270000
O      1.430383000      1.110928000      1.465270000
C      1.855029000     -0.027527000      1.846892000
C      2.931186000      0.025695000     -2.910668000
H      2.554020000     -0.485613000     -3.807790000
H      3.235522000      1.046275000     -3.168848000
H      3.801418000     -0.538773000     -2.546805000
```

```
C    -2.931186000    -0.025695000    -2.910668000
H    -2.554020000     0.485613000    -3.807790000
H    -3.235522000    -1.046275000    -3.168848000
H    -3.801418000     0.538773000    -2.546805000
C    -2.931186000     0.025695000     2.910668000
H    -3.235522000     1.046275000     3.168848000
H    -3.801418000    -0.538773000     2.546805000
H    -2.554020000    -0.485613000     3.807790000
C     2.931186000    -0.025695000     2.910668000
H     3.235522000    -1.046275000     3.168848000
H     3.801418000     0.538773000     2.546805000
H     2.554020000     0.485613000     3.807790000
C     0.000000000    -3.498369000     0.000000000
N     0.000000000    -4.675022000     0.000000000
C     0.000000000     3.498369000     0.000000000
N     0.000000000     4.675022000     0.000000000
```

CuPCH3.2CN: T$_M$(D$_2$): ADF (-7.94619279)
symmetry D(2)
occupations
A   20.0 // 20.0
B1 18.0 // 18.0
B2 20.0 // 18.0
B3 18.0 // 18.0
end
```
Cu    0.000000000    -1.306914000     0.000000000
Cu    0.000000000     1.306914000     0.000000000
O    -1.414693000    -1.128942000     1.554538000
O    -1.547925000    -1.131972000    -1.405339000
O     1.547925000    -1.131972000     1.405339000
O     1.414693000    -1.128942000    -1.554538000
C    -1.887674000     0.004214000     1.887457000
C    -1.887674000    -0.004214000    -1.887457000
O    -1.547925000     1.131972000     1.405339000
O     1.547925000     1.131972000    -1.405339000
C     1.887674000     0.004214000    -1.887457000
O    -1.414693000     1.128942000    -1.554538000
O     1.414693000     1.128942000     1.554538000
C     1.887674000    -0.004214000     1.887457000
C     2.960031000    -0.000191000    -2.960918000
H     2.565935000    -0.482111000    -3.866844000
H     3.290394000     1.017121000    -3.198415000
H     3.817429000    -0.595346000    -2.615456000
C    -2.960031000     0.000191000    -2.960918000
H    -2.565935000     0.482111000    -3.866844000
H    -3.290394000    -1.017121000    -3.198415000
H    -3.817429000     0.595346000    -2.615456000
C    -2.960031000    -0.000191000     2.960918000
H    -3.290394000     1.017121000     3.198415000
H    -3.817429000    -0.595346000     2.615456000
H    -2.565935000    -0.482111000     3.866844000
C     2.960031000     0.000191000     2.960918000
H     3.290394000    -1.017121000     3.198415000
H     3.817429000     0.595346000     2.615456000
H     2.565935000     0.482111000     3.866844000
C     0.000000000    -3.333568000     0.000000000
N     0.000000000    -4.508519000     0.000000000
C     0.000000000     3.333568000     0.000000000
```

```
N            0.000000000          4.508519000          0.000000000


CuPCH3.2NHC: T₀(C₂ᵥ): ADF (-12.97521013 a.u.)
symmetry C(2v)
occupations
A1    36.0 // 36.0
A2    18.0 // 16.0
B1    25.0 // 25.0
B2    25.0 // 25.0
end
Cu           0.000000000          0.000000000          1.384800000
O           -1.446100000         -1.432000000          1.135200000
O            1.446100000          1.432000000          1.135200000
O           -1.446100000          1.432000000          1.135200000
O            1.446100000         -1.432000000          1.135200000
C           -1.844800000         -1.845200000         -0.000700000
C           -1.844800000          1.845200000         -0.000700000
Cu           0.000000000          0.000000000         -1.385600000
O            1.436100000          1.444800000         -1.137900000
O           -1.436100000         -1.444800000         -1.137900000
O            1.436100000         -1.444800000         -1.137900000
O           -1.436100000          1.444800000         -1.137900000
C            1.844800000          1.845200000         -0.000700000
C            1.844800000         -1.845200000         -0.000700000
C           -2.888000000         -2.942700000          0.002000000
H           -3.505900000         -2.894300000         -0.903000000
H           -2.371900000         -3.915200000          0.014300000
H           -3.517800000         -2.878200000          0.897800000
C           -2.888000000          2.942700000          0.002000000
H           -3.505900000          2.894300000         -0.903000000
H           -3.517800000          2.878200000          0.897800000
H           -2.371900000          3.915200000          0.014300000
C            2.888000000          2.942700000          0.002000000
H            3.517800000          2.878200000          0.897800000
H            3.505900000          2.894300000         -0.903000000
H            2.371900000          3.915200000          0.014300000
C            2.888000000         -2.942700000          0.002000000
H            3.517800000         -2.878200000          0.897800000
H            2.371900000         -3.915200000          0.014300000
H            3.505900000         -2.894300000         -0.903000000
C            0.000000000          0.000000000         -3.573300000
N           -1.070100000          0.000000000         -4.424400000
N            1.070100000          0.000000000         -4.424400000
C            0.680500000          0.000000000         -5.754700000
C           -0.680500000          0.000000000         -5.754700000
H           -1.391000000          0.000000000         -6.573000000
H            1.391000000          0.000000000         -6.573000000
C            0.000000000          0.000000000          3.574400000
N            0.000000000         -1.070300000          4.425600000
N            0.000000000          1.070300000          4.425600000
C            0.000000000          0.680700000          5.756000000
C            0.000000000         -0.680700000          5.756000000
H            0.000000000         -1.391600000          6.574200000
H            0.000000000          1.391600000          6.574200000
C            0.000000000          2.467400000          3.998700000
H            0.000000000          2.489900000          2.905300000
H           -0.896800000          2.972600000          4.381700000
H            0.896800000          2.972600000          4.381700000
```

```
C          0.000000000       -2.467400000        3.998700000
H         -0.896800000       -2.972600000        4.381700000
H          0.000000000       -2.489900000        2.905300000
H          0.896800000       -2.972600000        4.381700000
C          2.466900000        0.000000000       -3.997100000
H          2.488500000        0.000000000       -2.903900000
H          2.972500000       -0.896500000       -4.380000000
H          2.972500000        0.896500000       -4.380000000
C         -2.466900000        0.000000000       -3.997100000
H         -2.488500000        0.000000000       -2.903900000
H         -2.972500000        0.896500000       -4.380000000
H         -2.972500000       -0.896500000       -4.380000000
```

CuPCH3.2NHC: T$_M$(C$_{2v}$): ADF (-12.97515986)
symmetry C(2v)
occupations
A1   36.0 // 35.0
A2   18.0 // 17.0
B1   25.0 // 25.0
B2   25.0 // 25.0
end
```
Cu         0.000000000        0.000000000        1.338100000
O         -1.495000000       -1.454300000        1.136200000
O          1.495000000        1.454300000        1.136200000
O         -1.495000000        1.454300000        1.136200000
O          1.495000000       -1.454300000        1.136200000
C         -1.885700000       -1.876600000        0.002700000
C         -1.885700000        1.876600000        0.002700000
Cu         0.000000000        0.000000000       -1.342800000
O          1.463300000        1.493000000       -1.133400000
O         -1.463300000       -1.493000000       -1.133400000
O          1.463300000       -1.493000000       -1.133400000
O         -1.463300000        1.493000000       -1.133400000
C          1.885700000        1.876600000        0.002700000
C          1.885700000       -1.876600000        0.002700000
C         -2.940600000       -2.969100000        0.007900000
H         -3.552100000       -2.926000000       -0.901700000
H         -2.431700000       -3.945200000        0.032700000
H         -3.576800000       -2.893800000        0.898200000
C         -2.940600000        2.969100000        0.007900000
H         -3.552100000        2.926000000       -0.901700000
H         -3.576800000        2.893800000        0.898200000
H         -2.431700000        3.945200000        0.032700000
C          2.940600000        2.969100000        0.007900000
H          3.576800000        2.893800000        0.898200000
H          3.552100000        2.926000000       -0.901700000
H          2.431700000        3.945200000        0.032700000
C          2.940600000       -2.969100000        0.007900000
H          3.576800000       -2.893800000        0.898200000
H          2.431700000       -3.945200000        0.032700000
H          3.552100000       -2.926000000       -0.901700000
C          0.000000000        0.000000000       -3.413300000
N         -1.075000000        0.000000000       -4.251200000
N          1.075000000        0.000000000       -4.251200000
C          0.680300000        0.000000000       -5.578500000
C         -0.680300000        0.000000000       -5.578500000
H         -1.391500000        0.000000000       -6.395800000
H          1.391500000        0.000000000       -6.395800000
```

```
C          0.000000000          0.000000000          3.409200000
N          0.000000000         -1.075100000          4.246100000
N          0.000000000          1.075100000          4.246100000
C          0.000000000          0.680500000          5.573800000
C          0.000000000         -0.680500000          5.573800000
H          0.000000000         -1.392600000          6.390500000
H          0.000000000          1.392600000          6.390500000
C          0.000000000          2.476200000          3.827600000
H          0.000000000          2.510800000          2.735700000
H         -0.897100000          2.973800000          4.218500000
H          0.897100000          2.973800000          4.218500000
C          0.000000000         -2.476200000          3.827600000
H         -0.897100000         -2.973800000          4.218500000
H          0.000000000         -2.510800000          2.735700000
H          0.897100000         -2.973800000          4.218500000
C          2.476200000          0.000000000         -3.834100000
H          2.511700000          0.000000000         -2.742400000
H          2.973500000         -0.897100000         -4.225700000
H          2.973500000          0.897100000         -4.225700000
C         -2.476200000          0.000000000         -3.834100000
H         -2.511700000          0.000000000         -2.742400000
H         -2.973500000          0.897100000         -4.225700000
H         -2.973500000         -0.897100000         -4.225700000
```

CuPCF3.2NHC: T₀(C₂ᵥ): ADF (-13.10982211 a.u.)
symmetry C(2v)
occupations
A1   45.0 // 45.0
A2   27.0 // 25.0
B1   34.0 // 34.0
B2   34.0 // 34.0
end

```
Cu         0.000000000          0.000000000          1.468200000
O         -1.437400000         -1.432800000          1.129400000
O          1.437400000          1.432800000          1.129400000
O         -1.437400000          1.432800000          1.129400000
O          1.437400000         -1.432800000          1.129400000
C         -1.803100000         -1.808500000         -0.015200000
C         -1.803100000          1.808500000         -0.015200000
Cu         0.000000000          0.000000000         -1.501700000
O          1.435700000          1.438500000         -1.159100000
O         -1.435700000         -1.438500000         -1.159100000
O          1.435700000         -1.438500000         -1.159100000
O         -1.435700000          1.438500000         -1.159100000
C          1.803100000          1.808500000         -0.015200000
C          1.803100000         -1.808500000         -0.015200000
C         -2.871000000         -2.943000000          0.013300000
C         -2.871000000          2.943000000          0.013300000
C          2.871000000          2.943000000          0.013300000
C          2.871000000         -2.943000000          0.013300000
C          0.000000000          0.000000000         -3.636700000
N         -1.071600000          0.000000000         -4.483600000
N          1.071600000          0.000000000         -4.483600000
C          0.680400000          0.000000000         -5.811300000
C         -0.680400000          0.000000000         -5.811300000
H         -1.392100000          0.000000000         -6.628300000
H          1.392100000          0.000000000         -6.628300000
C          0.000000000          0.000000000          3.598900000
```

```
N      0.000000000     -1.071500000      4.445500000
N      0.000000000      1.071500000      4.445500000
C      0.000000000      0.680400000      5.773500000
C      0.000000000     -0.680400000      5.773500000
H      0.000000000     -1.392800000      6.590000000
H      0.000000000      1.392800000      6.590000000
C      0.000000000      2.471500000      4.028900000
H      0.000000000      2.511200000      2.937000000
H     -0.897000000      2.972000000      4.416000000
H      0.897000000      2.972000000      4.416000000
C      0.000000000     -2.471500000      4.028900000
H     -0.897000000     -2.972000000      4.416000000
H      0.000000000     -2.511200000      2.937000000
H      0.897000000     -2.972000000      4.416000000
C      2.471900000      0.000000000     -4.067600000
H      2.513100000      0.000000000     -2.975900000
H      2.972200000     -0.896800000     -4.455400000
H      2.972200000      0.896800000     -4.455400000
C     -2.471900000      0.000000000     -4.067600000
H     -2.513100000      0.000000000     -2.975900000
H     -2.972200000      0.896800000     -4.455400000
H     -2.972200000     -0.896800000     -4.455400000
F      3.461100000     -3.121800000     -1.189500000
F      3.838900000     -2.672900000      0.927600000
F      2.276500000     -4.117100000      0.373400000
F     -3.461100000     -3.121800000     -1.189500000
F     -2.276500000     -4.117100000      0.373400000
F     -3.838900000     -2.672900000      0.927600000
F     -3.838900000      2.672900000      0.927600000
F     -3.461100000      3.121800000     -1.189500000
F     -2.276500000      4.117100000      0.373400000
F      3.838900000      2.672900000      0.927600000
F      2.276500000      4.117100000      0.373400000
F      3.461100000      3.121800000     -1.189500000
```

CuPCF3.2NHC: T$_M$(C$_{2v}$): ADF (-13.11965195 a.u.)
symmetry C(2v)
occupations
A1   45.0 // 44.0
A2   27.0 // 26.0
B1   34.0 // 34.0
B2   34.0 // 34.0
end
```
Cu     0.000000000      0.000000000      1.403900000
O     -1.488700000     -1.442900000      1.136300000
O      1.488700000      1.442900000      1.136300000
O     -1.488700000      1.442900000      1.136300000
O      1.488700000     -1.442900000      1.136300000
C     -1.856800000     -1.820500000     -0.005600000
C     -1.856800000      1.820500000     -0.005600000
Cu     0.000000000      0.000000000     -1.442400000
O      1.468900000      1.475600000     -1.148300000
O     -1.468900000     -1.475600000     -1.148300000
O      1.468900000     -1.475600000     -1.148300000
O     -1.468900000      1.475600000     -1.148300000
C      1.856800000      1.820500000     -0.005600000
C      1.856800000     -1.820500000     -0.005600000
C     -2.954000000     -2.925800000      0.019600000
```

C	-2.954000000	2.925800000	0.019600000
C	2.954000000	2.925800000	0.019600000
C	2.954000000	-2.925800000	0.019600000
C	0.000000000	0.000000000	-3.492700000
N	-1.076700000	0.000000000	-4.323400000
N	1.076700000	0.000000000	-4.323400000
C	0.680000000	0.000000000	-5.649400000
C	-0.680000000	0.000000000	-5.649400000
H	-1.392300000	0.000000000	-6.465500000
H	1.392300000	0.000000000	-6.465500000
C	0.000000000	0.000000000	3.454400000
N	0.000000000	-1.077200000	4.283300000
N	0.000000000	1.077200000	4.283300000
C	0.000000000	0.680300000	5.609600000
C	0.000000000	-0.680300000	5.609600000
H	0.000000000	-1.393500000	6.425000000
H	0.000000000	1.393500000	6.425000000
C	0.000000000	2.479900000	3.869400000
H	0.000000000	2.525700000	2.778600000
H	-0.897600000	2.974300000	4.261100000
H	0.897600000	2.974300000	4.261100000
C	0.000000000	-2.479900000	3.869400000
H	-0.897600000	-2.974300000	4.261100000
H	0.000000000	-2.525700000	2.778600000
H	0.897600000	-2.974300000	4.261100000
C	2.480100000	0.000000000	-3.912400000
H	2.529200000	0.000000000	-2.821800000
H	2.973700000	-0.897300000	-4.306200000
H	2.973700000	0.897300000	-4.306200000
C	-2.480100000	0.000000000	-3.912400000
H	-2.529200000	0.000000000	-2.821800000
H	-2.973700000	0.897300000	-4.306200000
H	-2.973700000	-0.897300000	-4.306200000
F	3.624100000	-3.012300000	-1.153800000
F	3.860900000	-2.699400000	1.005300000
F	2.370800000	-4.137800000	0.262100000
F	-3.624100000	-3.012300000	-1.153800000
F	-2.370800000	-4.137800000	0.262100000
F	-3.860900000	-2.699400000	1.005300000
F	-3.860900000	2.699400000	1.005300000
F	-2.370800000	4.137800000	0.262100000
F	-3.624100000	3.012300000	-1.153800000
F	3.860900000	2.699400000	1.005300000
F	2.370800000	4.137800000	0.262100000
F	3.624100000	3.012300000	-1.153800000

CuPCH3.2NHC: Symmetric TBP T_M: ORCA (-4803.96162140 Eh)

Cu	1.097364000	0.372482000	-0.447739000
O	-0.314327000	0.277554000	-2.051761000
O	1.204952000	-0.066626000	1.641484000
O	0.469115000	2.234959000	-0.036221000
O	1.706743000	-1.494323000	-0.869962000
C	-1.494596000	-0.133918000	-2.230816000
C	-0.716042000	2.352087000	0.431902000

```
Cu     -1.529168000      -0.736241000       0.533971000
O      -0.776154000      -0.866960000       2.391762000
O      -2.268629000      -0.609130000      -1.329261000
O      -0.250900000      -2.330545000      -0.095300000
O      -1.503726000       1.402045000       0.700160000
C       0.433601000      -0.481231000       2.551414000
C       0.967063000      -0.502465000       3.978025000
H       2.011451000      -0.870188000       3.987238000
H       0.977766000       0.537143000       4.367099000
H       0.335742000      -1.123424000       4.639856000
C       0.907004000      -2.451479000      -0.585910000
C       4.633820000       1.619539000      -2.427968000
H       5.233800000       1.632974000      -3.343596000
N       3.400212000       0.978692000      -2.348831000
C       2.860680000       1.105180000      -1.103822000
N       3.770398000       1.835012000      -0.398922000
C       4.867673000       2.166722000      -1.189316000
H       5.710457000       2.754620000      -0.811667000
C      -4.901071000      -2.767224000       2.110567000
H      -5.305351000      -3.655742000       2.606152000
N      -3.550785000      -2.630592000       1.799625000
C      -3.305398000      -1.435468000       1.192254000
N      -4.519553000      -0.820641000       1.123158000
C      -4.732388000       0.487910000       0.509516000
H      -5.424198000       1.082648000       1.135664000
H      -5.163768000       0.374364000      -0.504284000
H      -3.754341000       0.998488000       0.437970000
C      -5.517370000      -1.617786000       1.677843000
H      -6.566325000      -1.306928000       1.717934000
C       3.583287000       2.236968000       0.992982000
H       3.276658000       3.299725000       1.051056000
H       2.791993000       1.601749000       1.432193000
H       4.529909000       2.099941000       1.549407000
C       2.766657000       0.235253000      -3.435082000
H       1.697350000       0.104353000      -3.186121000
H       2.867896000       0.801611000      -4.380272000
H       3.241412000      -0.758532000      -3.552606000
C      -2.513446000      -3.612919000       2.103781000
H      -2.880059000      -4.627894000       1.859295000
H      -2.242354000      -3.571297000       3.176869000
H      -1.624291000      -3.376074000       1.491236000
C       1.432548000      -3.860217000      -0.831843000
H       1.848631000      -4.253484000       0.119543000
H       2.237319000      -3.863003000      -1.590306000
H       0.607950000      -4.530321000      -1.141038000
C      -1.218250000       3.773760000       0.649774000
H      -1.789192000       3.834359000       1.596514000
H      -1.914201000       4.033318000      -0.175218000
H      -0.387154000       4.502767000       0.655813000
C      -2.051435000      -0.095793000      -3.648207000
H      -3.150662000      -0.212892000      -3.657427000
H      -1.761576000       0.851201000      -4.143502000
H      -1.598556000      -0.925954000      -4.229548000
```

    0:        0.00 cm**-1
    1:        0.00 cm**-1
    2:        0.00 cm**-1
    3:        0.00 cm**-1
    4:        0.00 cm**-1

```
    5:          0.00 cm**-1
    6:         14.50 cm**-1
    7:         17.54 cm**-1
    8:         26.27 cm**-1
    9:         29.53 cm**-1
   10:         33.90 cm**-1
   11:         37.89 cm**-1
   12:         41.18 cm**-1
```

CuPCH3.2NHC: Asymmetric TBP T$_M$: ORCA (-4803.96120825 Eh)
```
Cu    -0.178189000     0.272126000     1.539137000
O     -1.668064000    -1.070840000     1.484093000
O      1.285877000     1.654157000     1.521618000
O     -1.459746000     1.628229000     0.646325000
O      1.319054000    -1.251364000     0.834838000
C     -1.969410000    -1.530737000     0.325968000
C     -1.727714000     2.028258000    -0.523671000
Cu     0.146613000     0.118597000    -1.514469000
O      1.598072000     1.426836000    -0.711913000
O     -1.405461000    -1.227078000    -0.760105000
O      1.462004000    -1.388387000    -1.419099000
O     -1.176737000     1.627334000    -1.603419000
C      1.868412000     1.928189000     0.415379000
C      1.759281000    -1.763157000    -0.227956000
C     -3.136051000    -2.510287000     0.275392000
C     -2.837467000     3.059487000    -0.680556000
C      2.961081000     2.988205000     0.482101000
C      2.702927000    -2.956266000    -0.120768000
C      0.069358000    -0.063356000    -3.521466000
N     -1.014048000    -0.306956000    -4.311090000
N      1.116477000     0.049797000    -4.386917000
C      0.699749000    -0.121577000    -5.704219000
C     -0.655177000    -0.345201000    -5.655839000
H     -1.382156000    -0.525576000    -6.454330000
H      1.389871000    -0.071133000    -6.552540000
C      0.047106000    -0.041698000     3.522887000
N      0.157311000    -1.227102000     4.187885000
N      0.013302000     0.905584000     4.504957000
C      0.094052000     0.326317000     5.767292000
C      0.187027000    -1.029608000     5.565149000
H      0.284200000    -1.857010000     6.275424000
H      0.088996000     0.918422000     6.688331000
C     -0.146401000     2.335289000     4.245155000
H      0.384558000     2.578197000     3.306995000
H     -1.219322000     2.593980000     4.143748000
H      0.285914000     2.909438000     5.084761000
C      0.207705000    -2.533700000     3.533985000
H      0.865155000    -3.205891000     4.117067000
H     -0.807729000    -2.971175000     3.468385000
H      0.612427000    -2.388249000     2.515094000
C      2.492820000     0.296258000    -3.966096000
H      2.944688000     1.077540000    -4.606320000
H      2.474422000     0.634628000    -2.914604000
H      3.094423000    -0.630606000    -4.040114000
C     -2.375296000    -0.454480000    -3.800491000
H     -2.314327000    -0.760996000    -2.739689000
H     -2.920859000     0.506544000    -3.874077000
H     -2.907243000    -1.224773000    -4.389798000
```

```
H          3.248446000        -3.134578000        -1.065856000
H          3.416840000        -2.802780000         0.711649000
H          2.102788000        -3.859487000         0.117379000
H         -4.026341000        -1.983102000        -0.126879000
H         -2.899888000        -3.339614000        -0.419324000
H         -3.381691000        -2.907720000         1.277299000
H         -2.881444000         3.724003000         0.202843000
H         -2.701000000         3.651002000        -1.605201000
H         -3.807120000         2.523508000        -0.754974000
H          3.396819000         3.050070000         1.496530000
H          2.512956000         3.974390000         0.237974000
H          3.750633000         2.782059000        -0.265284000

       0:         0.00 cm**-1
       1:         0.00 cm**-1
       2:         0.00 cm**-1
       3:         0.00 cm**-1
       4:         0.00 cm**-1
       5:         0.00 cm**-1
       6:        11.05 cm**-1
       7:        18.03 cm**-1
       8:        28.85 cm**-1
       9:        31.88 cm**-1
      10:        35.20 cm**-1
      11:        37.31 cm**-1
      12:        41.49 cm**-1
```

AZOGOL: [Zn$_2$(O$_2$CCH$_2$Ph)$_4$(NMes$_2$NHC)$_2$]: ORCA (-7242.98610438 Eh)

```
Zn         3.938230000        16.615161000         5.676933000
N          1.028353000        15.904828000         4.848262000
O          4.625792000        15.106677000         4.425428000
O          4.312647000        17.968203000         4.092885000
C          1.868587000        16.678899000         5.602709000
C         -0.310579000        16.236398000         5.066144000
H         -1.129829000        15.724946000         4.551414000
C          1.409431000        14.860375000         3.922968000
C          1.508281000        13.533802000         4.398200000
C          1.759721000        12.519586000         3.451553000
H          1.828028000        11.476378000         3.802046000
C          1.923426000        12.799477000         2.080010000
C          1.854493000        14.144922000         1.660310000
H          1.994283000        14.386411000         0.593123000
C          1.604860000        15.196405000         2.563502000
C          5.713114000        14.510884000         4.169228000
C          1.383866000        13.220684000         5.868435000
H          2.225616000        13.675971000         6.434519000
H          1.404130000        12.128842000         6.046451000
H          0.446266000        13.626792000         6.302700000
C          2.204502000        11.695205000         1.085852000
H          3.286466000        11.655286000         0.833523000
H          1.659347000        11.853783000         0.133558000
H          1.922138000        10.701658000         1.486483000
C          1.577740000        16.634670000         2.107008000
H          2.412028000        17.200737000         2.576577000
H          0.636856000        17.146864000         2.399594000
H          1.678174000        16.703989000         1.006274000
H          5.955728000        12.391074000         3.950290000
H          4.536651000        13.069735000         3.082250000
```

```
C       6.427003000      13.273525000       2.037490000
C       5.897390000      13.867094000       0.868820000
H       4.879201000      14.287273000       0.896804000
C       6.648402000      13.925842000      -0.317757000
H       6.214118000      14.389109000      -1.218449000
C       7.949880000      13.392347000      -0.358876000
H       8.538417000      13.434416000      -1.289360000
C       8.491597000      12.803270000       0.798017000
H       9.509352000      12.382612000       0.778106000
H       8.166451000      12.284092000       2.884936000
C       5.607415000      13.228302000       3.309247000
C       7.736480000      12.747784000       1.983036000
O       6.874496000      14.844327000       4.559372000
Zn      7.151271000      16.547740000       5.786033000
O       6.563904000      17.706414000       4.176658000
C       5.495628000      18.161543000       3.673127000
O       4.611653000      18.055433000       7.007595000
C       5.701815000      18.559352000       7.410121000
O       6.871842000      18.234177000       7.042685000
O       6.375979000      15.423795000       7.359739000
C       5.259806000      14.995267000       7.777254000
O       4.118344000      15.227435000       7.273114000
C      -0.313069000      17.250528000       5.984620000
N       1.024323000      17.503409000       6.297127000
C       1.398593000      18.530427000       7.244756000
C       1.626819000      19.843277000       6.770589000
C       1.867487000      20.847954000       7.727410000
H       2.036441000      21.879872000       7.376915000
C       1.897227000      20.573339000       9.111334000
C       1.704060000      19.242395000       9.531430000
H       1.745095000      19.004373000      10.607604000
C       1.458611000      18.198383000       8.616152000
C       1.299981000      16.770653000       9.079098000
H       2.122948000      16.142836000       8.672123000
H       0.347513000      16.322378000       8.725861000
H       1.320847000      16.706710000      10.184466000
C       2.161281000      21.678759000      10.108926000
H       3.217512000      22.020148000      10.055009000
H       1.971328000      21.347336000      11.148870000
H       1.528888000      22.567901000       9.907813000
C       1.645327000      20.145225000       5.292728000
H       2.498353000      19.629554000       4.800018000
H       1.751227000      21.231227000       5.108926000
H       0.722036000      19.795571000       4.784621000
H      -1.134994000      17.812326000       6.439061000
C       5.301590000      14.135909000       9.064402000
H       6.363727000      13.913593000       9.278146000
H       4.919944000      14.786443000       9.880888000
C       4.483845000      12.865019000       9.000742000
C       3.137607000      12.831035000       9.425486000
H       2.676038000      13.750342000       9.818819000
C       2.385079000      11.645378000       9.357886000
H       1.338438000      11.641840000       9.700949000
C       2.966557000      10.466123000       8.857302000
H       2.379914000       9.534854000       8.806106000
C       4.305450000      10.485780000       8.425363000
H       4.771348000       9.567725000       8.032194000
C       5.053682000      11.673578000       8.497106000
H       6.102060000      11.683206000       8.157184000
```

```
C      9.221622000     16.487168000      5.862628000
N     10.111884000     17.186158000      5.092509000
C     11.432562000     16.880206000      5.427315000
C     11.372148000     15.961303000      6.439215000
N     10.016326000     15.736421000      6.687424000
C      9.579240000     14.815513000      7.713471000
C      9.427990000     13.448617000      7.382412000
C      9.123068000     12.554199000      8.426834000
H      9.015280000     11.482319000      8.189826000
C      8.960039000     12.987673000      9.760083000
C      9.083263000     14.364479000     10.033238000
H      8.939052000     14.724995000     11.065114000
C      9.386318000     15.302511000      9.025118000
C      9.469027000     16.778765000      9.326654000
H      8.664821000     17.326827000      8.788956000
H     10.432303000     17.218629000      8.993473000
H      9.361183000     16.968365000     10.412020000
C      8.634635000     11.997803000     10.856080000
H      7.606264000     11.594404000     10.734561000
H      8.693193000     12.463669000     11.859231000
H      9.321427000     11.126500000     10.835686000
C      9.555164000     12.975225000      5.955196000
H      8.745673000     13.417965000      5.333323000
H      9.484184000     11.871659000      5.895400000
H     10.519292000     13.284500000      5.499563000
H     12.160868000     15.452273000      7.001857000
H     12.285196000     17.340705000      4.918721000
C      9.796352000     18.135318000      4.046938000
C      9.692877000     19.504781000      4.381822000
C      9.506853000     20.420512000      3.326872000
H      9.439286000     21.495129000      3.566343000
C      9.413015000     20.004811000      1.982272000
C      9.484505000     18.624397000      1.704153000
H      9.394401000     18.277506000      0.661344000
C      9.668493000     17.665678000      2.720445000
C      9.693693000     16.189645000      2.411451000
H      8.823154000     15.681050000      2.878848000
H     10.605423000     15.695209000      2.808052000
H      9.648434000     16.008881000      1.320869000
C      9.200175000     21.012050000      0.874562000
H      8.121886000     21.260816000      0.767061000
H      9.545529000     20.623956000     -0.104111000
H      9.730791000     21.963602000      1.078777000
C      9.746766000     19.962763000      5.817706000
H      8.866426000     19.579654000      6.379309000
H      9.738573000     21.067546000      5.886279000
H     10.652216000     19.588771000      6.340665000
C      5.567453000     19.639050000      8.510766000
H      4.527055000     20.013199000      8.473179000
H      5.680937000     19.093953000      9.473275000
C      6.561016000     20.775044000      8.445346000
C      7.791677000     20.720398000      9.136222000
H      8.033999000     19.826075000      9.732690000
C      8.705956000     21.786977000      9.077806000
H      9.657890000     21.723210000      9.629265000
C      8.406334000     22.934325000      8.320814000
H      9.118593000     23.774151000      8.277509000
C      7.187319000     23.000815000      7.621468000
H      6.941805000     23.894997000      7.026271000
```

```
C          6.276778000         21.931787000          7.684810000
H          5.324429000         21.991560000          7.133723000
C          5.657540000         19.005483000          2.385791000
H          6.740943000         19.172352000          2.237495000
H          5.293759000         18.366612000          1.552428000
C          4.902104000         20.316104000          2.393140000
C          3.610390000         20.427648000          1.834041000
H          3.145840000         19.540092000          1.375940000
C          2.914641000         21.649495000          1.851002000
H          1.908954000         21.712244000          1.406096000
C          3.500430000         22.788332000          2.432841000
H          2.959007000         23.747900000          2.444289000
C          4.785322000         22.691221000          2.998240000
H          5.253847000         23.577544000          3.455438000
C          5.476541000         21.467644000          2.978191000
H          6.480575000         21.397372000          3.426282000
```

```
 0:         0.00  cm**-1
 1:         0.00  cm**-1
 2:         0.00  cm**-1
 3:         0.00  cm**-1
 4:         0.00  cm**-1
 5:         0.00  cm**-1
 6:       -10.03  cm**-1
 7:         5.17  cm**-1
 8:         9.29  cm**-1
 9:        10.07  cm**-1
10:        12.16  cm**-1
11:        13.29  cm**-1
12:        15.03  cm**-1
```

The single negative value corresponds to a mesityl para-methyl group rotation which we do not consider significant.

AZOGOL[Cu]: [Cu$_2$(O$_2$CCH$_2$Ph)$_4$(NMes$_2$NHC)$_2$]: T$_M$ ORCA (-6965.69749889)

```
Cu     -0.000000000        -0.000000000          1.582852000
N      -0.434481000        -0.986990000          4.402243000
O      -0.209735000        -1.928356000          0.682783000
O      -1.987559000         0.255216000          1.564842000
C      -0.000051000        -0.000045000          3.570130000
C      -0.275991000        -0.627774000          5.744029000
H      -0.562971000        -1.292734000          6.564086000
C      -0.995415000        -2.230465000          3.943259000
C      -0.127297000        -3.248419000          3.497641000
C      -0.713657000        -4.453083000          3.064024000
H      -0.051637000        -5.261249000          2.713006000
C      -2.109128000        -4.640134000          3.043579000
C      -2.935137000        -3.584594000          3.479479000
H      -4.029599000        -3.700085000          3.433439000
C      -2.401295000        -2.362267000          3.923398000
C      -0.444196000        -2.488874000         -0.415078000
C       1.359103000        -3.032098000          3.425117000
H       1.598723000        -2.310085000          2.616804000
H       1.889834000        -3.974679000          3.195409000
H       1.765550000        -2.605942000          4.365243000
C      -2.716328000        -5.903535000          2.485391000
H      -3.019815000        -5.739915000          1.427339000
H      -3.628128000        -6.201477000          3.041558000
H      -1.999431000        -6.748162000          2.501660000
```

```
C     -3.285642000     -1.192098000      4.270624000
H     -3.092091000     -0.369484000      3.547929000
H     -3.083179000     -0.795785000      5.286934000
H     -4.354669000     -1.473038000      4.214442000
H     -0.775961000     -4.467701000     -1.256872000
H     -0.814777000     -4.368419000      0.547798000
C     -2.616542000     -3.672319000     -0.444221000
C     -3.243674000     -2.735263000      0.405130000
H     -2.630789000     -2.158177000      1.109985000
C     -4.629304000     -2.528733000      0.340239000
H     -5.099108000     -1.789642000      1.007969000
C     -5.415481000     -3.255559000     -0.572107000
H     -6.503049000     -3.090075000     -0.626165000
C     -4.800545000     -4.194400000     -1.419147000
H     -5.404067000     -4.767044000     -2.141099000
H     -2.930742000     -5.122161000     -2.032403000
C     -1.111713000     -3.863684000     -0.392995000
C     -3.410667000     -4.396629000     -1.356018000
O     -0.255043000     -1.988835000     -1.581808000
Cu     0.000025000     -0.000000000     -1.600469000
O     -1.931886000      0.217192000     -0.701280000
C     -2.488072000      0.450018000      0.399133000
O      0.209711000      1.928322000      0.682810000
C      0.444196000      2.488862000     -0.415040000
O      0.255077000      1.988839000     -1.581780000
O      1.931915000     -0.217212000     -0.701241000
C      2.488084000     -0.450047000      0.399178000
O      1.987555000     -0.255258000      1.564880000
C      0.275574000      0.627712000      5.744046000
N      0.434261000      0.986921000      4.402278000
C      0.995239000      2.230399000      3.943352000
C      0.127159000      3.248375000      3.497702000
C      0.713554000      4.453038000      3.064133000
H      0.051571000      5.261220000      2.713085000
C      2.109029000      4.640065000      3.043763000
C      2.934999000      3.584507000      3.479691000
H      4.029465000      3.699984000      3.433706000
C      2.401125000      2.362177000      3.923565000
C      3.285429000      1.191980000      4.270814000
H      3.091948000      0.369407000      3.548054000
H      3.082855000      0.795606000      5.287076000
H      4.354463000      1.472924000      4.214755000
C      2.716265000      5.903468000      2.485625000
H      3.019773000      5.739871000      1.427576000
H      3.628053000      6.201380000      3.041826000
H      1.999386000      6.748110000      2.501901000
C     -1.359237000      3.032065000      3.425096000
H     -1.598809000      2.309967000      2.616849000
H     -1.889940000      3.974629000      3.195250000
H     -1.765743000      2.606031000      4.365252000
H      0.562276000      1.292705000      6.564174000
C      3.860027000     -1.124901000      0.384585000
H      4.362393000     -0.847507000     -0.563060000
H      4.469425000     -0.779519000      1.240953000
C      3.656057000     -2.626486000      0.460766000
C      4.350238000     -3.409620000      1.404417000
H      5.065005000     -2.925031000      2.088292000
C      4.129434000     -4.795052000      1.490753000
H      4.678132000     -5.390817000      2.236486000
```

```
C       3.202615000      -5.416596000       0.635960000
H       3.023718000      -6.500739000       0.709589000
C       2.505406000      -4.641646000      -0.309137000
H       1.776724000      -5.117017000      -0.985046000
C       2.730822000      -3.259991000      -0.397547000
H       2.176685000      -2.652703000      -1.126086000
C       0.000069000       0.000012000      -3.589406000
N      -0.996814000       0.411202000      -4.421762000
C      -0.633857000       0.261514000      -5.763644000
C       0.634104000      -0.261284000      -5.763620000
N       0.997005000      -0.411097000      -4.421733000
C       2.247859000      -0.953678000      -3.959861000
C       2.395584000      -2.358044000      -3.931733000
C       3.620533000      -2.875962000      -3.476207000
H       3.748905000      -3.968938000      -3.426452000
C       4.663816000      -2.035661000      -3.037479000
C       4.462796000      -0.642310000      -3.070260000
H       5.260891000       0.030631000      -2.716662000
C       3.255032000      -0.071686000      -3.516759000
C       3.025634000       1.414139000      -3.462230000
H       2.287259000       1.657280000      -2.669523000
H       2.614539000       1.806962000      -4.415161000
H       3.961058000       1.954060000      -3.223301000
C       5.929126000      -2.626714000      -2.466277000
H       5.749368000      -2.968641000      -1.422938000
H       6.754115000      -1.888058000      -2.439593000
H       6.265693000      -3.512425000      -3.042158000
C       1.239377000      -3.257378000      -4.287530000
H       0.408530000      -3.075662000      -3.571372000
H       1.533595000      -4.322751000      -4.230365000
H       0.848511000      -3.058745000      -5.306786000
H       1.305596000      -0.533666000      -6.583540000
H      -1.305297000       0.534113000      -6.583536000
C      -2.247665000       0.953796000      -3.959909000
C      -2.395395000       2.358160000      -3.931796000
C      -3.620339000       2.876094000      -3.476280000
H      -3.748727000       3.969068000      -3.426556000
C      -4.663624000       2.035801000      -3.037549000
C      -4.462602000       0.642454000      -3.070347000
H      -5.260721000      -0.030456000      -2.716761000
C      -3.254845000       0.071808000      -3.516829000
C      -3.025479000      -1.414026000      -3.462330000
H      -2.287007000      -1.657207000      -2.669724000
H      -2.614539000      -1.806867000      -4.415324000
H      -3.960898000      -1.953916000      -3.223306000
C      -5.928936000       2.626843000      -2.466347000
H      -5.749209000       2.968705000      -1.422978000
H      -6.753950000       1.888207000      -2.439733000
H      -6.265463000       3.512589000      -3.042195000
C      -1.239210000       3.257489000      -4.287637000
H      -0.408297000       3.075710000      -3.571578000
H      -1.533401000       4.322865000      -4.230396000
H      -0.848428000       3.058903000      -5.306931000
C       1.111715000       3.863670000      -0.392902000
H       0.776021000       4.467702000      -1.256790000
H       0.814729000       4.368406000       0.547875000
C       2.616546000       3.672292000      -0.444048000
C       3.243613000       2.735208000       0.405314000
H       2.630683000       2.158112000       1.110120000
```

```
C      4.629237000      2.528633000      0.340479000
H      5.098984000      1.789507000      1.008213000
C      5.415481000      3.255439000     -0.571825000
H      6.503033000      3.089876000     -0.625870000
C      4.800615000      4.194333000     -1.418857000
H      5.404184000      4.766989000     -2.140762000
C      3.410740000      4.396610000     -1.355780000
H      2.930895000      5.122211000     -2.032148000
C     -3.860013000      1.124867000      0.384534000
H     -4.362390000      0.847466000     -0.563102000
H     -4.469409000      0.779486000      1.240904000
C     -3.656073000      2.626457000      0.460714000
C     -4.350302000      3.409576000      1.404342000
H     -5.065055000      2.924966000      2.088217000
C     -4.129557000      4.795017000      1.490661000
H     -4.678290000      5.390765000      2.236381000
C     -3.202759000      5.416588000      0.635867000
H     -3.023923000      6.500742000      0.709482000
C     -2.505482000      4.641650000     -0.309187000
H     -1.776799000      5.117034000     -0.985089000
C     -2.730836000      3.259984000     -0.397576000
H     -2.176654000      2.652703000     -1.126087000
```

```
 0:        0.00 cm**-1
 1:        0.00 cm**-1
 2:        0.00 cm**-1
 3:        0.00 cm**-1
 4:        0.00 cm**-1
 5:        0.00 cm**-1
 6:       13.71 cm**-1
 7:       15.56 cm**-1
 8:       17.10 cm**-1
 9:       18.66 cm**-1
10:       25.27 cm**-1
11:       25.41 cm**-1
12:       27.46 cm**-1
```